Author:
Cooper, Michael

Title:
What lies beneath

A radioglaciological study of Greenland

What lies beneath: A radioglaciological study of Greenland

Michael A. Cooper

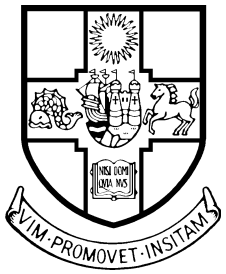

Bristol Glaciology Centre
School of Geographical Sciences
University of Bristol

This dissertation is submitted for the degree of
Doctor of Philosophy
21 September 2018

Abstract

The subglacial environment can exert strong controls on glacier dynamics, influencing the orientation and velocity of ice flow, as well as the modulation and distribution of basal waters and sediment. Bed geometry can also provide a long-term record of geomorphic processes, allowing insight into landscape evolution and inheritance with consequences for both palaeo- and contemporary ice dynamics. However, beneath the Greenland Ice Sheet (GrIS), many aspects of the subglacial environment remain poorly constrained, including both its bulk (*e.g.* geology, geometry, and presence of sediment and water) and inter-facial properties (*e.g.* basal roughness and geotechnical bed properties). There is, therefore, limited understanding of how spatially heterogenous subglacial properties relate to ice-sheet motion. A marked increase in the availability of radio-echo sounding (RES) (often referred to as ice-penetrating radar (IPR)) data, has not only improved the accuracy of derived basal topography products, but continues to facilitate wider analysis of the subglacial environment. The primary focus of this thesis is to use RES, and complementary data (*e.g.* ice velocities, basal thermal state, surface topography, etc.), to examine the complex interrelationships between Greenland's ice and the bed.

The first results chapter of this thesis presents evidence from RES data for a large, subglacial drainage network, radiating inland from Jakobshavn Isbræ, Greenland's largest outlet glacier. Topographic and basin morphometric analyses of an isostatically uplifted (ice-free) bedrock topography suggest that this catchment pre-dates ice-sheet initiation. This landscape has likely been instrumental in controlling the location and form of Jakobshavn Glacier, as well as influencing ice flow from the deep interior to the margin, both now and over several glacial cycles.

The second results chapter presents a new systematic analysis of subglacial

roughness beneath the GrIS. Using two decades of RES data, this chapter quantifies two near-independent subglacial roughness metrics enabling assessment of roughness anisotropy, and of finer-scale information, respectively. In fast-flowing regions 'topographic roughness' (defined by variation in sampled bed elevation) exhibits an exponential scaling relationship with ice velocity parallel, but not perpendicular, to flow direction. In many slow-flowing regions both roughness metrics indicate spatially-coherent signals, representative of 'smooth' bed; combined with analyses for underlying geology, it is concluded that these are likely due to the presence of a hard bed.

The third results chapter focuses on the assessment of how the subglacial environment is expressed at the surface of the ice sheet. This is undertaken through the use of a new high-resolution surface topography (ArcticDEM), and its potential to provide enhanced insights into basal and englacial ice-sheet processes. Notable surface features—quantified using a calculated 'residual surface elevation' (RSE)—are observed coincident with previously documented subglacial channels. Additionally, 'new' smaller-scale tributaries ($< \sim$2,000 m in width) and complex valley-like structures are revealed with particular clarity. RSE also allows the extents of basal ice units to be mapped, providing support to the theorized genesis of these these features, and that they act as 'false bottoms,' likely due to a rheological contrast in the ice column.

Ultimately, this thesis not only provides significant advances in the quantification of subglacial properties of the GrIS, the results and data presented herein will facilitate further assessment of the bed and its influence on, and interrelationship with ice motion. It is, therefore, hoped that this thesis works to improve the understanding of glacial response to contemporary climatic perturbation, and to improve projections of future contributions to global sea level.

Declaration

I declare that the work in this dissertation was carried out in accordance with the requirements of the University's [of Bristol] Regulations and Code of Practice for Research Degree Programmes. The work is original to the candidate, except where indicated by special reference in the text, and no part of the thesis has been submitted for any other academic award. Collaborative work undertaken, or with the assistance of others, is indicated as such. Any views expressed in this thesis are those of the author.

Michael A. Cooper
September, 2018

Acknowledgements

I would, first and foremost, like to acknowledge my supervisor, Prof. Jonathan Bamber, for his ongoing assistance, support, and advice since the inception of this project—without which this research would surely be lacking. Further, for his supervisory approach that has truly helped forge the start of my own academic career through this research. Secondly, Drs. Tom Jordan and Chris Williams who have both proved fundamental throughout the evolution of this project, providing key insight both academically and worldly. And, as the final member of my pseudo-supervisory team, I would like to extend my gratitude to Prof. Martin Siegert, whose friendly chats always instilled me with confidence, and shared my excitement for 'what lies beneath.'

I must also express my gratitude to my ever-supporting family and friends, many of whom I have somewhat neglected over the past four years within my own PhD 'bubble.' To Emily and Rose, and the rest of the 'après-ski' group, for being the most-caring and thoughtful friends I could ask for; to Moya Macdonald and Guillaume Lamarche-Gagnon for making our house a home; and, to James Crosby for always being great company, and someone to deplore the world with.

The 'Browns' community should get a look in too; that great bunch of fellow postgraduate students that I have had the great pleasure of ~~hardly working~~ working hard alongside over my time in Bristol. Where my particular thanks go to: Ed'd, Gaz, Izzy, Erik, Tim, Jenny, Alice, Stefan, Bea, and Sam.

To the myriad cafés that allowed me to sit for hours on end in the final stages of this research, plying me with coffee and toast and marmalade. And to Mum and Dad, who I am sure will be as glad and I am, if not more so, to see this thesis submitted.

Although not a traditional subject matter for the acknowledgements section of a thesis—a place reserved for thanks and well wishes—I would like to address

this last part to anyone that is currently embarking upon a PhD of their own. This is to 'acknowledge' the depression I have been suffering with throughout most of my time in Bristol. This, obviously, is not a comment of thanks or appreciation for such, but neither is this a slight on the dealings and nature of the University of Bristol or any member of its staff; to reiterate, support from both staff and students within the faculty, and at the Students' Health- and Counselling Services here have certainly made my life easier—through 'opening up,' through counselling, and, without forgetting, through SSRI anti-depressants...! I would like to note that I have, in some ways, really rather struggled through these past four years, and although the PhD process, and my thesis cannot be wholly 'blamed' for this, it has certainly been a contributor.

Perhaps in noting this, it may seem that I am attempting to undertake some egotistical exercise, with an air of 'look what I have accomplished, despite;' however, I want to make clear that this is here instead for posterity, for understanding, and perhaps more meaningfully, for the purpose of solidarity. The process of obtaining a PhD is a difficult beast, even if this difficulty comes mostly through gruelling endurance and persistence 'despite.' This is a difficulty that deserves to be noted, to be acknowledged, for the sake of the mental health of the students it affects. The epigraph of this thesis, opening after the contents pages, consists of three poems (or self-styled 'grooks') by Danish scientist, Piet Hein; whilst I cannot confess that these verses have carried me through my PhD, I believe that their sentiment, like much of Hein's work, carries both wisdom and meaning. Above poetry and whimsy, however, it is important to know that help is there if you need it: please make sure you lend a voice to your feelings, to talk about your mental health, be open, and if you need it, to ask for help—I wish I had done so sooner myself. To take an important quote from Gaz (given in his TEDx talk), who, and whose impact on me, I have already mentioned above: "ultimately, talking about your mental health is not just good for you, it's good for everyone."

Contents

List of Figures

Problems worthy
of attack
prove their worth
by hitting back.

Problems
Piet Hein

Put up in a place
where it's easy to see
the cryptic admonishment
T.T.T.

When you feel how depressingly
slowly you climb,
it's well to remember that
Things Take Time.

TTT
Piet Hein

The road to wisdom? — Well, it's plain
and simple to express:

Err
and err
and err again
but less
and less
and less.

The Road to Wisdom
Piet Hein

Chapter 1

Introduction

Whilst the total potential sea level rise (SLR) of the Greenland Ice Sheet (GrIS) is relatively well constrained by geophysical survey (∼7.42 m; Morlighem et al., 2017), projections of future SLR contributions remain challenging (Joughin et al., 2004; Bamber and Aspinall, 2013). As the GrIS experiences accelerating mass loss (Velicogna and Wahr, 2006; Rignot et al., 2011), a push to provide better constraints on predicted future losses has led to the successive release of subglacial topography beneath Greenland (*e.g.* Bamber et al., 2001, 2013a; Morlighem et al., 2014, 2017). As an integral boundary condition used within numerical models, subglacial topography can exert strong controls on glacier dynamics, both influencing the orientation and velocity of ice flow (Clarke, 2004; Joughin et al., 2009; Bingham and Siegert, 2009), as well as the modulation, and distribution, of basal waters and sediment (Baroni et al., 2005; Rose et al., 2014; Jamieson et al., 2016; Wright et al., 2008). Whilst the influence of these and other basal properties on ice motion is well understood theoretically, such characteristics remain either poorly constrained, or are not yet incorporated into predictive ice-sheet modelling. There is, therefore, limited understanding of how spatially-heterogeneous aspects of the subglacial environment influence contemporary ice dynamics, and to what degree.

Distilling this picture is made more complex by the time-transgressive nature of the subglacial environment. Basal morphology provides a record of long-term landscape evolution (*e.g.,* Young et al., 2011; Hall et al., 2013), not only reflecting the present-day influence of an overlying ice sheet, but also detailing the history of ice-sheet development and former patterns of ice flow (Siegert et al., 2005;

Bingham and Siegert, 2009; Rose et al., 2013).

A recent marked increase in the availability of radio-echo sounding data presents an opportunity not only to quantify aspects of the subglacial environment, but when used alongside complementary datasets (*e.g.* contemporary ice velocity, basal thermal state, and surface topography, etc.) to elucidate the complex inter-relationships between Greenland's ice and the underlying bed, acting both contemporaneously and for past glacial cycles.

Chapter 2

Background

This chapter provides a broad background to introduce this thesis's scope, highlight the context to relevant research aims and objects, as well as within the wider field of glaciology. This is done with reference to aspects of the solid earth (*i.e.* underlying geology); the observed and theorised influence of the subglacial environment, and basal processes on ice motion; and, the key geophysical method employed within this study, RES. Finally, this chapter identifies major research gaps within current understanding, and outlines the research aims and objectives that arise from these.

2.1 Greenland and the Greenland Ice Sheet

2.1.1 Geological setting and geothermal history

Dominated by crystalline rocks of the Precambrian (Henriksen et al., 2009), Greenland has experienced an ancient history of development spanning more than 3,800 million years (Ma) (Henriksen, 2008). As much of the island lies unexposed under the GrIS, only limited direct information regarding the geology beneath the ice is available. However, the island's ice-free margins present a thorough geological history of Greenland's bedrock and surrounding continental shelf, a geology that is most likely to be shared with the island's interior (Figure 2.1; Henriksen, 2008; Henriksen et al., 2009).

Methods used to better constrain coast-to-coast correlation involve the direct observation of rocks at nunataks (isolated rocks or peaks projecting from the

Figure 2.1: Geological map of Greenland with interpretation of sub-ice bedrock in terms of major provinces (after Dawes 2009). Ice-free geology (darker shades) is modified from Henriksen (2008); grey, dashed line, delineates the division of Proterozoic crust after Dahl-Jensen et al. (2003). Small map, Canadian–Greenland correlations in the Precambrian shield showing the Palaeozoic Franklinian Basin blanketing its northern margin.

ice's surface) or at drill sites (Dawes, 2009) (see Figures 2.1 and 2.2 for borehole locations). The sparse drill sites, however, not only prove to be a costly, but are ineffectual in determining underlying geology (Dawes, 2009). Most notably, the only *in situ* rock sampled using this technique was collected at GISP 2 (Figure 2.1), where other boreholes have revealed information regarding subglacial till and debris rather than substratum composition (Fountain et al., 1981). Alternatively, magnetic geophysical survey allows transitions between provinces, and the intrusion of igneous rocks (*e.g.* Tinto et al., 2015), to be better mapped (Dawes, 2009). Additionally, inferences made about the crustal (lithosphere) thickness and geothermal history of Greenland can present implications for the island's geodynamic evolution (Martos et al., 2018). In the first case, crustal thickness, derived using seismology and gravity data, supports a 'stabilisation' of the Greenland basement during the Early Proterozoic, after which tectonic reworking of the continent was limited (Martos et al., 2018; Braun et al., 2007). Measures of contemporary geothermal heat flux (GHF) (*e.g.* Martos et al., 2018), providing a proxy for geothermal history, have elucidated the role of mantle plumes and the movement of the Iceland hot-spot beneath Greenland. The influence of this hot-spot is not limited to the island's geology, but has also been linked to the onset of fast flow at the North East Greenland Ice Stream (NEGIS) (Fahnestock et al., 2001).

The basement, crystalline rocks were formed following a succession of ancient orogenic events (creating fold belts) during the Archaean and Palaeoproterozoic (3,200–2,600 Ma and 2,000–1,750 Ma Before Present [B.P.], respectively) (Henriksen et al., 2009). At ∼1,600 Ma B.P., Greenland's basement stabilised as a coherent block, as noted above, forming part of the wider Laurentian shield present across north-eastern North America (Henriksen, 2008). Subsequent geologic developments were localised to the margins of the shield. Limited sedimentary basins were developed across three discrete periods, during the Proterozoic (1,740–542 Ma B.P.), the Cambrian–Silurian (542–416 Ma B.P.) and the Devonian–Neogene (416–0 Ma B.P.) (Henriksen, 2008). Younger mountain chains, formed by the Caledonian (∼420 Ma B.P.) and the Ellesmerian fold belts (∼350 Ma B.P.) run parallel to the coast in north-east and northern Greenland, respectively (Henriksen, 2008; Henriksen et al., 2009). Localised volcanic intrusions are documented following the Gardar rift (∼1,350–1,125 Ma B.P.) in southern Greenland in which basaltic sequences were deposited. Later volcanic

units (∼60–55 Ma ago) in the west and east of Greenland were developed in connection with the North Atlantic sea floor spreading (Henriksen, 2008; Henriksen et al., 2009).

The current geology can be broadly split into three: localised Archaean basement, unaffected by later Proterozoic orogenies (now only seen in the southern tip of Greenland; Henriksen, 2008); Archaean terranes reworked during Palaeoproterozoic (across much of south-east and west of the island); and, the terranes composed of juvenile Palaeoproterozoic rocks (north, north-east) (Henriksen, 2008; Henriksen et al., 2009). Owing to the limited development of sedimentary basins, much of the island, comprised of a crystallised craton, will be resistant to any large-scale glacial erosion.

2.1.2 Climate, and the inception of the inland ice

Palaeoclimatic records, in the form of marine and terrestrial indicators, show that the past changes in the GrIS have occurred alongside temperature changes, having consistently lost mass in response to climatic warming, and gained mass in response to cooling (Alley et al., 2010).

The earliest evidence of glaciation on Greenland dates back to between ∼38–30 Ma B.P. (late Eocene–Oligocene), with the observation of ice-rafted debris in sediment records from the Norwegian–Greenland Sea (Eldrett et al., 2007); whilst this record indicates a glacial source (rather than from sea ice), it does not suggest the scale of glaciation present at this interval and could represent either isolated valley glaciers, or more extensive ice-sheet cover (Alley et al., 2010). However, increases of ice-rafted debris documented across sediment records ∼14 Ma (middle Miocene) and again from ∼3.5–2.4 Ma B.P. suggest large-scale, stepwise initiation of extensive glaciation across Greenland (Kleiven et al., 2002) as the Earth cooled following the hot conditions of Cretaceous (Alley et al., 2010). Alongside climatic cooling, Bartoli et al. (2005) propose that the closure of the Central American Seaways at Panama (∼3.0 Ma) intensified moisture supply to the Northern Hemisphere facilitating the build-up of the GrIS.

Ten Brink and Weidick (1974) and Fleming and Lambeck (2004) present descriptions of the fluctuations of the GrIS since the Last Glacial Maximum (LGM). It is clear that the ice sheet has progressively retreated since the LGM (∼175 km) (Ten Brink and Weidick, 1974), where, the position of the GrIS at that time was

some distance beyond modern-day shorelines (extending to the edge of the continental shelf in west and north-west Greenland (Fleming and Lambeck, 2004)). Dated moraine systems of West Greenland show that this retreat has been interrupted by moderate re-advances in extent (Ten Brink and Weidick, 1974), which is echoed in the complex fluctuations of isostatic sea level (Fleming and Lambeck, 2004).

The comparatively short length of Greenland's glaciation, paired with the fluctuation (waxing and waning) in ice-sheet extent and expansive erosion-resistant geology prove pertinent when regarding the origin of landscape systems beneath the GrIS. This is more explicitly discussed in research Chapter 4, with reference to observed subglacial 'palaeo-landscapes' (see also Section 2.3).

2.1.3 The contemporary Greenland Ice Sheet

As a result of recent climatic perturbation, mass loss from the GrIS is accelerating (Velicogna and Wahr, 2006; Rignot et al., 2011). Greenland is currently the largest contributor to global sea level rise (SLR) (from the three major ice sheets; the GrIS, and the West and East Antarctic Ice Sheets) at a rate of 0.8 mm a^{-1}, which is set to continue in the coming decades (Bamber and Aspinall, 2013; Vaughan et al., 2013). Latest estimates for the volume of the contemporary GrIS stand at approximately 2.9 million km^3, giving a total potential sea level rise (SLR) of ∼7.42 m (Morlighem et al., 2017). Projections of future mass loss and SLR contributions, however, remain challenging. Inherent system variability and the dynamic response of the ice sheet to both climatic and local factors are not yet fully realised (Joughin et al., 2004; Bamber et al., 2013b). A notable example of dynamic response to warming, and accounting for around half of estimated mass loss from the GrIS, is the increased rate at which solid ice is discharged across the grounding line at outlet glaciers (van den Broeke et al., 2009).

Influencing rates of basal motion, ice-sheet dynamic response is controlled by various properties of the subglacial environment (see Sections 2.2 and 2.3). To better constrain numerical modelling for future change, focus has centred towards the accurate characterisation of both ice thickness and bed elevation over Greenland using airborne geophysical survey (*e.g.* Bamber et al., 2001, 2013a; Morlighem et al., 2014, 2017). Other basal properties relevant to ice dynamics include, but are not limited to, subglacial roughness, basal thermal

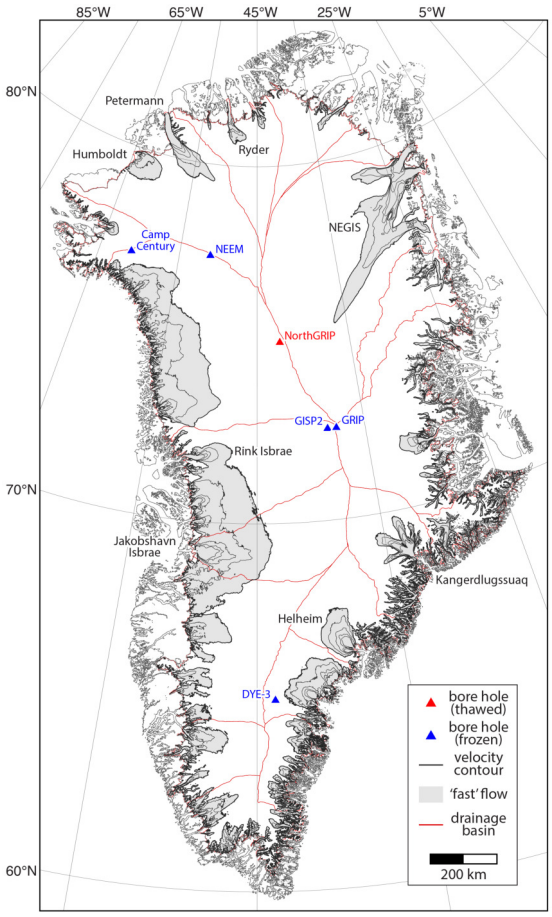

Figure 2.2: The Greenland Ice Sheet, labelled as per various 'glaciological landmarks' to provide a setting for the scope of this thesis. Deep boreholes, and observed basal thermal state, are marked and named. Thick black contour delineates the onset of 'fast' flow ($|v| > 50$ ma^{-1}, shaded grey), subsequent velocity contours are spaced at 100 ma^{-1} intervals (Joughin et al., 2016, 2017). Important outlet glaciers referenced in research Chapters 4–6 are named. Ice-drainage systems of the GrIS, as delineated by (Zwally et al., 2012).

regime, and the presence of basal water and deformable sediments (Clarke, 2004). Whilst the influence of these is well understood theoretically (Sections 2.2 and 2.3), these characteristics remain either poorly constrained, or have not yet been incorporated into predictive ice-sheet modelling.

The recent increase in available geophysical survey coverage (Section 3.1) provides an opportunity for new physical constraints to be placed upon bed, and explored in parallel with both palaeo- and present day ice flow, as per the overlying aim of this original research. The extent of the contemporary GrIS is shown in Figure 2.2; this outlines specific outlet glaciers referenced explicitly within this study, alongside other fast flow units ($|v|$ (speed) > 50 ma^{-1}) and ice-drainage basins.

2.2 Radio-echo sounding

2.2.1 Context

Radio-echo sounding (RES), often also referred to as ice-penetrating radar (IPR; chiefly US), enables the widespread study of ice sheets, ice caps, and mountain/valley glaciers, globally. It is an active geophysical survey technique whereby a radio-wave is emitted through an ice mass. This wave propagates from the source, travels through the ice column before a return signal, or echo, is ultimately recorded by the receiving antenna. The power of returned signals is quantified in decibels (dB), and measured through time. Variations in the returned power are caused as the radio-wave interacts with, or passes through, surfaces of differing dielectric properties (*i.e.* electrical permittivity, and/or conductivity) (Plewes and Hubbard, 2001). The time-delay between ice-surface and ice-bottom 'peaks' in the returned power are fundamentally used to extract measurements of ice thickness (Plewes and Hubbard, 2001; Rodriguez-Morales et al., 2014); however, RES observations can also capture information regarding basal conditions (*e.g.* the presence of basal water) and properties relating to the internal structure (*e.g.* englacial deformation) of the ice mass (Siegert, 1999; Plewes and Hubbard, 2001).

This section provides a brief history and theory behind RES, and its uses within glaciology. As RES data comprise a major analytical component of this thesis, specific data used and considerations are broadly described in Chapter 3, with more specific methods employed for analysis are outlined within each

research chapter (Chapters 4–6).

Since the initial reports of ice being effectively transparent to the radio-waves emitted from radar altimeters during the mid-1940s (Waite and Schmidt, 1962), improvements in the theoretical understanding of how radio-waves propagate through ice, as well as through ground-truthing and *in situ* experiments, have enabled RES to become an important technique for glaciological investigation (Plewes and Hubbard, 2001). However, owing to the heterogeneous nature of ice, both through depth in the ice column, and spatially over an ice mass, there still remain a number of issues that can lead to 'incomplete' or non-interpretable readings. A common reason for this is due to power attenuation (loss with depth) as a result of the thermal properties of ice (see Figure 3.2; Jordan et al., 2016). This is clearly evidenced when looking at the maximum observed values of ice thickness, where depths of ∼4000 m and ∼1500 m for cold and temperate ice, respectively, have been sounded (Evans et al., 1972; Nolan et al., 1995).

2.2.2 Role within glaciology

Ice thickness and bed elevation

As previously noted, the time delay between the bed- and surface-returns (see Figure 3.2) is used to estimate ice thickness. This is bounded physically by the speed at which radio-waves travel/ propagate through the ice column. However, errors within thickness estimates are introduced by the uncertainty in geo-positioning of the aircraft (and radar sounder); the varied dielectric properties of the ice column; and, interpretation errors when defining the bed-echo itself ('peak' power identification) (Rodriguez-Morales et al., 2014). For example, within the CReSIS systems used across the GrIS, and in this study (Chapter 3), the error is found to be in the order of tens of metres (accounting for only a small percentage of estimated thickness) (Rodriguez-Morales et al., 2014).

RES can provide ice thickness for both floating (*i.e.,* ice shelves), and land-based ice. Thickness values help to define ice volume, and water equivalent, estimates (*e.g.* the total potential contribution for the GrIS Morlighem et al., 2017); additionally, these estimates are used to infer bed elevation/ topography (*e.g.,* Bamber et al., 2013a; Morlighem et al., 2017). To do this, thickness is differenced from surface elevation obtained from contemporaneous laser altimetry data (as in Bamber et al., 2013b), or from a surface topography product (*i.e.,*

GIMP DEM (Howat et al., 2014), as in Morlighem et al., 2017).

These observations of ice thickness (and thus bed elevation) are used to produce spatially-complete bed digital elevation models (bed DEMs) through interpolation (Section 3.1.4), providing an important boundary condition for predictive ice-sheet modelling. Additionally, as in this study, bed topography products are variously used to describe landforms, geomorphic processes, and landscape evolution (specifically Chapter 4).

Basal characteristics

RES is also instrumental in elucidating basal characteristics, pertinent to ice motion, and ice dynamics. These properties are related to the 'shape' of the bed-echo, providing information regarding the returned-power and scattering at the bed, rather than travel-time (as with ice thickness) (Plewes and Hubbard, 2001). Basal conditions and characteristics which are obtained through RES include: bed roughness (described in Chapter 5), subglacial debris and sedimentation(*e.g.,* Rippin et al., 2006), basal thermal state and the presence of basal water (wet/thawed–frozen/dry) (*e.g.,* MacGregor et al., 2016; Oswald et al., 2018), or indeed subglacial lakes (Siegert, 1999; Plewes and Hubbard, 2001).

Englacial structure and properties

Finally, RES data are used to examine aspects of the ice column itself, providing information regarding englacial structure and properties. This information is extracted as a result of changing dielectric properties within the ice column, which are, generally, referred to as the 'radio-stratigraphy' within radargrams (presenting as (predominantly) linear, laterally extensive horizons (see Figure 3.2).

Englacial stratigraphy can be used as isochrons, helping to characterise age and accumulation of properties of the ice sheet, when constrained with ice cores (Plewes and Hubbard, 2001). Changes within this layering, or layer 'distribution' has also recently been used to assess fast flow due to deformation, and highlight palaeo-flow configurations (*e.g.,* Karlsson et al., 2012). Units of severe disruption, situated within the lower portion of the ice column, have been identified across Greenland (*e.g.,* Bell et al., 2014) and Antarctica (*e.g.,* Wrona et al., 2017). These features are variously termed 'basal units,' or 'units of disrupted radio-

stratigraphy,' and are suggestive of various basal and englacial processes further described in Chapter 6. Furthermore, internal changes in reflectivity can provide information with respect to changing crystal fabric and rheology (Fujita et al., 2006; Matsuoka et al., 2012), and in turn, may lead to effects upon ice dynamics (as described in Chapter 6).

2.3 Interactions between rock and ice

2.3.1 A 'chicken-and-egg' problem?

The higher-order relationship between bed topography and the flow of ice is seen to be intuitive; where, large-scale topography is seen to exert strong controls upon ice motion, influencing both flow configuration (the direction of flow) and speed (Cuffey and Paterson, 2010; van der Veen, 2013). However, through its movement, ice and ice sheets are an effective erosive force, producing key 'landscapes of erosion,' with the potential to 'scour' vast areas, leading glacial 'erasure' (Sugden, 1974; Sugden and John, 1976); and, by limiting mountain heights through a glacial 'buzzsaw' (Egholm et al., 2009; Hall and Kleman, 2014). Understanding the role of ice sheets, and the effect they impose on landscapes has, until recently, been limited to deglaciated beds (*i.e.* the sites of former large ice sheets, Sugden and John, 1976; Kleman, 1994; Kleman and Hättestrand, 1999; Kleman et al., 2008; Stroeven et al., 2006; Ebert et al., 2015). However, RES can provide understanding of landscape development beneath contemporary ice sheets (*e.g.,* Siegert et al., 2005; Bingham and Siegert, 2009; Jamieson et al., 2010, 2014); where further assessment and observation at outlet glaciers has helped to constrain estimates of (high) rates of erosion through sediment transport across the grounding line (Koppes and Montgomery, 2009; Cowton et al., 2012; Overeem et al., 2017).

Most notably, however, there has been recent 'discovery' of what are thought to be preserved pre-glacial (prior to ice sheet inception) landscapes and landforms beneath Greenland (*e.g.,* Cooper et al., 2016; Livingstone et al., 2017) and Antarctica (*e.g.,* Siegert et al., 2005; Rose et al., 2015). As such, the relationship between bed topography and ice is called into question – is the underlying bed affected more by the overlying ice (through erosive means), or the ice by the bed (through topographic steering)?

This thesis, through its overarching aim and research objectives, poses this question at varying spatial scales for the Greenland Ice Sheet. As discussed within each research chapter, this requires more detailed discussion relating, but not limited, to: underlying geology, length of glaciation, and glacial cycles, contemporary basal thermal sate, ice velocity, and higher-order topographic constraint, is needed in order to disentangle the inter-relationships between rock and ice (Sugden and John, 1976; Summerfield, 1991; Clarke, 2004).

2.3.2 Role in contemporary ice dynamics

As noted, bedrock topography demonstrably exerts strong controls on ice dynamics, determining where ice flows, as well as the response and stability of outlet glaciers and ice streams to external forcing (Siegert et al., 2005; Bingham and Siegert, 2009; Joughin et al., 2009; Cuffey and Paterson, 2010; Jamieson et al., 2010; Durand et al., 2011; Rippin et al., 2014; Carr et al., 2015). Additionally, it is important in the modulation, distribution, and routing of both basal waters and sediment (Baroni et al., 2005; Wright et al., 2008; Rose et al., 2014; Jamieson et al., 2016), in turn affecting ice motion and its dynamic response (Clarke, 2004; Cuffey and Paterson, 2010; van der Veen, 2013).

At a more localised scale, various properties of the subglacial environment, including, but not limited to: basal thermal regime; presence of basal water (and effective pressure); geotechnical bed properties (*i.e.* presence of sediment and, its viscosity/deformability); and, basal friction/traction (*i.e.* resistance from roughness) (Weertman, 1957; Nye, 1970; Clarke, 2004; Iverson and Zoet, 2015; Durand et al., 2011; Brondex et al., 2017; Stearns and van der Veen, 2018), have direct influence on ice motion (notably sliding velocity).

2.3.3 'Palaeo-' landscapes, and landscape inheritance

As alluded to previously, bed topography can provide a long-term record of geomorphic processes, allowing insight into landscape evolution (*e.g.,* Kleman, 1994; Kleman and Hättestrand, 1999; Young et al., 2011; Hall et al., 2013), as well as defining the history of ice-sheet development and former patterns of ice flow (Siegert et al., 2005; Bingham and Siegert, 2009; Rose et al., 2013). Furthermore, knowledge of basal geometry can be used to determine previous hydrological

pathways, which may have been instrumental both prior to ice-sheet inception, or through successive glacial cycles (*e.g.,* Baroni et al., 2005; Wright et al., 2008; Bamber et al., 2013b; Cooper et al., 2016; Livingstone et al., 2017).

Studies have shown relict 'pre-glacial' landforms preserved at the beds of former ice sheets, surviving successive periods of glaciation (*e.g.,* Kleman, 1994; Kleman and Hättestrand, 1999; Hall et al., 2013). Crucially, the effects of ice-sheet erosion will be superimposed onto the pre-glacial topography (Sugden, 1974), presenting a palimpsest of geomorphic origin and landscape evolution. The nature of these landscapes and, as such the "type" of glacial erosion, is often distinct (Sugden, 1974). Regions marked by evidence of "selective linear erosion" are characterized by landscape preservation directly adjacent to areas of intense erosion, due to the interplay of pre-existing basal topography and geometry (Sugden, 1974; Sugden and John, 1976; Drewry, 1986). In the case of ice-sheet inception over pre-glacial fluvial surfaces, selective linear erosion will act to deepen river valleys, while preserving the spatial pattern of the channels, suggestive of more nuanced inter-relationships between basal topography and the overlying ice, often termed 'landscape inheritance' (Hall et al., 2013; Gunnell, 2015).

As is discussed further in Chapter 4, the geological setting and glacial history of Greenland yield conditions amenable to the long-term conservation of subglacial landscapes. This is facilitated by comparatively-hard Precambrian crystalline, gneissic basement rocks and limited sedimentary deposits (Henriksen, 2008; Henriksen et al., 2009); additionally there has only been extensive ice cover for approximately the last 3.5 million years (Ma) (Kleiven et al., 2002; Alley et al., 2010). To date, most analysis of subglacial geomorphology, and basal landscape origin, has been focused on Antarctica (*e.g.,* the"Ellsworth Subglacial Highlands" (Ross et al., 2014), and "pre-glacial erosional (planation) surfaces" of the West Antarctic Ice Sheet (Rose et al., 2015)), with little focus on such associations in Greenland. However, a large subglacial mega-canyon in northern Greenland, thought to be of palaeofluvial origin, has recently been discovered (Bamber et al., 2013b), allowing new insights into Greenland's landscape history and past processes of landscape evolution. These inherited landscapes are seen to influence modern ice flow, and the routing of contemporary subglacial water (Bamber et al., 2013b; Cooper et al., 2016; Livingstone et al., 2017; Jordan et al., 2018).

2.4 Current gaps in understanding

As outlined above, there are many facets of Greenland's subglacial environment that are left understood. Although the theoretical understanding of certain inter-relationships between basal characteristics and ice sheet cover is well founded, a lack of definitive examination *in situ*, and particularly within Greenland, present several gaps in current understanding.

Macro-scale landscape genesis

Previous works regarding the characterisation of 'landscapes of glacial erosion' (after (Sugden, 1974; Sugden and John, 1976) typifies the examination of landscape evolution of both contemporary- and palæo- ice sheets (with the current exception of the landscape beneath the GrIS, as discussed above; Section 3.2). Whilst this is a useful practise in the assessment of broad-scale landscape morphology, its intent is to define all landscape characteristic through solely glacial means (by glacial erosion). An approach following this style of assessment was attempted for Greenland as a pilot study (see Section 3.2).

However, recent work regarding contemporary ice sheets, primarily the Antarctic Ice Sheet (Rose et al., 2014; Ross et al., 2014; Rose et al., 2015), as well as the (palæo-) Fennoscandian Ice Sheet (Kleman, 1994; Kleman and Hättestrand, 1999; Kleman et al., 2008), examines morphologies documenting markers of previous, non-glacial modification. This, therefore, suggests an ability for ancient landscapes formed through other erosive/ depositional means, to be left 'preserved' beneath active ice sheets. However, it should be noted that any landscape will be somewhat 'modified' through subsequent, and contemporary, glacial erosion.

It is in this context that, particularly within Greenland, there is a current lack of understanding in the 'true' control on (or of) the underlying landscape, presenting the following key questions:

i In Greenland, is glacial erosion the dominant modifier in the genesis of the morphology underlying the Greenland Ice Sheet?

ii Are remnants of ancient (pre-glacial), or palæo-landscapes left preserved under the contemporary ice sheet? And if so, to what extent has the ice sheet modified these landscapes since its inception, ad to what extent is landscape evolution dominated through glacial means?

iii To what extent does underlying geometry control the movement of ice, and is the contemporary flow configuration a result of pre-glacial landscapes?

Ice sheet flow and roughness characteristics

The measurement of subglacial roughness has long been established within glaciological literature. The scope of such studies have not only provided detailed assessments of roughness beneath individual valley glaciers, ice caps, and outlet glaciers, but also across both the contemporary ice sheets (GrIS, and the Antarctic Ice Sheets). As discussed above there are various behavioural relationships established and theorised behind aspects of roughness and overlying ice; however, due to the variation in measurement scales, and presence of other subglacial factors, there is still more to be understood.

Within Greenland there have been few subglacial roughness studies, with a singular ice-sheet-wide study to date employing the widespread RES data from OIB missions (see Rippin, 2013). The current major gaps within roughness research present the following key questions:

i Is there a relationship between subglacial roughness and basal sliding in Greenland? If so, to what magnitude does this relationship exist?
ii Over which length-scale(s) of subglacial roughness affect basal sliding, and is there a critical threshold?
iii Does subglacial roughness exhibit direction dependence (anisotropy) with respect to ice flow across Greenland?
iv Does roughness derived from radar-scattering exhibit different characteristics from roughness calculated from along-track topography?
v Is subglacial roughness, in Greenland, controlled by largely glacial erosion, or does it exert control upon the overlying ice sheet?

Observational limitations

Finally, albeit standing as a limitation in observational data, rather than in theoretical understanding, the true nature of the bed geometry for large parts of the ice sheet interior is unknown (see Figure 3.1); consequently, this results in several aspects of the interrelationships between the contemporary ice sheet, the underlying bed to not be fully understood. However, it is beyond the scope of this

thesis to provide additional observational data (through radio-echo sounding) of the bed.

The next section outlines the principal aim of this thesis, pointing towards objectives as to how this is achieved, and how these research gaps are addressed.

2.5 Aim, and research objectives

Overarching thesis aim: To identify and better constrain the inter-relationships between aspects of the subglacial environment and the Greenland Ice Sheet, with specific reference to subglacial processes, ice-sheet motion and the solid earth.

To approach this aim, multiple objectives have been identified; these are outlined below according to the relevant research chapter of this thesis (Chapters 4–6). Assessment and quantification of the subglacial environment rely primarily on the use of radio-echo sounding (RES) data and derived basal topography, alongside complementary ice sheet-wide glaciological parameters (*e.g.* ice velocity, and basal thermal state). Broadly, this is to explore the influence, or 'control,' of the subglacial environment upon overlying ice motion, and vice versa.

Chapter 4 research objectives

4 i to identify the the broad geomorphic origin of Greenland bed topography at the landscape scale;

4 ii to establish the potential for palaeo- landscape 'preservation' beneath the ice, evaluating the long-term influence upon ice-sheet motion, with reference to 'landscape inheritance.'

Chapter 5 research objectives

5 i to improve upon previous quantifications of subglacial roughness beneath the GrIS, by providing both a systematic assessment of anisotropy, with respect to ice-flow direction, as well as fine-scale roughness information for the first time;

5 ii to determine relationships present between subglacial roughness and ice motion, in attempt to evaluate control/causality between the bed and overlying ice;

5 iii to interpret the spatial distribution of, and any observed relationships within quantified subglacial roughness with specific reference to basal processes (*e.g.,* erosion/deposition, and/or presence of deformable sediment).

Chapter 6 research objectives

6 i to determine the expression of basal and englacial processes at the ice's surface, with a view to establish the potential for spatially-complete ice surface topographies to improve understanding where RES data are sparse;

6 ii to characterise the influence of basal geometry and englacial processes upon ice motion.

Chapter 3

Data, materials and methodological overview

The purpose of this chapter is to outline the data used for the analysis presented in results Chapters 4–6, alongside a brief overview of the methodologies undertaken. This is done with reference to the overarching aims and objectives given above (Section 2.5) in order to further elucidate the inter-relationships between the GrIS and its subglacial environment. This chapter is split across two broad sections. Firstly, it builds upon the context given in Chapter 2, regarding the use of radio-echo sounding data in glaciology more generally. The specific RES data used over Greenland, its spatial coverage, and 'levels' of pre-processing are introduced. This also covers specific examples of RES application within this study, outlining the approaches undertaken to assess specific basal and englacial conditions, in conjunction with basal topography, an RES-derived product. Secondly, this chapter introduces complementary ice sheet-wide datasets that provide key glaciological parameters relating to ice motion and dynamics. The methods of acquisition, production and/or derivation of each dataset is described, and where relevant, this chapter discusses any assumptions made in the use of the data, as well as limitations and uncertainty affecting the context of this study.

Whilst this chapter acts to provide a broad explanation of each dataset used, due to the differences in scope between the research undertaken in Chapters 4–6, readers are referred to the relevant methods sections for the specific subsets of data and exact techniques used for analysis.

3.1 RES, and derived products

As described above (Section 2.2), RES is a technique through which the analysis of the propagation and reflectance of a radio-wave through an ice mass can be used to derive thickness, internal structure characteristics, and properties of the ice–bed interface. In this thesis, RES, and derived bed topography, provides the basis through which properties of the subglacial environment are studied.

3.1.1 Greenland coverage and availability

The 'raw' RES data (*i.e.* outside of derived bed topographies, Section 3.1.4) used here are obtained through airborne geophysical survey campaigns undertaken, and made available, by the Center for the Remote Sensing of Ice Sheets (CReSIS) and NASA's Operation IceBridge (OIB) programme. For analysis in this thesis, both Level 1B (L1B) and Level 2 RES products are used. Geospatial information (*i.e.* latitude, longitude, and instrument (aeroplane) elevation) is included across both processing levels; however, L1B contains power information from the returned radio-signal, and L2 data contain quantified measures of ice thickness and bed elevation.

Figure 3.1 depicts the spatial coverage of airborne radio-echo sounding data used in this study. These data were collected by CReSIS between March and May over the years 1993–2016, using a succession of radar instruments. These included the: Improved Coherent Radar Depth Sounder (ICORDS); ICORDS version 2; Advanced Coherent Radar Depth Sounder (ACORDS); Multi-Channel Radar Depth Sounder (MCRDS), Multi-Channel Coherent Radar Depth Sounder (MCoRDS), and MCoRDs version 2 (v2) (Paden, 2017). Centre-frequencies for these instruments are 149 MHz (for ICORDS and ICORDS v2), 150 MHz (for ACORDS and MCRDS) and 195 MHz (for MCoRDs and MCoRDS v2). Three airborne platforms have been used for collection, where the aforementioned instruments have been variously mounted upon the P-3B Orion (P3), DHC-6 Twin Otter (TO), and Douglas DC-8 (DC8) aircraft (Paden, 2017). Functional developments made to these instruments through time, as well as advances in the processing of returned signals, have improved ice sheet, and ice–bed observation. Penetration depth has increased, allowing bed-echoes to be received across larger parts of the ice sheet, and notable increases in depth-range (vertical) and along-

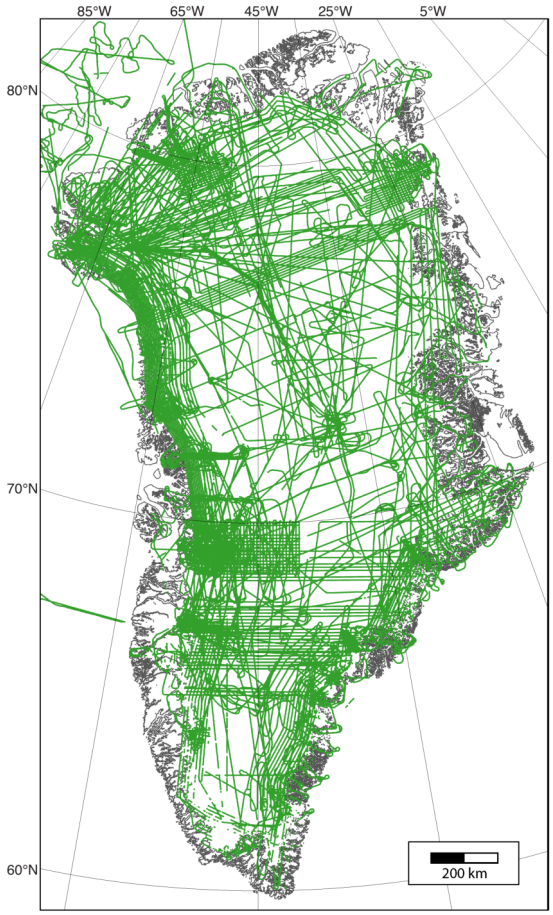

Figure 3.1: Coverage of CReSIS airborne radio-echo sounding used in this study. Data shown span campaigns flown between March and May in the years 1993–2016.

track (horizontal) resolutions have led to an improved accuracy in recorded ice thickness, as well as improved sampling density, respectively (Rodriguez-Morales et al., 2014; Gogineni et al., 2014; Paden, 2017).

In Chapter 5, RES data are used across both product levels (L1B and L2) in order to quantify two metrics of subglacial roughness (see Section 3.1.3). Specific information relating to the subsets of RES data used for in-depth analysis within this thesis, including sampling resolution, data quality flags, and caveats for data combination, is noted within Chapter 5. For the remaining results chapters (Chapters 4 and 6), where more visual inspection of RES data is undertaken using radargrams (described below), the nuances of radar instrumentation (*e.g.* centre-frequencies and/or sampling resolution) are not so relevant.

3.1.2 Echo- and radar-grams

When considering the properties of the radar signal (provided within L1B data), RES data are commonly presented in either echo- or radar-grams. These visualise the change in returned power (dB) over depth. Figure 3.2 displays an example of these formats, from which analysis of the ice column, and subglacial characteristics, can be made.

Echograms, sometimes termed A-scopes, (right, Figure 3.2) display returned power over depth for a single radio-wave, or pulse, providing a spatial 'snapshot' through the ice column. Radargrams, sometimes termed Z-scopes, comprise echograms that are stacked side-by-side to prove a longitudinal cross-section, or 'image,' of the ice mass as sampled along-track (left, Figure 3.2). The 'brightness' of this image is representative of the power of the return, where darker bands signify a higher returned power, or a 'stronger' reflection. Sometimes referred to as Z-scopes in the literature (Plewes and Hubbard, 2001), these images are, for the purposes of this thesis, termed 'radargrams.'

Both echo- and radar-grams, such as those displayed in Figure 3.2, facilitate the visualisation of the reflective surfaces within the ice column, as well as clearly demarcating its 'top' (the ice surface) and 'bottom' (the bed). The ice surface is marked by a distinct and abrupt peak in power (Figure 3.2). At the ice bottom, after which the radio-wave can no longer propagate, a final, large peak is returned above the noise floor, termed the bed-echo (red; Figure 3.2). Numerous internal (englacial) reflectors, identified by large variation in returned power, are

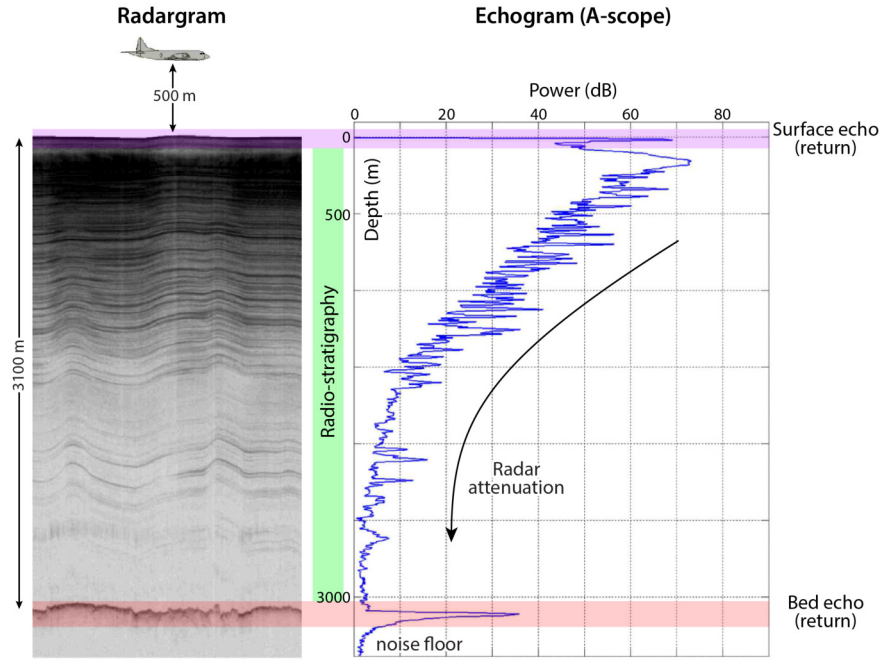

Figure 3.2: Annotated illustration of echo- and radar-grams from airborne radio-echo sounding. Individual echogram (or A-scope) is displayed, **right**, documenting variations in returned signal power (dB) over depth (m). Stacked echograms (side-by-side) produce the greyscale radargram (or Z-scope), **left**. The surface return (or echo) from the top of the ice column is highlighted in purple. The bed return (or echo) from the ice bottom is highlighted in red. Marked variation in returned power over the majority of the ice column depicts englacial radio-stratigraphy, highlighted in green. Attenuation of the radio-wave is visible by the gradual decrease in radar power, labelled and highlighted by the arrow. (adapted from C. Allen, CReSIS, 2008)

also often sampled within the ice column. This 'layering,' or radio-stratigraphy, presents as dark lateral horizons within the radargram (green; Figure 3.2). Radio-stratigraphy is not commonly visible throughout the entire depth of the ice column, however, largely as a result of the attenuation of the radar signal with depth (arrow; Figure 3.2; Section 2.2; Plewes and Hubbard 2001).

3.1.3 Elucidating the ice–bed interface

This study relies on L1B RES data to extract information regarding aspects of subglacial topography, the ice–bed interface, and structures within the ice column. Whilst some of this analysis is undertaken purely visually from radargrams, more complex analyses of echogram characteristics (*i.e.* the behaviour of the waveform) are also employed. In the first instance, radargram profiles are used to extract the width and relative depth of observed subglacial channels and basal features; these metrics are used as part of a wider analytical tool to determine the geomorphic origin and landscape evolution of west Greenland (Chapter 4). Additionally, such profiles are also used to visualise englacial features in north-west Greenland, facilitating both the interpretation of these and related sub- and en-glacial processes (Chapter 6).

More quantitatively, however, the behaviour of individual bed-echo data are analysed to determine properties of subglacial roughness over the ice sheet in Chapter 5. This involves characterising how diffuse (or specular) the reflection at bed is. This is used in order to make assumptions regarding fine-scale characteristics at the ice–bed interface. Quantified values for bed elevation, provided by L2 RES data, is also used in this chapter (5) to measure more large-scale changes at the ice–bed interface; principally, variation in the sampled bed elevation provides an additional metric for bed roughness. Additionally, although used singularly, this thesis employs echogram properties with a view to identify anisotropic-reflectance behaviour within ice column (see Chapter 6). This involves measuring the difference in returned power between two radar pulses, recorded at an orthogonal crossover.

3.1.4 Bed topographies

More broadly, this study relies on the use of Greenland bed topography for the assessment of subglacial features, wider landscape systems, and basal processes (in Chapters 4 and 6), as well as to make inferences regarding underlying bed geology (Chapter 5). The latest product, in a succession of bed topographies, is 'BedMachine, version 3' (Morlighem et al., 2017). This product provides a spatially-complete bed elevation product, at a 150 m posting-resolution. Bed elevation is provided subglacially, as well as surface elevation (in ice-free margins) and bathymetry data (sea bed elevation) extending to, and over the continental shelf. Figure 3.3 depicts BedMachine, v3 (Morlighem et al., 2017), clipped to the modern-day coastline for the purposes of the research presented in this thesis. The clipping mask used was the provided ice–land mask (Zwally et al., 2012; Morlighem et al., 2017).

Whilst this bed product is derived using various geophysical sources, only RES can provide an accurate bed elevation over the ice sheet. As stated in Section 2.2, subglacial bed elevation is inferred from ice thickness, derived from the time-delay between the surface- and bed-echoes. Figure 3.4 (a) depicts the full geophysical survey coverage used for the production of BedMachine, v3 (Morlighem et al., 2017), where RES surveys are denoted by the coloured lines. Readers will note that over the ice sheet there is a coverage discrepancy between RES surveys used in this thesis (depicted in Figure 3.1) and those used for the production of BedMachine, v3. This thesis limits analysis to the publicly-available CReSIS data only. This is due to the advantages of improved consistency within documentation, signal processing techniques, and instrumentation, which enables analysis *en masse* to be undertaken more easily, and facilitates data combination when quantifying bed-echo characteristics in Chapter 5.

As spatially-complete coverage of the entire ice sheet using airborne RES data is not feasible, a 'prediction' must be made for bed elevation between observations. This is done statistically via methods of spatial interpolation. Across the GrIS several methods of interpolation are used, whereby the technique employed is limited primarily by the nature of surface ice velocity. The spatial extent of the interpolation techniques used are shown in Figure 3.4 (b). Within fast-flowing outlet glacier regions, where the uncertainty of velocity magnitude is low, a 'mass conservation' technique is applied to predict basal topography with improved

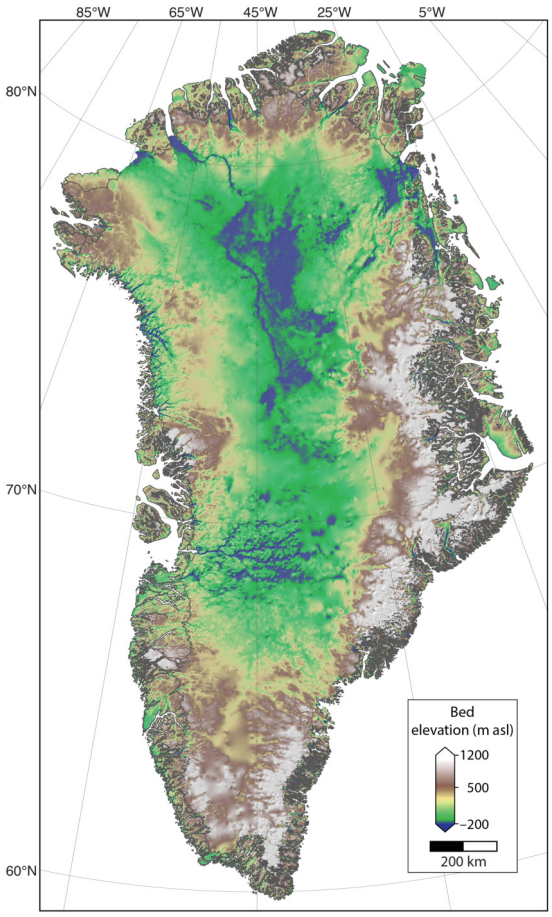

Figure 3.3: Greenland bed topography supplied from BedMachine, v3 (Morlighem et al., 2017). Topography is clipped to modern-day coast line, using land–ice mask provided at data source. Bed elevation is given in metres with reference to mean sea level (metres above sea level).

accuracy (Morlighem et al., 2011, 2017). This method calculates the flux of ice through a region, constrained by both the observed speed and thickness of surrounding ice (Morlighem et al., 2011). Dense, gridded sampling regimes over many outlet glaciers (*e.g.* near Petermann Glacier; Figure 3.4 (a)) can further improve the use of this technique allowing it to be employed over a greater spatial extent (Morlighem et al., 2011). In the ice sheet interior, however, where RES data are more sparse and the speed of ice is slow and less accurately constrained (Joughin et al., 2016, 2017), more simple methods of spatial interpolation are used (*i.e.* ordinary kriging). Other sources for bedrock topography, such as surface altimetry in ice-free regions, are also shown in Figure 3.4 (b), and outlined in Morlighem et al. (2017). As these sources are not used to determine subglacial topography used in the scope of this research, these are not discussed in detail here.

Initial Greenland bed topography products (*e.g.* Bamber et al. 2001, 2013a; Morlighem et al. 2014) were provided at a spatial posting-resolution of 1 km. The notable increase in spatial resolution (to 150 m) has in part been driven by an increase in geophysical survey coverage and the advanced implementation of aforementioned sophisticated interpolation techniques (*i.e.* mass conservation). However, it is important to note that the true accuracy of predicted bed elevation is limited by observation density. This is largely controlled by track spacing and differences within sampling regimes used over fast-flowing outlet glacier regions, and the ice sheet interior. For example, in the interior of the ice sheet, where track spacing can reach up to 75 km, the 'improvement' in spatial resolution is somewhat of a misnomer. The spatial distribution of errors within the predicted bed topography product is detailed in Morlighem et al. (2017) (Figure S3). Chapter 6 (Figure 6.1), concerned with the expression of basal features at the ice's surface, highlights the artefacts and omissions in the interpolated bed topography as a result of interpolation error in data-sparse regions.

In addition to the 'contemporary' bed topography, this thesis also makes use of an isostatically adjusted (ice-free) bed topography in Chapter 4 (Bamber et al., 2013b). This product, based on an earlier iteration of the bed (Bamber et al., 2013a), accounts for the flexural rebound, after removing the 'weight' of the modern ice sheet, and yields a bed configuration closely representing pre-glacial elevation. This surface is used to make inferences about a subglacial landscape system, and its geomorphic origin, as well as in the pilot study discussed above

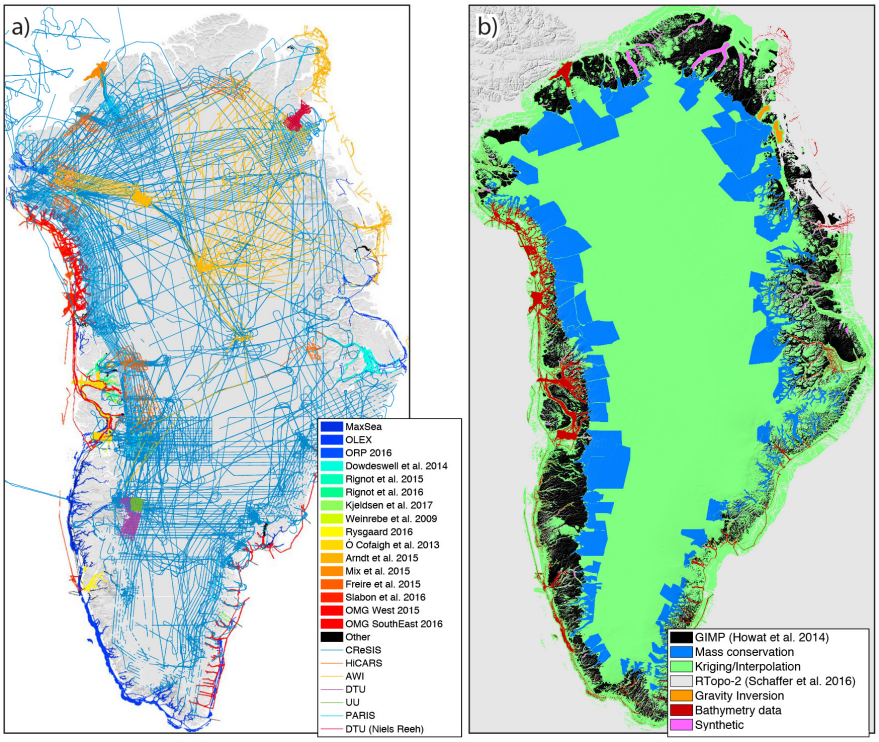

Figure 3.4: Geophysical survey coverage, and interpolation methods, used to derive BedMachine, v3. (a) Geophysical data coverage including CReSIS (as used directly this study; Figure 3.1) and other radio-echo sounding surveys and ocean bathymetry. (b) Bed topography sources, including methods of spatial interpolation used subglacially, and for ice-free regions are shown. For more detail of these, readers are referred to Morlighem et al. (2017).

(Section 3.2).

3.2 Pilot study: Landscape classification of Greenland

As discussed so far within chapter 2, various efforts have previously been made with a view to interpret subglacial geomorphology with respect to glacial erosion (*e.g.* Rose et al. 2013, 2015; Jamieson et al. 2014). These methods rely on the analysis of extracted surface metrics such as relief (elevation range), peak density, slope, curvature, and hypsometry (distribution of elevation over area), as well as hydrological drainage form, or flow routing.

The initial research undertaken as part of this thesis echoed this, and with specific reference to work presented by Jamieson et al. (2014), made an attempt to broadly characterise, or 'classify,' the underlying bed morphology as 'landscapes of erosion.' Jamieson et al. (2014), presents a method based on a number of metrics (as an extension to earlier research completed by Sugden and John (1976)) to describe the glacial geomorphology associated with the Antarctic Ice Sheet. This method classifies the bedrock topography into three types, or 'landscapes,' as a result of their morphology, each suggesting a distinct glacial geomorphic origin; these landscapes, defined by Sugden and John (1976), are said to be characterised by 'areal scour,' 'selective linear' erosion, and 'mainly alpine' morphology. These classes reflect the influence of glacial erosion occurring with different intensities and time periods, from most to least. Landscapes of 'areal scour' are expected within the interior of the ice sheet, characterised by a low mean elevation, small relief, and without any independent peaks. Contrastingly, 'selective linear' landscapes have high relief and a bimodal hypsometry to reflect the dominance of incised valleys dissecting upland plateaux. The 'mainly alpine' classification presents high regional relief, many independent peaks, and a near-normal hypsometric distribution (Sugden and John, 1976; Jamieson et al., 2014).

Following the method outlined by Jamieson et al. (2014), using an isotatically-compensated bed topography (further described in Chapter 3), landscape classification maps were produced for Greenland over two output sizes (Figure 3.5). The results of this classification are broadly in line with what is expected in

conjunction with the geological history and development of Greenland, and the configuration of the GrIS; the Caledonian mountain range along the east coast is highlighted by 'mainly alpine' landscapes, landscapes of 'selective linear' erosion surround the ice sheet margins reflecting the incised valleys of the many outlet glaciers, and 'areal scour' landscapes are seen in the interior reflecting the relatively flat and smooth morphology underneath much of the GrIS. The variable resolution of this classifier allows different-scale morphologies to be realised; for example, at the 50 km output resolution (Figure 3.5 (b)) more landscapes of selective linear erosion are identified at the margins, and are observed cut inland towards the island's interior. A particular example of this is the dendritic channelised system of the Jakobshavn Isbræ catchment (JI, Figure 3.5; Cooper et al. 2016). Interestingly, however, the palaeofluvial mega-canyon of northern Greenland (Bamber et al., 2013b) remains unidentified.

It was concluded that due to scale-sensitivities inherent within both the underlying metrics, and decision tree used to classify different landscapes of erosion, this assessment of the bed was not taken further. Whilst it may prove useful to provide a superficial understanding of how landscapes are broadly shaped, or perhaps 'controlled,' by the overlying ice sheet, this method does little to assess any influence of palaeo-genesis, from erosive forces prior to the inception of the ice sheet. Furthermore, the results shown (Figure 3.5) the information gained provides little more than what visual analysis of the bed topography could determined.

However, this premise of this pilot study lead onto the work presented in the first results chapter (Chapter 4), where a more in-depth analysis of topographic and morphometric analysis of the underlying bed was undertaken to better describe the influence of the GrIS on the underlying bed, and vice-versa.

3.3 Complementary datasets

The assessment, and interpretation, of the inter-relationships between the GrIS and the bed, as per this studies aims, also necessitates the integration of parameters relating to ice motion and dynamics. For this, this thesis draws on various datasets to complement the use of the described RES data and derived subglacial topography. So far, this chapter has focused on how basal proper-

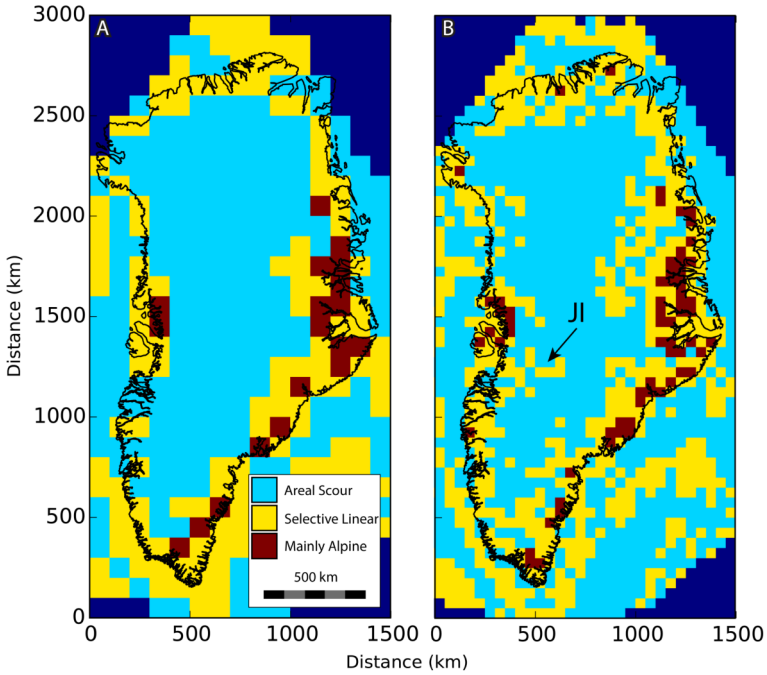

Figure 3.5: Classified 'Landscapes of Glacial Erosion' (defined by Sugden and John 1976 and Jamieson et al. 2014), at a 100 km (**a**) and 50 km resolution (**b**), respectively. These show regions characterised by 'mainly alpine' landscapes (red), 'selective linear' erosion (yellow), and 'areal scour' (blue). Label JI denotes the location of the channelised system in the vicinity of Jakobshavn Isbræ, and its 'classification' as a landscape of selective linear erosion.

ties (*i.e.* bed elevation) and characteristics of the subglacial environment (*i.e.* subglacial roughness) are retrieved. Whilst it is clear that RES can be used to illuminate parameters relating to ice dynamics, and ice-sheet motion directly (see Section 2.2), the scope of this thesis does not warrant such analysis. To better understand the basal characteristics and processes observed, this thesis opts to use independent, spatially-complete observations with less inherent uncertainty. This includes ice velocity (Jordan et al., 2016) and ice surface topography product (Morin et al., 2016), alongside a new synthesis of the basal thermal state.

3.3.1 Contemporary ice surface velocity

The ice velocity product used for analysis in this thesis is the MEaSUREs multi-year Greenland Ice Sheet velocity mosaic (Joughin et al., 2016, 2017). This product presents a near-spatially complete map for flow velocity, provided at a 250 m spatial resolution (Figure 3.6). Observations from both from synthetic aperture radar (SAR) and optical imagery (from Landsat 8) were used to compile an averaged ice velocity over a 20-year period (between 1995–2015). Interferometric analysis of SAR data, as well as speckle- and optical feature-tracking are used within the ice sheet interior and at the margins, respectively. The accuracy of the final product is high, with an uncertainty of $\sim$1–3 ma^{-1} in slow-flowing regions.

Whilst yearly- or seasonal velocity maps are also available, the spatial coverage of these does not fit the requirements of this study. As this thesis principally is interested in the influence of ice motion upon the underlying bed, and vice versa, high temporal resolution, or rather seasonal change in flow speed is not required. The multi-year mosaic, presenting an average of both velocity magnitude and direction, allows references to be drawn not only to the speed of ice, but also to the long-term flow configuration. In this thesis, observations of velocity are important for several reasons. In Chapter 4 comparison is made between contemporary ice flow configuration and observed subglacial topography. This highlights the influence of large-scale topographic control on the movement of ice, leading to an established role of 'landscape inheritance' within the region. In Chapter 5, basal characteristics derived from RES data are directly compared to both ice flow speed and direction in order to assess roughness anisotropy with respect to ice motion. And finally, in Chapter 6, ice flow direction is compared to observed surface manifestations of basal–englacial processes as part of the interpretation

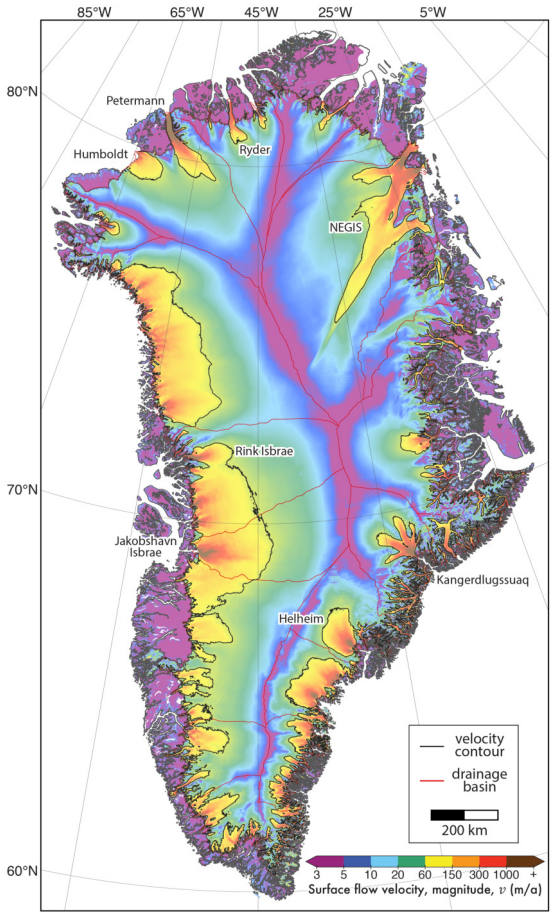

Figure 3.6: MEaSUREs multi-year Greenland Ice Sheet velocity mosaic (Joughin et al., 2016). Ice surface velocity magnitude ($|v|$) in units of ma^{-1}. Black contour delineates the onset of 'fast' flow ($|v| > 50$ ma^{-1}) as used for further analysis. Ice-drainage systems of the GrIS, as delineated by Zwally et al. (2012) (red).

of the genesis of coincident features (basal units).

3.3.2 Ice surface topographies

The final major dataset used within this thesis is a subset of the newly-released 'ArcticDEM.' This is a pan-Arctic collection of earth surface DEMs produced from high-resolution (∼0.5 m) optical satellite imagery. Supplied to the public by the Polar Geospatial Center (PGC) (Morin et al., 2016), an automated process is used to co-register overlapping stereo-pair imagery. The source images, collected by DigitalGlobe, Inc., are not publicly available. The ArcticDEM is available in two formats, offering surface topographies at a 2- or 5-metre spatial resolution, respectively. The latter product is used within this thesis, owing to the improved data quality, due to further pre-processing at source.

As the core analytical 'tool' within Chapter 6, surface topography over specific subsets of the GrIS is used to determine the influence of both basal and englacial features observable from the ice's surface. This research demonstrates the potential for high-resolution surface topography to elucidate these, alongside basal–englacial processes, with previously unobtainable clarity.

3.3.3 Basal thermal state

Alongside the consideration for characteristics of the ice column, and ice sheet itself (*i.e.* ice thickness, surface elevation, and velocity), this thesis makes use of a recent synthesis and prediction regarding the ice–bed interface.

The basal thermal state of the GrIS—whether it is frozen or thawed at the bed—presents an important constraint upon dynamics, influencing the nature of the ice-sheet's evolution and response to external forcing (MacGregor et al., 2016). Principally, a thawed basal state (hereafter termed 'thawed bed') is a necessary condition for basal sliding, and the deformation of subglacial sediment or till (MacGregor et al., 2016). Therefore, through knowledge of the spatial distribution of frozen and thawed beds, or indeed, delineation of this transition, alongside observations of ice velocity, can provide a good proxy for enhanced basal motion. Basal thermal state is observed *in situ* using ice cores, or deep bore holes. Marked on Figures 2.2 and 3.7 are locations of such boreholes across the GrIS, and the recorded basal thermal state. Since such observations are sparse, the

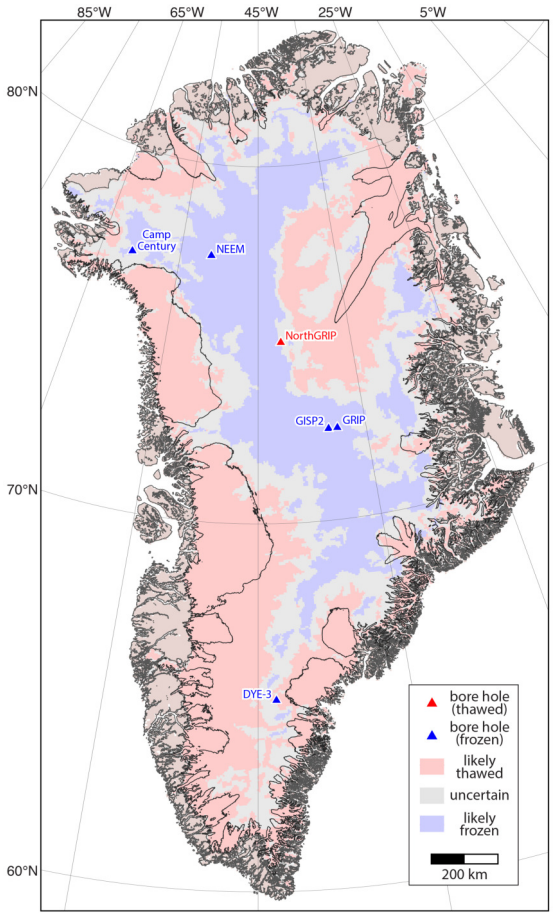

Figure 3.7: Predicted likely basal thermal state of the GrIS (after MacGregor et al. 2016). Locations, and known basal thermal state of deep boreholes are marked and named. Black contour delineates the onset of 'fast' flow ($|v| > 50$ ma^{-1}) as per Figure 3.6.

inference of basal thermal state though the use of RES or thermo-mechanical models has become a research priority (MacGregor et al., 2016).

A recent prediction of the likely basal thermal state of the GrIS has been released (MacGregor et al., 2016), and is used within this thesis. This is produced through the synthesis of existing outputs from thermo-mechincal models, as well as information from radio-stratigraphy, ice velocity, and surface imagery. Figure 3.7 presents these predictions, noting regions that are 'likely' thawed or frozen at the bed. In this thesis, this product is used principally with regard to defining a proxy for enhanced basal motion as noted above, and as such, enhanced rates of erosion with reference to subglacial roughness anisotropy (see Chapter 5).

Chapter 4

Palaeofluvial landscape inheritance for Jakobshavn Isbræ catchment, Greenland.

4.1 Preface

For the most part, this chapter has been published in *Geophysical Research Letters*, under the full citation:
Cooper, M. A., Michaelides, K., Siegert, M. J., and J. L. Bamber (2016), Paleofluvial landscape inheritance for Jakobshavn Isbræ catchment, Greenland. *Geophys. Res. Lett., 43,* 6350–6357, doi:10.1002/2016GL069458.

Analysis, interpretation, and writing were conducted by M. A. Cooper, with the remaining authors providing guidance, insight, and review. Further insight was provided by David Sugden and an anonymous reviewer during the review process. There have been fairly minor changes made to this work presented here. The published 'supplementary information' for this paper, regarding an extended methodology, has been added in-line where appropriate. An additional section, which remains unpublished, regarding the 'nature of erosion (Section 4.5.1), has been added.

4.2 Abstract

Subglacial topography exerts strong controls on glacier dynamics, influencing the orientation and velocity of ice flow, as well as modulating the distribution of basal waters and sediment. Bed geometry can also provide a long-term record of geomorphic processes, allowing insight into landscape evolution, the origin of which may pre-date ice-sheet inception. Here, we present evidence from ice-penetrating radar data for a large dendritic drainage network, radiating inland from Jakobshavn Isbræ, Greenland's largest outlet glacier. The size of the drainage basin is ∼450,000 km^2 and accounts for about 20% of the total land area of Greenland. Topographic and basin morphometric analyses of an isostatically uplifted (ice-free) bedrock topography suggest that this catchment pre-dates ice sheet initiation and has likely been instrumental in controlling the location and form of Jakobshavn Glacier, and ice flow from the deep interior to the margin, now and over several glacial cycles.

4.3 Introduction

Recent efforts to characterise ice thickness and subglacial bed elevations of large ice masses have involved detailed, and repeated, geophysical surveys using ice-penetrating radar (IPR) over Antarctica and Greenland (often referred to also as radio-echo sounding (RES)) (*e.g.*, Bamber et al., 2001, 2013a; Fretwell et al., 2013). Such data provide a rich source of information that can be used to explore landscape origin and evolution (*e.g.*, Young et al., 2011), as well as hydrological processes (*e.g.*, Wright et al., 2008). Quantifying attributes of subglacial morphology and landscape origin can provide insights into past and present erosional regimes, ice-sheet development and former patterns of ice flow (Siegert et al., 2005; Bingham and Siegert, 2009; Rose et al., 2013), the distribution of basal water, and ancient subglacial hydrological pathways (Baroni et al., 2005; Rose et al., 2014; Jamieson et al., 2016).

Morphological studies have shown relict 'preglacial' landforms preserved at the beds of former ice sheets, surviving successive periods of glaciation (*e.g.* Kleman, 1994; Kleman and Hättestrand, 1999; Hall et al., 2013). These have raised discussions on the efficiency of glacial erosion and 'erasure,' as well as on the glacial and geological conditions that facilitate landscape preservation beneath

ice sheets (Sugden and John, 1976; Kleman, 1994; Koppes and Montgomery, 2009). Crucially, the effects of ice-sheet erosion will be superimposed onto the preglacial topography (Sugden, 1974), presenting a palimpsest of geomorphic origin and landscape evolution. The nature of these landscapes and, as such the 'type' of glacial erosion, is often distinct (*e.g.*, Sugden, 1974). Regions marked by evidence of 'selective linear erosion' are characterized by landscape preservation directly adjacent to areas of intense erosion, due to the interplay of pre-existing basal topography and geometry, rock type, and basal thermal regime (Sugden, 1974; Sugden and John, 1976; Drewry, 1986). In the case of ice-sheet inception over preglacial fluvial surfaces, selective linear erosion will act to deepen river valleys, while preserving the spatial pattern of the channels.

The geological setting and glacial history of Greenland yield conditions amenable to the long-term conservation of subglacial landscapes. The island is dominated by Precambrian crystalline, gneissic shield rocks with limited sedimentary deposits (Henriksen, 2008; Henriksen et al., 2009), and has only been extensively ice covered for about the last 3.5 million years (Ma) (Kleiven et al., 2002; Alley et al., 2010). To date, most analysis of subglacial geomorphology, and basal landscape origin, has been focused on Antarctica (*e.g.,* the "Ellsworth Subglacial Highlands" (Ross et al., 2014) and "preglacial erosional (planation) surfaces" of the West Antarctic Ice Sheet (Rose et al., 2015)), with little focus on such associations in Greenland. However, a large subglacial "megacanyon" in northern Greenland, thought to be of palaeofluvial origin, has recently been discovered (Bamber et al., 2013b), allowing new insights into Greenland's landscape history and past processes of landscape evolution. Despite several decades of airborne geophysical surveys, providing accurate and detailed bed topography for Greenland (Bamber et al., 2013a), studies of the long-term subglacial landscape evolution, and the effects of topography on both subsequent glaciation and contemporary ice dynamics, have been limited.

In this paper, we use RES and derived data to measure and analyze the subglacial morphology of southern Greenland and, from this, present evidence for an extensive drainage basin of palaeofluvial origin, directly beneath a major glacial outflow unit. Further, we consider the impact this topography has on past and contemporary ice dynamics (namely, flow velocity and orientation), revealing the importance of landscape inheritance on ice-sheet evolution.

4.4 Calculating land surface water flow paths

Topographic analyses and hydrologic basin calculations were conducted on an isostatically compensated digital elevation model (DEM) of Greenland, presented by Bamber et al. (2013b), referred to hereafter as the "iDEM." The initial bed elevation for this iDEM was derived from a combination of extensive RES ice thickness surveys and satellite-derived surface altimetry and was compiled at a 1 km posting resolution (Bamber et al., 2013a). The iDEM accounts for a flexural rebound of the bed, following the removal of the modern ice sheet load, and yields a configuration of bed topography that closely represents preglacial elevation. It is important to note that the preglacial morphology of Greenland cannot be recreated, and the iDEM studied here assumes a landscape not significantly altered by the ice sheet since its inception. This assumption is supported by the fact that glacial erosion is largely selective, and the flow of ice is constrained by preexisting topography (Sugden and John, 1976; Summerfield, 1991). The iDEM facilitates the identification of large-scale landform features, and their analysis, to determine predominant erosional processes and landscape origin.

The iDEM of southern Greenland displays a dendritic network of valleys, radiating inland from Jakobshavn Isbræ, Greenland's largest outlet glacier (Echelmeyer and Clarke, 1991) (Figure 4.1). Due to the nature of the RES coverage across the island (Bamber et al., 2013a) the ability to resolve topography in this region degrades at about 300 km inland from the coast, coinciding with more sparse flight line coverage (see Figure 4.1). Errors in bed elevation are primarily a function of distance from flight lines (see Bamber et al., 2013a). RES observations remain relatively "dense" throughout the majority of the basin, particularly in the south and immediately surrounding Jakobshavn Isbræ, with the eastern and north-eastern limits being more sparsely sampled. Here dense regions are defined as areas with greater than 1000 ice thickness measurements within a 50 km radius. Full details of the accuracy and uncertainties of this dataset are given in Bamber et al. (2013a).

In order to ascertain the geomorphic origin of this region and to determine the potential influence of preglacial surface waters on the landscape and thus the flow of ice, topographic and morphometric analyses were undertaken. Initially, hydrographic basins and flow routing networks were calculated for the region using two separate software packages (SAGA-GIS; (Conrad and Olaya,

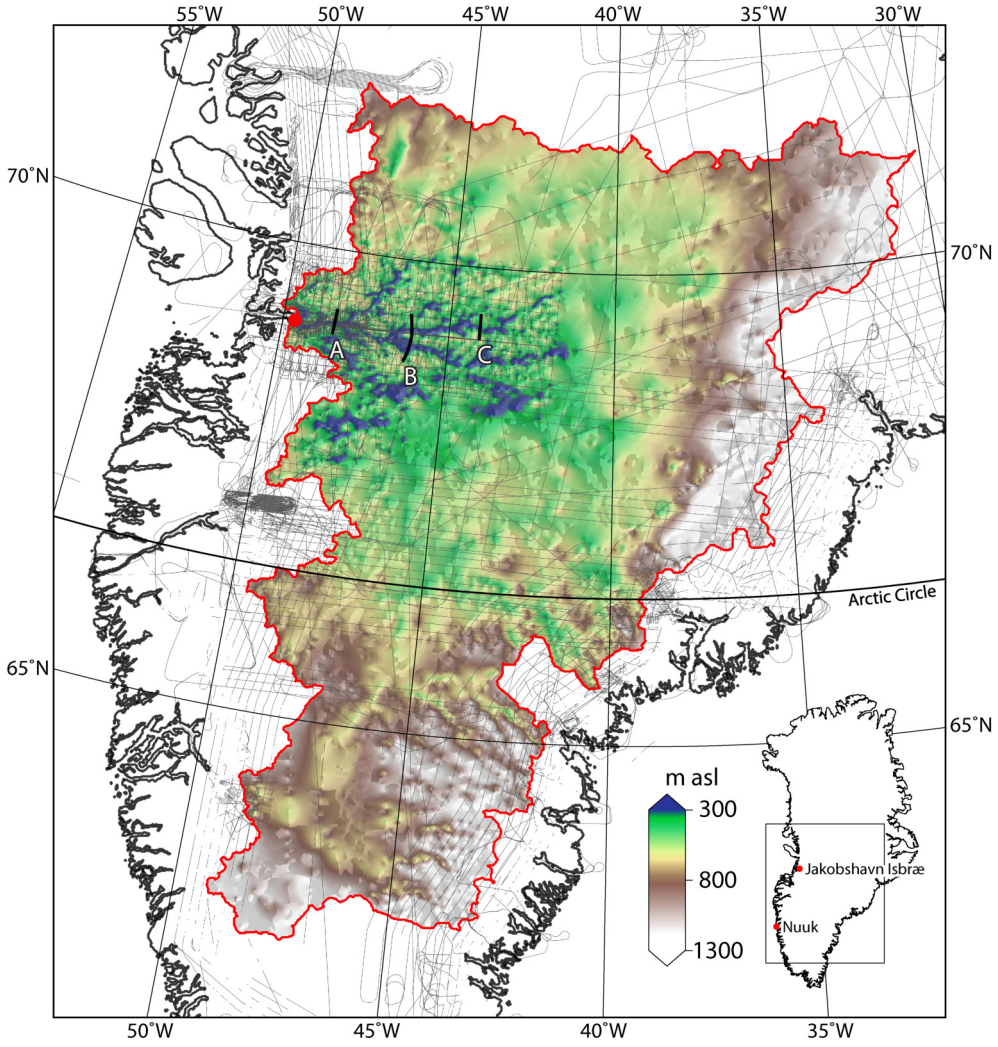

Figure 4.1: Bed elevation (between 300 and 1300 m above sea level (asl)) for southern Greenland, and the wider Jakobshavn Isbræ area. The area plotted is indicated by the black box in the inset. The calculated water divide of the Jakobshavn Isbræ hydrographic basin is delineated in red. Airborne ice-penetrating radar flight lines (collected between 2006 and 2014) are shown in grey, and three bed profiles (A–C) plotted in Figure 4.4 are shown by the respective solid lines.

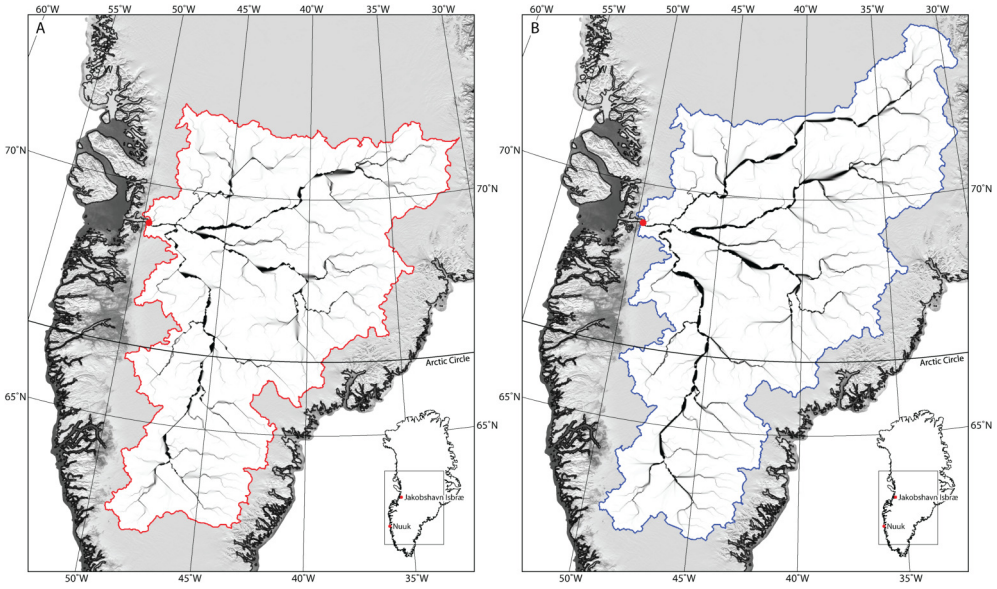

Figure 4.2: Hydrographic basins and flow routing networks calculated for the Jakobshavn Isbræ region from the iDEM using two separate software packages. A and B depict flow accumulation from the Land Surface Dynamics Topography Tool Box (LSDTopoToolBox) [red bound] and SAGA-GIS [blue bound], respectively.

2004; Böhner and Conrad, 2007) and Land Surface Dynamics Topography Tool Box (LSDTopoToolBox); (Mudd et al., 2013)) in order to test the robustness of the resultant basin. "Sinks" within the iDEM were filled prior to calculation, a general step used in hydrological analysis to remove any topographic lows in the DEM which prevent discontinuities in calculated flow paths, and the subsequent network. The drainage network was extracted from the interior to the present-day coastline based on a steepest-descent algorithm. The difference in area of the drainage basins between the two approaches was not significant, providing confidence that the depiction of the drainage system is robust. The total areas varied by ∼62,000 km^2 (∼10%). Furthermore, the network structure and watershed boundary of both basin calculations were nearly identical (Figure 4.2), with only a slight difference in the north-eastern corner where RES track spacing is most sparse. The smaller of the two basins (delineated in Figures 4.1 and 4.2(a)) was used for subsequent analysis.

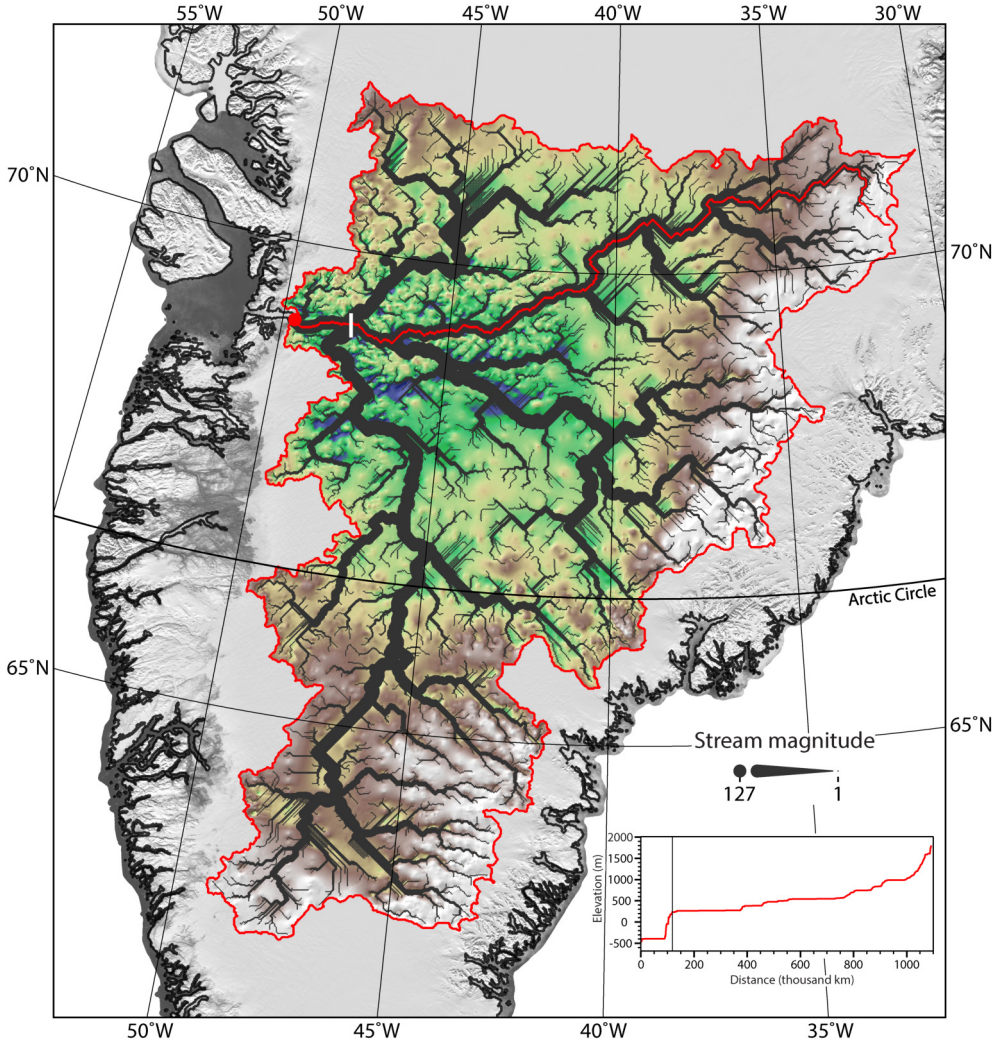

Figure 4.3: Flow routing network and Shreve (Shreve, 1966) stream magnitude for the palaeofluvial Jakobshavn Isbræ basin. A main stream of the catchment is marked by the solid red line, with its longitudinal profile inset. A downstream knickpoint of this channel is marked by the solid white and black lines on the main and inset figures, respectively.

4.5 Network characteristics

Figures 4.1 and 4.3 present the calculated drainage basin for the catchment incorporating Jakobshavn Isbræ and its flow routing network, respectively. The calculated basin size is 442,584 km^2, comparable with the Ohio River basin, USA, and accounts for about 20% of the total land area of Greenland. Much of the basin is relatively low-lying and smooth (Figure 4.1; with low relief, an average elevation ∼748 m and slope of 0.8°); however, the eastern limit gives rise to a more mountainous, high-elevation terrain, as a result of the Caledonian fold belt (formed ∼420MaB.P.) (Henriksen, 2008). The relief (elevation range) of the basin is 3382 m, with a minimum elevation at the outlet, of ∼458 m below sea level.

Figure 4.3 shows Shreve (1966) stream magnitude (number of upstream unbranched streams) calculated for the basin, presenting a metric for basin scale and network arrangement. The dendritic and sinuous nature of the calculated flow routing (Figure 4.3), as well as magnitude and tributary hierarchy, suggests that the hydrological system may have once been a viable drainage network prior to the inception of the ice sheet. In addition to analysis of the structure of the calculated flow paths, channel and basin morphology (long-profile and cross-section geometry) were considered with regard to their geomorphic process origin and erosion rates.

Figure 4.4 shows airborne RES profiles at three points along the calculated channel network. Figure 4.4(a) was taken nearest the outlet (the topographic low point along the basin boundary), through which the entire network drains, coincident with the present-day Jakobshavn Isbræ; Figures 4.4(b) and 4.4(c) present cross sections upstream from this point, documenting some of the main channels of this dendritic system. The RES data indicate that the channels are very large with a relative depth up to about 1400 m and a width of ∼12 km; dimensions that exceed parts of the north Greenland mega-canyon, reported previously by Bamber et al. (2013b).

Channel cross-section geometry and calculation of valley width-to-depth ratios are used to differentiate between U- and V-shaped valleys and, therefore, between predominantly glaciated (*i.e.*, glacially (re)modified) and solely fluvially incised geometries, respectively (Graf, 1970; Bull and McFadden, 1977). The ratio for the channels shown in Figure 3 range from between 1.2 and 8.89, indicating that

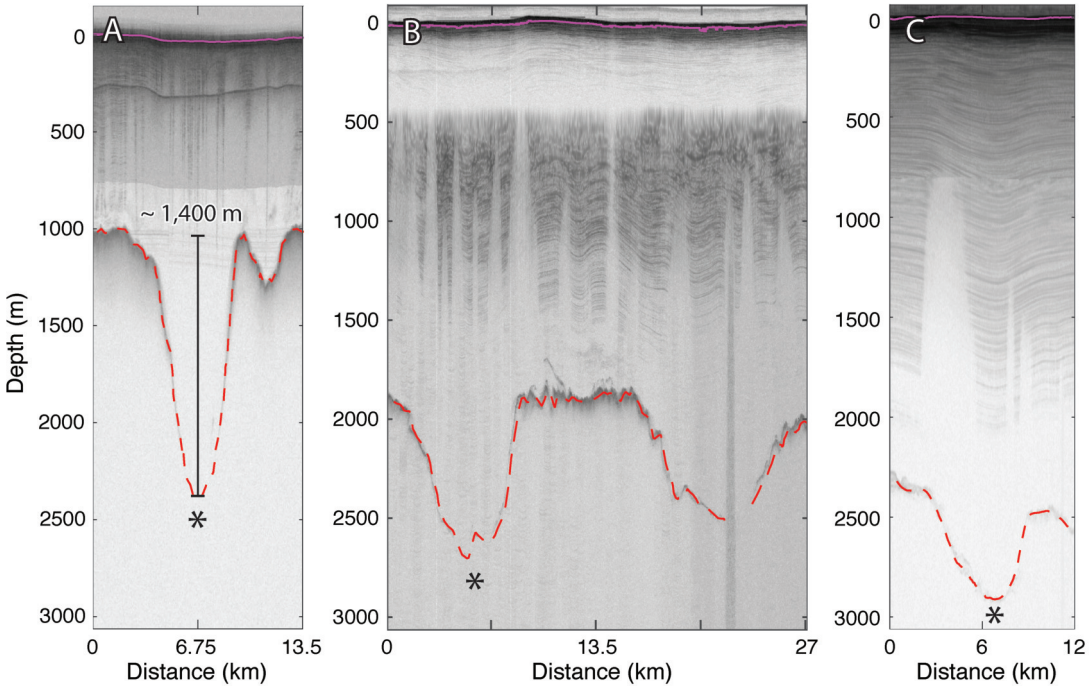

Figure 4.4: Ice-penetrating radargram profiles across the flow network at three locations (a–c). These locations are indicated in Figure 4.1 by A–C (solid black lines). There is an exaggeration in the vertical by a factor of 13. The bed return has been picked, the dashed red line, showing bedrock depth relative to the ice surface, the solid purple line. Cross sections of the main channel, as seen in Figure 4.4 (solid red line), are marked with the asterisk.

fluvial incision has been the dominant channel-forming process. Higher ratios, whereby a channel is relatively broad and shallow, are more characteristic of glacially worked channels, with those solely from glacial erosion having lower incision rates (Graf, 1970).

The longitudinal profile of one of the main channels is concave up and involves a series of steps and flats (Figure 4.3; inset). At the headwaters, the profile shows a relatively sharp change in gradient from the Caledonian mountain region. This morphology is indicative of headwater streams, documenting high rates of incision and low sinuosity. As the channel continues downstream toward lower elevations, the long profile becomes relatively smooth, reflecting the nature of a broadening and graded fluvial system. The long profile terminates following a large "knickpoint" (an abrupt break in slope) (Figure 4.3; black and white solid lines), coincident with the confluence of three channels (see Figures 4.1, 4.3, and 4.5(c)) and onset of fast glacial flow (>750 m a^{-1} (Joughin et al., 2010); see Figure 4.5(b)).

4.5.1 Nature of erosion

In order to ascertain the relative effectiveness of fluvial processes in creating the derived basal topography, calculations were carried out to compare the potential magnitude of incision rates by fluvial and glacial processes based upon the properties of the regional geology and glacial history (namely, length of glaciation). The basement rocks in the basin are gneisses (Henriksen et al., 2009) having a typical tensile strength of 5–20 MPa (Winkler, 1973), with no record of sedimentary sequences laid down in this region (Henriksen, 2008; Henriksen et al., 2009). Assuming a steady and uniform fluvial incision rate into rocks of ∼0.3 mm a^{-1} into bedrock of this order of tensile strength (Stock et al., 2005), yields a conservative estimate of around 2.3 Ma to incise to the observed channel depths (as big as 1,400 m). Alternative mechanisms for channel formation include extreme floods as a result of glacial lake outbursts, or increased flow during interglacial periods where a retreating GrIS ice margin would have stood north of Jakobshavn Isbræ (Siegert, 2001). Extreme flood events have the potential to cause dramatic landscape change over short periods of time (hours–days), and therefore the observed channel system may have been created over much a shorter timescale (than the conservatively estimated 2.3 Ma), in as few as 3 or 4 ma-

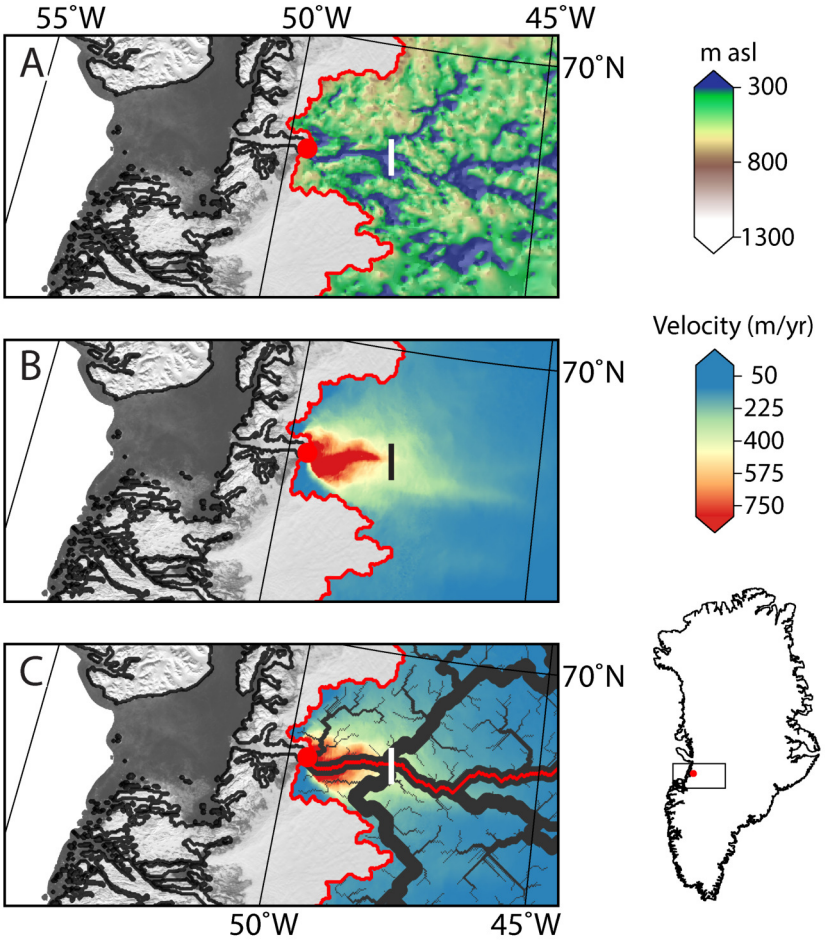

Figure 4.5: Influence of subglacial topography, and palaeofluvial network, on contemporary ice dynamics at the basin outlet, Jakobshavn Isbræ. (a) iDEM, as Figure 4.1, omitting flightlines; (b) 2008/2009 MEaSUREs surface ice velocity (Joughin et al., 2010); (c) as in Figure 4b but with flow routing network from Figure 4.3 overlaid with line weight decreased by half. The solid white and black cutlines mark the location of the longitudinal knickpoint shown in Figure 4.3. Surface velocity of Jakobshavn Isbræ at the outlet exceeds 10 km a^{-1}.

jor flood episodes (Baynes et al., 2015; O'Connor and Baker, 1992). However, palaeofluvial discharge events and corresponding hydraulic conditions are poorly constrained, and therefore, robust estimates of past episodic erosion rates are currently challenging to achieve.

Assessing the erosional potential of the ice sheet since its inception is also difficult. Where basal sliding occurs, glacial bedrock erosion rates are proportional to ice-sliding velocities squared (Herman et al., 2015). Across much of the present-day ice sheet the bed is frozen (cold-based ice), in which case, abrasion is very limited, and bedrock erosion ineffective (Drewry, 1986; Hallet et al., 1996). Whilst field-based assessments of the magnitude of glacial erosion are available, rates vary widely by geology and climate (over four orders of magnitude (Hallet et al., 1996)). Furthermore, where available, these rates are only representative of hydrologically-active portions of the glacial catchment, where surface melt waters are able to access the bed and evacuate sediment (Cowton et al., 2012). For glaciers in west Greenland, Andrews et al. (1994) present basal erosion rates of between 0.01–0.04 mm a^{-1}. Extrapolating this rate as a lower bound for glacial erosion, and assuming uniformity throughout over 3.5 Ma, a total incision of 35–140 m results. This is not consistent with the sizeable channels observed under the ice (with a depth of up to 1,400 m; Figure 4.4), suggesting that glacial erosion is unlikely to be the dominant geomorphic process for landscape development in this basin. A more recent study by Cowton et al. (2012) suggests an equivalent rate of 4.80 $\pm$ 2.60 mm a^{-1}, which could present a total incision of $\sim$16,800 $\pm$ 9,100 m over the same time period. Whilst this higher incision rate, if treated as an upper bound, could perhaps explain the channels identified, it should be noted that this rate is not representative of erosion conditions in the ice sheet's interior (*i.e.* of cold-based, hydrologically-inactive ice), and may only explain rapid erosion around the ice sheet margins. Furthermore, it is suggested that contemporary rates, particularly when measured only over short time-scales, should not be used to project over long periods of time ($>$ 1000 years) as the current warming period increases meltwater availability to the bed, enhancing erosion and sediment evacuation (Koppes and Montgomery, 2009).

These calculations offer an initial qualitative assessment of the efficacy of fluvial versus glacial origins for the basin. Owing to the capability of bedrock to present a palimpsest of geomorphic processes, and long-term history of landscape evolution, it is inappropriate to suggest that the bed topography remains

unaltered since the onset of extensive glaciation, however. Subsequent selective glacial erosion is likely to have adjusted the palaeofluvial basin, amplifying, and modifying, pre-existing topography.

4.6 Discussion

The topographic and morphometric analyses undertaken for the Jakobshavn Isbræ region largely point toward an inherited fluvial landscape of a preglacial (prior to extensive glaciation) origin. The calculated hydrologic basin and drainage network are seen to be well developed and extensive, with both a dendritic and sinuous structure (Figure 4.3). The concave up long profile presented is typical of fluvial networks, and V-shaped valley bottom geometries are suggestive of a dominant signal of fluvial incision. While the underlying topography will have been subject to glacial erosion, the influence of a slow-flowing and cold-based interior in this region, owed partly to divergent flow and ice divides (Sugden and John, 1976; Drewry, 1986), will have led to minimal glacial erosion and incision throughout much of the basin.

It is widely documented that under certain glacial and geological conditions, landforms are able to be left largely unmodified by subsequent glaciation and erosion, particularly in the case of larger, more "robust" features (Kleman, 1994). Our analysis reveals that the Greenland Ice Sheet has modified the landscape only in a highly selective manner, as constrained by the pre-existing topography (Sugden, 1974; Sugden and John, 1976). Modification, through glacial erosion, will be enhanced in hydrologically active portions of the ice sheet (where surface meltwater is able to access the bed), as well as in regions of altered (warmer) basal thermal regime, increased ice velocity, and ice thickness (Sugden, 1974; Sugden and John, 1976; Drewry, 1986), characteristics that are largely influenced by large-scale basal topography (Ignéczi et al., 2018). The observed knickpoint toward the basin outlet (Figure 4.3 (inset)) is a likely candidate for such enhanced selective erosion following the onset of glaciation, excavating further a valley formed by the action of preglacial fluvial activity. Figure 4.5 documents a coincident ice convergence zone and increase in ice surface velocity. Lateral convergence of ice gives rise to enhanced glacial erosion rates (Sugden, 1974; Sugden and John, 1976; Drewry, 1986), which can lead to the formation of a "glacial stair-

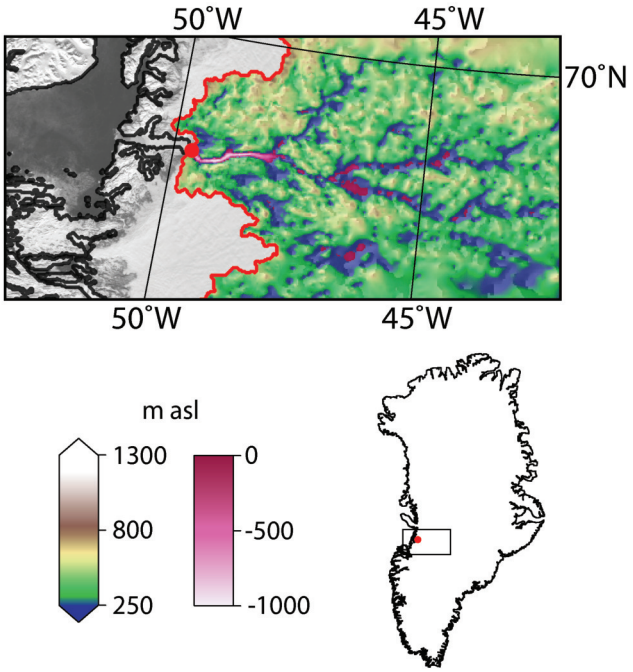

Figure 4.6: Over-deepenings in bed elevation present in the Jakobshavn Isbræ palaeo-catchment. iDEM bed elevation [between -1000 and 1300 m above sea level (asl)]. The area plotted is indicated by the black box in the inset. Possible over-deepenings (elevations below sea level) are clearly indicated in pinks.

way" (stepped long profiles), as documented in numerous valley glacier systems (Anderson et al., 2006). Such a feature is observed throughout the long profile documented here (Figure 4.3, inset). Glacial overdeepening is also present at other confluences in the subglacial channel network (see Figures 4.6 and 4.7), further confirming an erosive signal of the ice sheet superimposed upon the preglacial fluvial landscape, through selective means.

Aside from the geomorphic impact of the Greenland Ice Sheet upon the underlying topography, it is also important to consider the controls of bed geometry on ice dynamics. Figure 4.5b shows surface ice velocity for 2008/2009 (MEaSUREs) (Joughin et al., 2010) for Jakobshavn Isbræ alongside bed elevation. Surface velocity increases by many orders of magnitude toward the outlet, following the observed knickpoint in the longitudinal profile (Figures 4.3 and 4.5 (solid white and black lines)), and confluence of major subglacial channels; increases in surface velocity are also documented to fork upstream, mapping the underlying subglacial channels (Figures 4.5(b) and 4.5(c)). While these increases are perhaps unsur-

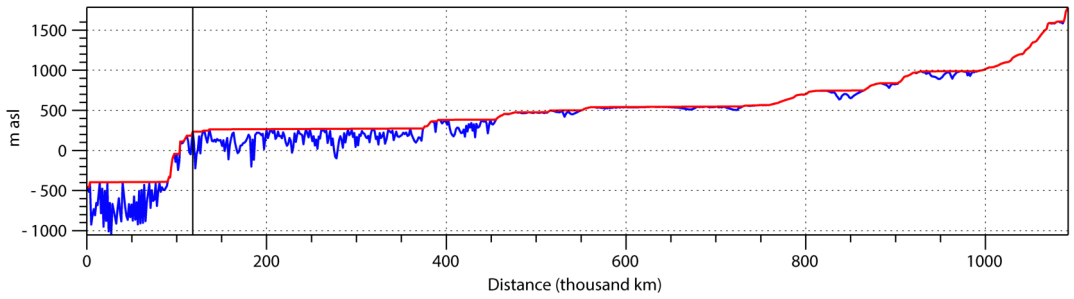

Figure 4.7: Longitudinal profile of the calculated mainstream (as in Figure 4.3) from the 'filled' iDEM (red), and un-'filled' iDEM (blue).

prising, owing to ice convergence and increased ice thickness (as ice velocity is proportional to the fourth power of ice thickness (Cuffey and Paterson, 2010)), it is remarkable to consider that the ancient bed topography has such a marked influence on the location of surface velocities and ice dynamics, where the flow of ice itself is usually seen as an important control upon bedrock topography from an erosional standpoint. It is reasonable to assume that a similar arrangement between ice flow and topography existed previously; hence, the fluvial system documented here is likely to have affected the flow of the Greenland Ice Sheet since its inception, at least in the study area presented here.

4.7 Conclusions

We have presented a detailed study on the subglacial geomorphology of southern Greenland and, through topographic and morphometric analysis, documented evidence for a large-scale drainage basin of likely palaeofluvial origin. We believe the delineated basin and flow routing network to be robust, and while track spacing is variable across the region, the error for the majority of catchment is $<$ 125m (Bamber et al., 2013a). Where the track spacing is more sparse, the topography is generally smoother (the island's interior) and a more coarse and interpolated measurement is seen as adequate (Bamber et al., 2013a).

While this region has been subject to glacial erosion throughout the history of the GrIS, the preexisting fluvial landscape, made evident by the dendritic nature of the system and V-shaped valley bottoms, is likely to have led to subsequent processes of selective glacial erosion. These processes have since modified the dimensions of parts of the basin, most notably toward the basin outlet, through a

long-term process of landscape evolution. The ancient bed topography presents, through landscape inheritance, a defining influence on the modern ice sheet configuration and contemporary dynamics, constraining the flow of ice, helping to explain the location, size, and velocity of the Jakobshavn Isbræ, Greenland's largest outlet glacier. It stands to reason that former ice cover in Greenland has been similarly influenced.

This paper has opened discussion on this region and landscape, providing the first interpretation of Greenland's underlying topography with respect to the established literature on the selective nature of glacial erosion, and landscape inheritance (*e.g.*, Hall et al., 2013; Sugden, 1974; Sugden and John, 1976). This work allows future interpretation into the two-way relationship between ice sheet glacial erosion and pre-existing topography, as well as providing new information to understanding long-term landscape evolution. Further, it adds to the growing collection of research on preglacial landscape inheritance both in Greenland and Antarctica.

Chapter 5

Subglacial roughness of the Greenland Ice Sheet

5.1 Preface

This chapter is currently in preparation for submission to *The Cryosphere*, under the following citation:
Cooper, M. A., Jordan, T. M., Schroeder, D. M., Siegert, M. J., Williams, C. N., and J. L. Bamber (in prep.), Subglacial roughness of the Greenland Ice Sheet: relationship with contemporary ice velocity and geology, *The Cryosphere*.

Additionally, the two subglacial metrics for subglacial roughness here defined are published and publicly available for download from the Polar Data Centre (URL: http://doi.org/ckqg; please be aware these data are embargoed until the publication of the above paper). The digital or object identifier for these data is: 10.5285/6071926f-32e0-4681-a50d-aab08f42c08a.

The vast majority of work presented in this chapter was conducted by M. A. Cooper; this includes analysis, interpretation, and writing. The derivation of the electromagnetic scattering-derived roughness metric (Section 5.4.3) was undertaken by T. M. Jordan, and is described in full in Jordan et al., 2017, a paper on which I am second author but which does not contribute direct text to this thesis.

Some of this chapter draws upon the material in Jordan et al., 2017 to introduce the scattering-roughness metric. For this chapter, I was responsible for

applying the scattering metric across the Greenland Ice Sheet, and undertook the analysis and interpretation of the results.

5.2 Abstract

The subglacial environment of the Greenland Ice Sheet (GrIS) is poorly constrained, both in its bulk (*e.g.* geology, sediment and presence of water) and interfacial properties (*e.g.* roughness and geotechnical bed properties). There is, therefore, limited understanding of how spatially heterogenous subglacial properties relate to ice-sheet motion. Here, via analysis of two decades worth of CReSIS radio-echo sounding data, we present a new systematic analysis of subglacial roughness beneath the GrIS. We use two independent methods to quantify subglacial roughness. First, we use the variability of along-track topography (enabling assessment of roughness anisotropy), and second, we infer roughness from bed-echo scattering (enabling assessment of finer-scale information).

We depict the spatial distribution of subglacial roughness and quantify the relationship with ice velocity (magnitude and flow direction). In fast flowing regions 'topographic roughness' exhibits an exponential scaling relationship with ice velocity parallel, but not perpendicular, to flow direction. In many slow flowing regions both roughness methods indicate spatially coherent regions of smooth bed, which, combined with analyses for underlying geology and lithology, we conclude is likely due to the presence of a hard bed. In this vein, this study provides scope for a spatially variable hard bed/soft bed boundary constraint for ice-sheet models.

5.3 Introduction

The rate of global sea level rise contributions from the Greenland Ice Sheet (GrIS) has accelerated over the past two decades (Velicogna and Wahr, 2006; Rignot et al., 2011). To constrain projections for future change, primarily driven by mass loss over the grounding line, models must parametrise characteristics influencing ice-sheet motion and dynamics (*e.g.,* Huybrechts, 1994; Nick et al., 2013). Outlet regions, and in particular fast flow, are principally characterised by enhanced basal motion (basal sliding) (Cuffey and Paterson, 2010; van der Veen,

2013). Conditions attributed to, and rates of, sliding at the bed are influenced by various properties of the subglacial environment, including, but not limited to: basal thermal regime; presence of basal water (and effective pressure); geotechnical bed properties (*i.e.* presence of sediment and, its viscosity/deformability); and basal friction/traction (*i.e.* resistance from roughness) (Weertman, 1957; Nye, 1970; Durand et al., 2011; Clarke, 2004; Iverson and Zoet, 2015; Brondex et al., 2017; Stearns and van der Veen, 2018). Although the influences of these properties upon ice dynamics are generally well understood (at least theoretically) (Cuffey and Paterson, 2010; van der Veen, 2013), these basal properties are not currently incorporated directly into ice sheet modelling. Understanding of spatial variation in subglacial conditions and processes remains restricted by the paucity of observations; as such, necessary parameters are often inverted or inferred, where observation-led interrogation is required to understand the presence, and magnitude of, different subglacial characteritics *in situ*.

Fundamentally, ice-sheet models rely on the application of sliding laws to approximate the rate of basal-motion with regards to subglacial characteristics, such as those described above. Though several sliding laws exists, each variously influencing the behaviour and sensitivity of modelled glacier response (Brondex et al., 2017), most models rely on a Weertman-style hard-bed sliding law (Weertman, 1957, 1972; Stearns and van der Veen, 2018). In this case, sliding velocity, and thus broad characteristics of ice dynamics, are controlled by frictional stresses at the ice-bed interface owing to a result of undulations within bed topography (order 1-metre) (Weertman, 1957; Nye, 1970; Iverson and Zoet, 2015; Stearns and van der Veen, 2018). Direct observation of such small-scale obstacles is not possible through conventional subglacial roughness quantification methods utilising RES data (described below). As such, within forward modelling, basal traction is primarily simulated (inferred/inverted) using satellite-derived surface velocity (e.g., Joughin et al., 2009; Durand et al., 2011; Arthern et al., 2015).

Nevertheless, quantification of subglacial roughness, and the subsequent evaluation with regard to ice velocity, have been the focus of many studies in recent years across Antarctica (*e.g.,* Siegert et al., 2005; Rippin et al., 2006, 2014; Bingham and Siegert, 2007, 2009; Schroeder et al., 2014), and Greenland, though to a lesser extent (*e.g.,* Layberry and Bamber, 2001; Rippin, 2013; Lindbäck and Pettersson, 2015; Jordan et al., 2017). Subglacial roughness has been concluded to exert control on the location of fast-flowing, streaming ice (Siegert et al., 2004;

Rippin et al., 2006; Bingham and Siegert, 2007, 2009; Rippin et al., 2014).

However, the influence/behaviour of subglacial roughness with respect to ice motion is not universal. Existing roughness maps of Greenland (*i.e.,* Rippin, 2013; Jordan et al., 2017) show that fast flow is typically associated with rougher beds, where slow-flowing regions are more smooth. A recent high-resolution assessment of the bed beneath Pine Island Glacier has concluded that small-scale roughness does indeed influence ice motion, but that principally occurs through form drag, controlled by the orientation and size of subglacial obstacles (Bingham et al., 2017). Furthermore, characterisation of the majority of Greenland's outlet glaciers implies that basal traction is not a major control on basal sliding within the GrIS, where effective basal water pressure, and the availability of deformable sediment, are more important/influential (Stearns and van der Veen, 2018). Additionally, when considering rough and smooth beds, various geomorphic interpretations have been made (Bingham and Siegert, 2009). For example, the majority of roughness studies of the West Antarctic Ice Sheet have associated low roughness with the presence of deformable sediment (e.g. Rippin et al., 2006, 2011, 2014; Bingham and Siegert, 2007); however, it is also evident that streamlined bedrock (hard beds) promote smooth beds (e.g. Siegert et al., 2005; Rippin et al., 2014). Altogether, this suggests not only that a consideration of orientation/anisotropy within the interpretation of subglacial roughness is necessary, but also relies on the influence of other factors (*i.e.,* basal thermal state, or geographical setting Bingham and Siegert, 2009).

Conclusions drawn from previous quantifications of subglacial roughness in Greenland are limited. Whilst the broad, ice sheet-wide distribution of roughness has been mapped (Layberry and Bamber, 2001; Rippin, 2013), systematic comparison to ice motion, and in particular reference to anisotropy, has not been fully considered. Rippin (2013) presents the most recent, ice sheet-wide consideration of subglacial roughness in Greenland. Whilst this highlighted the spatial distribution of roughness information across the island, a non-uniform/ mixed conclusion was made with regard to the speed of ice flow (velocity magnitude, $|v|$). Furthermore, the method employed aggregated information across various length-scales, working to eliminate more fine-scale information. More recently, Lindbäck and Pettersson (2015) present an albeit spatially-limited study highlighting the importance of considering roughness anisotropy, with respect to ice motion. The recent increase in coverage of radio-echo sounding (RES) data over

the GrIS (Rodriguez-Morales et al., 2014; Morlighem et al., 2017) provides new scope to increase understanding of the subglacial environment, enabling an ice sheet-wide description of spatially heterogeneous bulk (*i.e.,* geology, and presence of sediment) and interfacial properties (*i.e.,* roughness, and geotechnical bed properties) with previously unused data.

Subglacial roughness information can be obtained from airborne RES data in two different ways. The first is, via the statistical properties of along-track topography (e.g. Taylor et al., 2004; Siegert et al., 2005; Rippin, 2013; Jordan et al., 2017); and the second is, via the electromagnetic scattering properties of the bed-echo waveform (e.g., Oswald and Gogineni, 2008; Schroeder et al., 2013; Young et al., 2016; Jordan et al., 2017). Topography-derived roughness can be obtained using both space domain (*e.g.* measuring the root-mean-square height as a function of horizontal length-scale) and frequency domain, or spectral methodologies (e.g., performing a Fourier transform Shepard et al., 1995, 2001; Smith, 2014). The length-scale over which topographic roughness is assessed is limited to be greater than the horizontal resolution of the RES measurements (typically 30 m or greater) (Taylor et al., 2004; Li et al., 2010; Jordan et al., 2017). Scattering-derived roughness is sensitive to the radio wavelength in ice (typically 1–5 m for most radar systems), and reveals more-fine scale geometric information about the subglacial interface than topographic analysis (Shepard et al., 2001; Berry, 1973; Schroeder et al., 2015; Jordan et al., 2017).

One simple approach to mapping subglacial information from electromagnetic scattering is to use the 'abruptness' (or 'pulse-peakiness') of the bed-echo waveform (Oswald and Gogineni, 2008, 2012; Young et al., 2016; Jordan et al., 2017). This parameter, defined as the ratio of peak to integrated bed-echo power, gives an indication of the relative contributions of specular reflection (higher abruptness and associated with fine-scale smooth beds) and diffuse scattering (lower abruptness and associated with fine-scale rough beds). RES flight-track maps for the bed-echo abruptness in northern and central Greenland demonstrate clear spatial structure (Oswald and Gogineni, 2008, 2012; Jordan et al., 2017). For example, there are near-continuous regions of high abruptness in the interior (*e.g.*, near the Camp Century and NorthGRIP ice cores; Oswald and Gogineni, 2008, 2012; Jordan et al., 2017), whereas many ice margin regions have lower abruptness (*e.g.*, the main trunk of Petermann Glacier; Jordan et al., 2017). The original geophysical interpretation of the larger-scale high abruptness regions (typically

100s of km^2) was that they often represent extended, electrically-deep bodies of basal water (Oswald and Gogineni, 2008, 2012). However, this picture is largely inconsistent with ice core temperature data and existing knowledge of the basal thermal state (MacGregor et al., 2016; Jordan et al., 2017). An alternative explanation is that the larger-scale high abruptness regions typically indicate smooth and hard bedrock, with deep water only likely being present in more localised patches (Jordan et al., 2017). This primarily lithological interpretation of the bed-echo abruptness has, however, yet to be fully explored and integrated with existing knowledge of ice dynamics and the geological record.

In this paper, using two decades worth of CReSIS radio-echo sounding data, we present a new systematic analysis for subglacial roughness beneath the Greenland Ice Sheet (GrIS). We outline two independent methods for quantifying roughness using information obtained via both statistical analysis of sampled bed elevation (hereafter termed 'topographic roughness'), and the scattering properties quantified from the bed-echo waveform (hereafter termed 'scattering-derived roughness'), respectively. First, along-track variability in bed topography is used to provide an assessment of roughness anisotropy; and second, we infer roughness from bed-echo scattering behaviour to extract more fine-scale information about the bed.

For the first time, this study performs an integrated analysis of 'topography-derived' and 'scattering-derived' roughness at the scale of the GrIS. We map the spatial distribution of subglacial roughness across the GrIS, and document a marked spatial heterogeneity using both metrics. We then assess roughness anisotropy, providing clear evidence for direction-dependence between topographic roughness and the speed of surface ice in fast-flowing regions, both at the ice sheet-scale, and locally surrounding important outlet glaciers. Finally, to better understand the observed coherent signal of 'smooth' beds in regions of slow flow we compare scattering-derived roughness with complementary information and present an alternative to basal water discrimination.

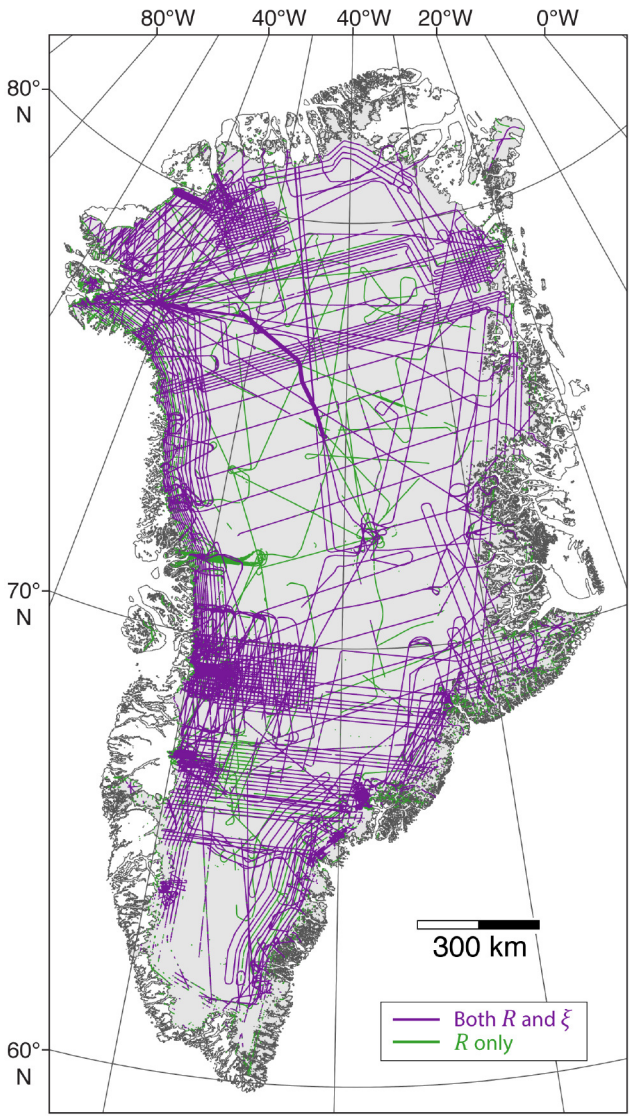

Figure 5.1: Coverage of radar sounding surveys over the GrIS used in this study. Topography-derived (topographic) roughness (R) is calculated using all available CReSIS survey data between 1993–2016, where scattering-derived roughness (ξ) uses only a subset of these (further explained in section 5.4.3). Displayed using a polar stereographic north projection (71° N, 39° W), as with all other spatial plots.

5.4 Methods

5.4.1 Ice-penetrating radar systems and survey coverage

The airborne RES data used in this study were collected by the Center for Remote Sensing of Ice Sheets (CReSIS) over the years 1993–2016, with more recent campaigns undertaken as part of the wider Operation IceBridge (OIB) programme (post–2009). Surveys were typically flown between the months March and May, using three airborne platforms for collection; radar instruments have been variously mounted upon the P-3B Orion (P3), DHC-6 Twin Otter (TO), and Douglas DC-8 (DC8) aircraft (Paden, 2017). The instruments used were, successively, the: Improved Coherent Radar Depth Sounder (ICORDS); ICORDS, version 2; Advanced Coherent Radar Depth Sounder (ACORDS); Multi-Channel Radar Depth Sounder (MCRDS), Multi-Channel Coherent Radar Depth Sounder (MCoRDS), and MCoRDs, version 2 (v2) (Paden, 2017). Centre frequencies for the radar instruments are 149 MHz (for ICORDS and ICORDS, v2), 150 MHz (for ACORDS and MCRDS) and 195 MHz (for MCoRDs and MCoRDS, v2). The vertical (depth-range) resolution varies from $\sim$ 4.3 to 20 m, where the horizontal (along-track) resolution is typically $\sim$30 or 60m. Precise breakdown of the radar data coverage by field season and radar instrument class can be found in MacGregor et al. (2015a) (Fig. 1) and Jordan et al. (2018) (Fig. 1), respectively.

For measures of topographic roughness (Sect. 5.4.2) data across all campaigns were used; however, for scattering-derived roughness analysis (Sect. 5.4.3), only a subset of these is incorporated (indicated in Fig. 5.1), including ACORDS, MCRDS and MCoRDS, and MCoRDs v2 data, only. The rationale for this, relating to internal consistency when combining data from differing radar instruments and the signal-to-noise (SNR) ratio of the bed echo, is described in Sect. 5.4.3. The quantification of topographic roughness makes use of many more years of data; however, owing to the preference for 'repeat fly-bys' in airborne sampling regimes, and the marked increase in survey kilometres in recent years (Rodriguez-Morales et al., 2014; Morlighem et al., 2017), the final spatial coverage of both roughness metrics is not dissimilar (Fig. 5.1).

Method-specific data pre-processing (*i.e.* the handling of quality flags) is described below. For full information regarding the multiple radar instruments used (including radar wavelength) in this analysis readers are referred to the

user's guide (available from (http://data.cresis.ku.edu/data/rds/rds_readme.pdf; Paden, 2017); additionally, detailed signal processing steps, and information regarding data segmentation, are described in several previous works (*i.e.,* Gogineni et al., 2001; Rodriguez-Morales et al., 2014; Gogineni et al., 2014; MacGregor et al., 2015a; Paden, 2017).

5.4.2 Subglacial roughness from along-track topography

Calculating rms height, R

As noted, subglacial roughness information can be determined via the statistical analysis of vertical variation in along-track bed topography (*e.g.*, Siegert et al., 2004, 2005; Taylor et al., 2004; Rippin et al., 2006, 2011, 2014; Bingham and Siegert, 2007, 2009; Bingham et al., 2007, 2017; Li et al., 2010; Rippin, 2013). The most prevalent method in glaciological literature employs spectral methods to do this (*i.e.* the application of fast Fourier transforms (FFTs) first employed across the Antarctic Ice Sheet by Taylor et al. (2004)). Alternative space-domain methods exist, however, and are frequently used within earth and planetary sciences (Shepard et al., 2001; Smith, 2014).

Here, the first metric for subglacial roughness we present, hereafter termed 'topographic roughness' (or R) is quantified by the root mean square (rms) height in along-track topography (RES sampled bed elevation). Rms height (referred to also as standard deviation of bed elevation (*e.g.*, Rippin et al., 2006, 2014) provides several benefits over the use of FFTs. Firstly, it enables all the collation of all CReSIS survey campaigns despite the variable sample spacing (horizontal resolution) without requiring along-track interpolation/ re-sampling the data. Secondly, this method allows the use of a shorter length-scale than FFT, not only facilitating subsequent anisotropic analysis at cross-overs (Sect. 5.4.2), but also providing a finer-scale roughness information with reference to basal friction. A final advantage of is that rms height calculations are unit-preserving (*i.e.* quantifying variation at the bed in metres (m)), providing a more physically intuitive metric. More critically, however, the spatial distribution of roughness values quantified by FFT and rms height methods have been noted to be similar (Rippin et al., 2014; Falcini et al., 2018).

Sampled elevation was obtained from all available CReSIS RES surveys (1993–2016). We use Level 2 data where both the ice surface and ice bottom (bed) were

recorded. Where applicable, data were filtered using the provided quality flags denoting the confidence of the bed pick accuracy (Paden, 2017), ensuring only bed elevations with 'high' confidence were used. RES data obtained during OIB campaigns prior to 2008, with the exception of the reprocessed '2006 TO' survey, do not hold quality flags, and as such all sampled bed elevations were used. As a result of the increased sampling resolution in more recent surveys (post–2006), data for these in these campaigns were rarefied (to include every other sample point), to ensure only independent measures of bed elevation were used (Paden, 2016, pers. comms.).

Topographic roughness, R, is given by

$$R = \left[\frac{1}{n-1} \sum_{i=1}^{n} (z(x_i) - \overline{z})^2 \right]^{\frac{1}{2}}, \tag{5.1}$$

where n is the number of sample points, $z(x_i)$ is the height of the surface point at point x_i, and $\overline{z}$ is the mean height of the profile over all x_i. Rms height R was calculated using a window length or bin size, L, of 200 m using all recorded bed elevations, regardless of spatial density within the bin, provided $n \geq 3$. R is given for the spatial midpoint of each window. Regions of greater roughness, quantified by a larger variation in bed elevation within the window, have greater R values. An example of R calculated along-track using sampled bed elevation is presented in Fig. 5.2.

$L = 200$ m was chosen to enable the finest-scale of R to be quantified whilst maintaining the largest spatial, and intrinsically temporal, coverage of the resultant metric by using all available survey data. Furthermore, this allows for a more appropriate consideration with regard to basal traction in a Weertman-style hard-bed sliding theory (Weertman, 1957; Nye, 1970) influenced by small-scale bedforms (Durand et al., 2011; Iverson and Zoet, 2015). It is, however, possible to quantify R at a finer scale using only more recent survey data the expense of spatial coverage for a length-scale not less than 100 m. It should be noted that not all bins have constant n, due to the variation in sampling regime, the resolution of the different radar instruments, and data quality. R was not calculated for bins where $n < 3$.

R was calculated at additional length-scales, where $L = 500$ m, 1000 m, and 5000 m, respectively. The broad spatial patterns observed using these length-

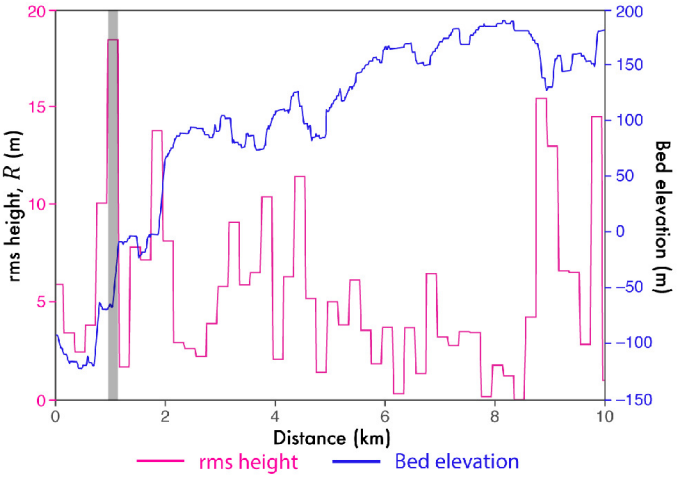

Figure 5.2: Along-track example of calculated topographic roughness (R). This demonstrates the length-scale (200 m) over which R is calculated from sampled bed elevation. Grey bar depicts a limitation of topographic roughness calculation over large step-changes in bed elevation (described in section 5.6.4).

scales were similar to those presented in Sect. 5.5, albeit 'smoothed,' as details of smaller wavelength subglacial features are not provided (Falcini et al., 2018). The scaling relationships exhibited and described below also held for these values of L.

Filtering R with respect to ice surface velocity

To evaluate, and more completely understand, how the spatial distribution of subglacial roughness influences, or perhaps is influenced by, ice-sheet motion, we compare R to ice surface velocities. We use the InSAR-derived MEaSUREs velocity mosaic (Joughin et al., 2016, 2017) to provide full spatial coverage over the GrIS. This mosaic also helps to capture long-term information (using 1995–2015 observations) regarding flow configuration, minimising inter- and intra-annual variation in both ice speed and direction. As R is quantified using two decades worth of RES data, we assume an inherent constancy in roughness over time. The MEaSUREs data provide magnitude (speed, $|v|$) and direction at a 250 m resolution (Figs. 5.3(a) & (b)); however, for our analysis, we performed a bilinear aggregation (to 1000 m) in order to smooth small-scale variation or 'noise.'

With regard to surface flow speed we delineate regions of 'fast' ($|v| \geq 50$ ma^{-1}) and 'slow' ($|v| \leq 5$ ma^{-1}) flow (Fig. 5.3 (a). We use these distinctions for two

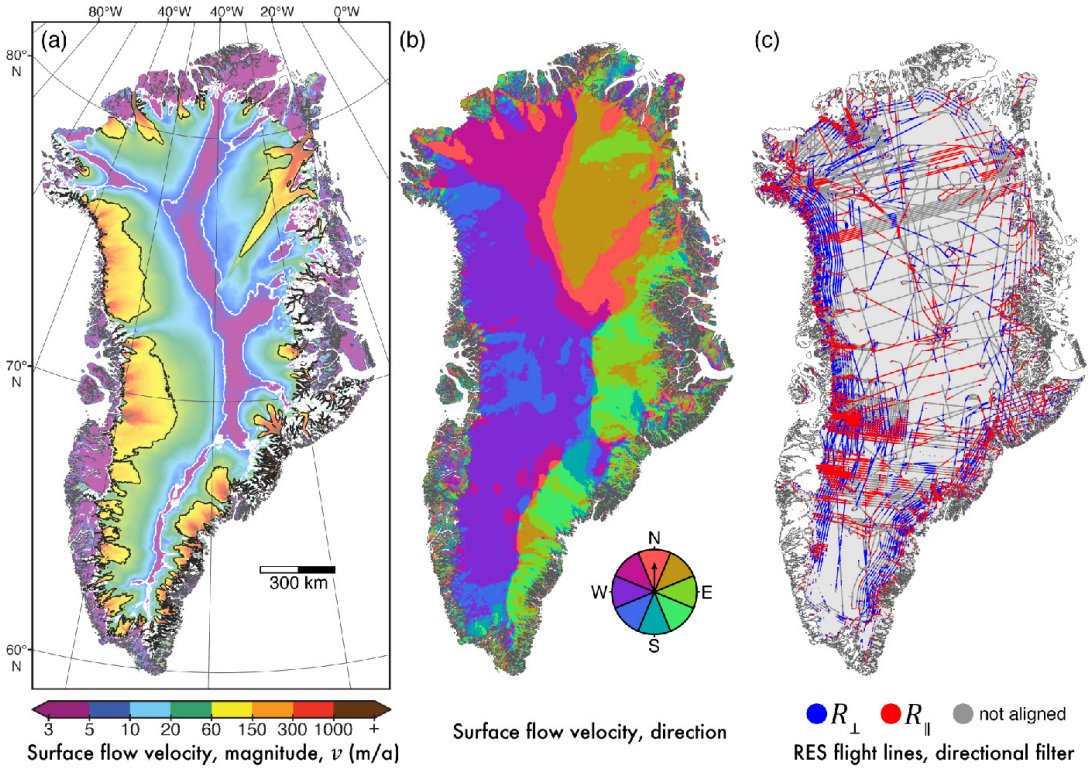

Figure 5.3: Observed surface ice velocity characteristics of the GrIS used in the filtering of R. (a) InSAR-derived surface velocity magnitude (m a^{-1}) (Joughin et al., 2016); regions of fast ($|v| > 50$ ma^{-1}) and slow ($|v| < 5$ ma^{-1}) flow are demarcated by the black and white contour lines, respectively. (b) Direction of ice surface velocity, from (a); coloured pin-wheel denotes direction of surface ice flow, where North is at the top of the page. (c) Radar sounding surveys as in Fig. 5.1 filtered for alignment with surface flow direction (b); flight tracks are categorised as aligned either parallel ($R_\parallel$) or perpendicular ($R_\perp$) to surface flow direction for the analysis of topographic roughness anisotropy.

reasons. First, where $|v|$ exceeds 50 ma^{-1}, ice is not only likely to be decoupled from the bed (*i.e.* sliding), but the rate of ice motion here cannot be achieved by internal deformation alone (MacGregor et al., 2016; Stearns and van der Veen, 2018). As we have noted above, basal traction, a principal constraint on basal sliding (Weertman, 1957), may be influenced by subglacial roughness (Siegert et al., 2004, 2005; Bingham et al., 2017). Secondly, where ice motion is limited in slow-flowing regions, rates of erosion are minimal, and thus the influence on subglacial topography is reduced (Bingham and Siegert, 2009). Whilst we do make some observations regarding scattering-derived subglacial roughness (later defined; Sect. 5.4.3) and the speed of ice $|v|$, this is to a lesser extent (Sects. 5.6 & 5.6.3).

However, as R is quantified along-track, there is an inherent directionality in its characterisation of the subglacial environment. To assess anisotropy at the bed, with particular reference to ice motion, we classify R through its alignment with local flow direction. Sample windows were filtered for their linearity to remove measures of R over corners and bends in RES flight-lines/transects; a deviation threshold of $\geq 10\%$ was chosen for this (as per Bingham et al., 2015). Roughness bins were then filtered by their alignment to local surface ice flow direction (Fig. 5.3 (b)) with a 20° threshold; figure 5.3 (c) shows classified measures of R aligned perpendicular $R_{\perp}$ or parallel $R_{\parallel}$. From this, we draw conclusions based on the relationship between subglacial roughness and the speed of overlying ice.

Where coincident measures of $R_{\perp}$ and $R_{\parallel}$ are available (the near-orthogonal ($\pm$ 20°) cross-overs between flight-lines) the degree of anisotropy can be calculated. This is achieved through a normalised difference ratio, herein termed 'anisotropy ratio' (Smith, 2014), given by

$$\Omega = \frac{R_{\parallel} - R_{\perp}}{R_{\parallel} + R_{\perp}}. \tag{5.2}$$

Using Ω we map the distribution of roughness anisotropy across the GrIS and assess any relationship between $|v|$ and Ω in both fast- and slow-flowing regions. Values of Ω are interpreted such that -1 dictates a complete dominance of smoothness parallel to flow direction, where $+1$ a dominance of smoothness perpendicular to flow (*i.e.* parallel roughness), and values of 0 suggest roughness isotropy.

5.4.3 Subglacial roughness from radar scattering

The abruptness (peakiness) of the bed-echo waveform

Bed-echo waveform properties are related to electromagnetic scattering from the glacier bed, and hence also provide information upon subglacial roughness (Oswald and Gogineni, 2008; Oswald et al., 2018; Jordan et al., 2017). Radar bed-echoes range from sharp pulse-like returns (associated with specular reflection from a smooth glacier bed), to echoes that have a trailing edge which extends greatly over the original pulse length (associated with diffuse scattering from a smooth glacier bed). A convenient way to parametrise the relative spread of the bed-echo waveform is to use the waveform 'abruptness' parameter defined by

$$A = \frac{P_{peak}}{P_{agg}}, \tag{5.3}$$

where P_{peak} is the peak power of the bed echo and P_{agg} is the aggregated (integrated) power over the echo envelope (Oswald and Gogineni, 2008; Jordan et al., 2017). Three examples of bed-echo waveforms and their abruptness values are shown in Fig. 5.4(c). Higher values of A are associated with specular reflection, and lower values with diffuse scattering. However, the maximum value for A (which is constrained by the ratio of the image sample rate to depth-range (vertical) resolution (Jordan et al., 2017) can differ between different CreSIS field seasons with values ranging between 0.5–0.8. Since the radar bed-echo results from a superposition of along-track and cross-track energy, the abruptness is a (near) isotropic parameter (Young et al., 2016), and therefore obscures information regarding the anisotropy of the glacier bed.

The procedure used to extract the bed-echo abruptness from CReSIS Level 1B data is outlined in Jordan et al. (2017). Briefly, this consists of the following steps. Firstly, CReSIS Level 2 picks are used as initial estimates for the depth-range bin of bed-echo power peak. Secondly, a local re-tracker is used to locate peak-power. Thirdly, the power is integrated over the bed-echo envelope applying a 'quality control' measure such that the peak power is 10 dB over the noise floor. This final step results in some regions, primarily in Southern Greenland, having reduced coverage (see Fig. 1(b) in Jordan et al., 2018)).

Deriving fine-scale roughness and the 'peakiness index'

The scattering of the radar pulse by the glacier bed is underpinned by the physics of electromagnetic diffraction (Berry, 1973; Ulaby et al., 1982). As roughness increases, energy is scattered over a wider range of angles, which results in the peak-power decreasing and the fading length of the echo increasing. The mathematical formulation of this relationship depends upon the physical model for electromagnetic interference (phase coherence, or incoherence) and the statistical model for the subglacial interface (Berry, 1973; Peters et al., 2005). The most commonly employed scattering model for the RES of glacier beds assumes phase-coherent interference, 'smoothly undulating' Gaussian statistics for rms roughness, and radial isotropy (Berry, 1975; Peters et al., 2005; MacGregor et al., 2013; Grima et al., 2014; Schroeder et al., 2015). We consider this scattering model for two reasons: firstly, as a way of estimating 'fine-scale roughness' from the abruptness; and, secondly as a way of combining the abruptness for different radar systems to derive an (approximately) system-independent 'peakiness index' (Λ).

Following a similar approach to that described by Schroeder et al. (2015) and Jordan et al. (2017), under assumptions of energy conservation the scattering model can be use to predict the relationship between A and rms height ξ ('fine-scale' roughness). In this context ξ is not strictly equivalent to the values obtained from topography, and a length-scale separation is performed with respect to a reference plane (Berry, 1973). The relationship between A and ξ is given by

$$A = A_{max} \exp(-g^2) I_0^2 \left(\frac{g^2}{2} \right), \tag{5.4}$$

where

$$g = 4\pi \xi f_c \sqrt{\epsilon}_{ice} / c, \tag{5.5}$$

is the rms phase variation, with A_{max} the maximum abruptness, I_0 a zeroth-order Bessel function of the first kind, f_c is the centre-frequency of the radar pulse, c is the vacuum speed of the radar pulse, and $\epsilon_{ice} = 3.15$ is the relative dielectric permittivity of glacier ice (Peters et al., 2005). Since the radar wavelength in ice is $\lambda_{ice} = c/f_c\sqrt{\epsilon}_{ice}$, eq. (5.5) can be expressed as

$$g = 4\pi \xi / \lambda_{ice}, \tag{5.6}$$

and hence ξ is scaled by the radar wavelength in ice (either 0.87 m or 1.13 m for the 195 MHz and 150 MHz systems, respectively). There are therefore two degrees of freedom in eq. (5.4) that can vary for different CReSIS field seasons: A_{max} and f_c. The different parameter combinations are shown in Fig. 5.4(a), and from these relationships it is possible to estimate ξ from A (and thus obtain a measure of fine-scale roughness that is similar between different radar systems). However, since the values of f_c and A_{max} differ between field seasons a cross-over bias is present for 'raw' abruptness values. In order to combine abruptness data we back-substituted the value of ξ to obtain the value of A as if it were the most spatially extensive radar system (the blue curve in Fig. 5.4(a)), and then re-scaled amplitude on the interval $[0, 1]$ to give the 'peakiness index' (from herein referred to as Λ). These steps combine the measurements via the system-independent relationship between Λ and wavelength-scaled rms height ξ/λ (Fig. 5.4(b)).

The inter-season data combination was validated by performing cross-over analysis for ξ and Λ, with the allowed tolerance for the cross-over bias 5 % of the parameter range. Seasons which did not meet this criteria (primarily the older ICORDS data, but also the 2010 P3 season which is known to have noise-floor issues (Paden, 2017)) were discounted. Although the data combination scheme employed here, across CReSIS platforms, is seen to work well, it should be noted that combining data from any instrument, particularly those with a larger difference in center frequencies, may not be so effective.

It is important to note that obtaining ξ from eq. (5.4) is just one way of estimating fine-scale roughness. Self-affine (fractal) statistics (Shepard and Campbell, 1999) can also be applied to scattering models of glacier beds (Jordan et al., 2017). Additionally, in reality, fine-scale roughness is anisotropic as revealed by the 'specularity' scattering metric (Schroeder et al., 2013; Young et al., 2016). We therefore recommend that ξ should be interpreted in a qualitative manner, with lower values indicating 'fine-scale smooth' and higher values indicating 'fine-scale rough' regions of the glacier bed. In regions of complex bed topography, and in particular at outlet glacier regions, off-nadir scattering may adversely influence the signal, and lead to a breakdown in the interpretation of this metric (see Sect. 5.6.4).

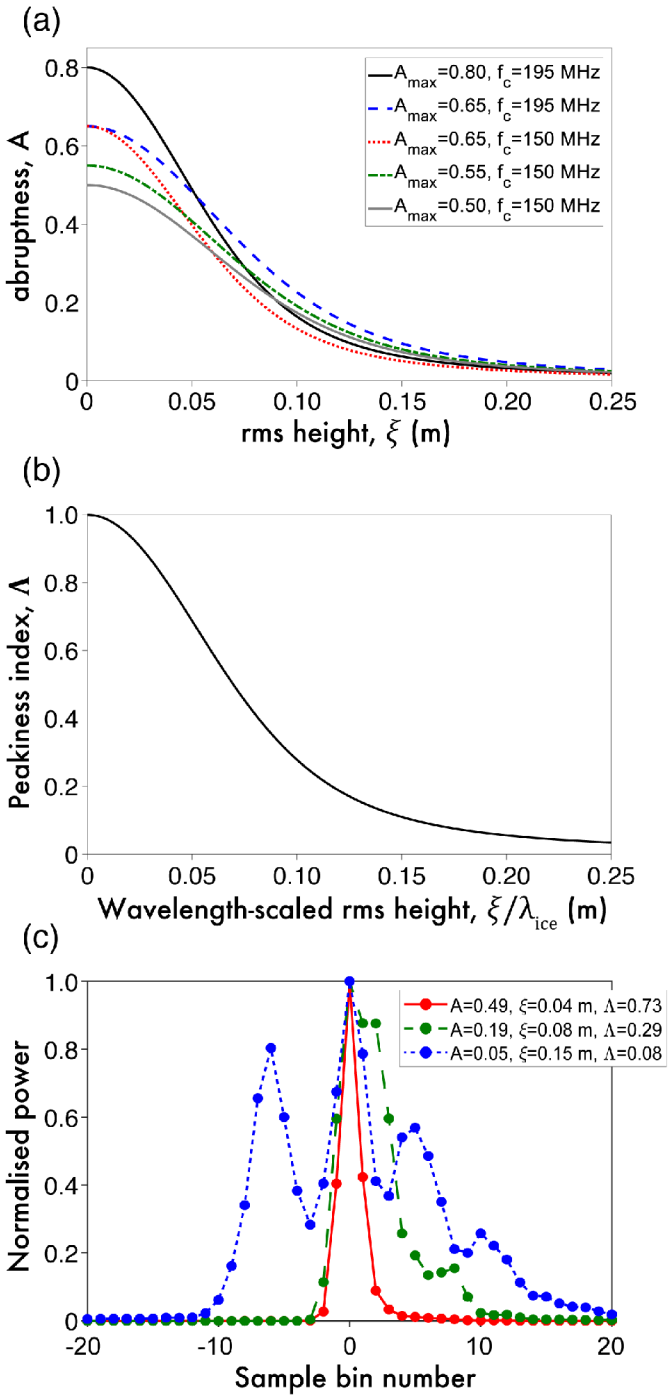

Figure 5.4: Determination of scattering-derived roughness and data combination for bed-echo peakiness. (a) Abruptness as a function of rms height for different CReSIS field seasons: solid black curve, 2010 DC8; long dashed blue curve, 2011 TO, 2011 P3, 2012 P3, 2013 P3 and 2014 P3; dotted red curve, 2006 TO; tray-dashed green curve, 2005 TO; solid grey curve, 2008 TO and 2009 TO. (b) Peakiness Index as a function of wavelength-scaled rms height. (c) Example bed-echo waveforms, their abruptness, A, peakiness-index, Λ, and scattering-derived roughness, ξ. The plots are for the 2011 P3 field season which has maximum A $\sim$0.65.

5.5 Results

5.5.1 Spatial distributions for subglacial roughness

Topographic roughness, R

Across the ice sheet, unfiltered (with respect to surface flow direction) R shows clear spatial heterogeneity (Fig. 5.5(a)); coherent signals, representing contiguous regions of both 'smooth' (low R values) and 'rough' (high R values) beds, are visible. Generally, the margins of the ice sheet have the roughest beds, where the interior is notably smooth. Ice sheet-wide, the lowest values of R are observed in the north and north-west of the island, discounting the majority of fast-flowing catchments here, notably the larger rougher 'patches' within the basins surrounding Humboldt and Petermann Glaciers. However, localised to the main 'trunks' of Petermann and Humboldt Glaciers, at the point of highest $|v|$ immediately before the grounding line, there are small patches of smooth bed observed. Broadly speaking, across the ice sheet, fast-flowing regions exhibit rough beds, though, as exemplified here, this behaviour is somewhat spatially-variable around the perimeter of Greenland. Notable examples of contiguous smooth beds near the margins include: northwest of the Camp Century (CC) drilling site; immediately north of Rink Isbræ; and, a region near the outlet of the North East Greenland Ice Stream (NEGIS) (these are marked on Fig. 5.5(a)). Perhaps understandably, the highest values of R trace the Caledonian fold belt mountain range (formed $\sim$420 Ma B.P., Henriksen, 2008) and the deep inland fjord-like systems along the east and south-eastern margins of the island (Fig. 5.5(a)).

Figures 5.5 (b) & (c) present directionally-filtered values for topographic roughness, aligned perpendicular ($R_\perp$) and parallel ($R_\parallel$) to ice surface flow direction, respectively. For improved visualisation, maps for $R_\perp$ and $R_\parallel$ were interpolated (using inverse-distance weighting) to a limit of 10 km (Figs. 5.5 (d) & (e)). This interpolation distance is representative of the average track-spacing used in the 'gridded' airborne sampling regimes in fast-flowing regions (*e.g.,* surrounding Jakobshavn Isbræ and Petermann Glacier; see Fig. 5.1). Initial comparison shows a marked difference between $R_\perp$ and $R_\parallel$, most notably within fast-flowing regions. Across the ice sheet, values for roughness suggest a more smooth aligned parallel to flow. In the ice sheet interior (where $|v| < 50$ ma^{-1}) the subglacial environment is mostly smooth in both directions (*i.e.* isotropic); however, in

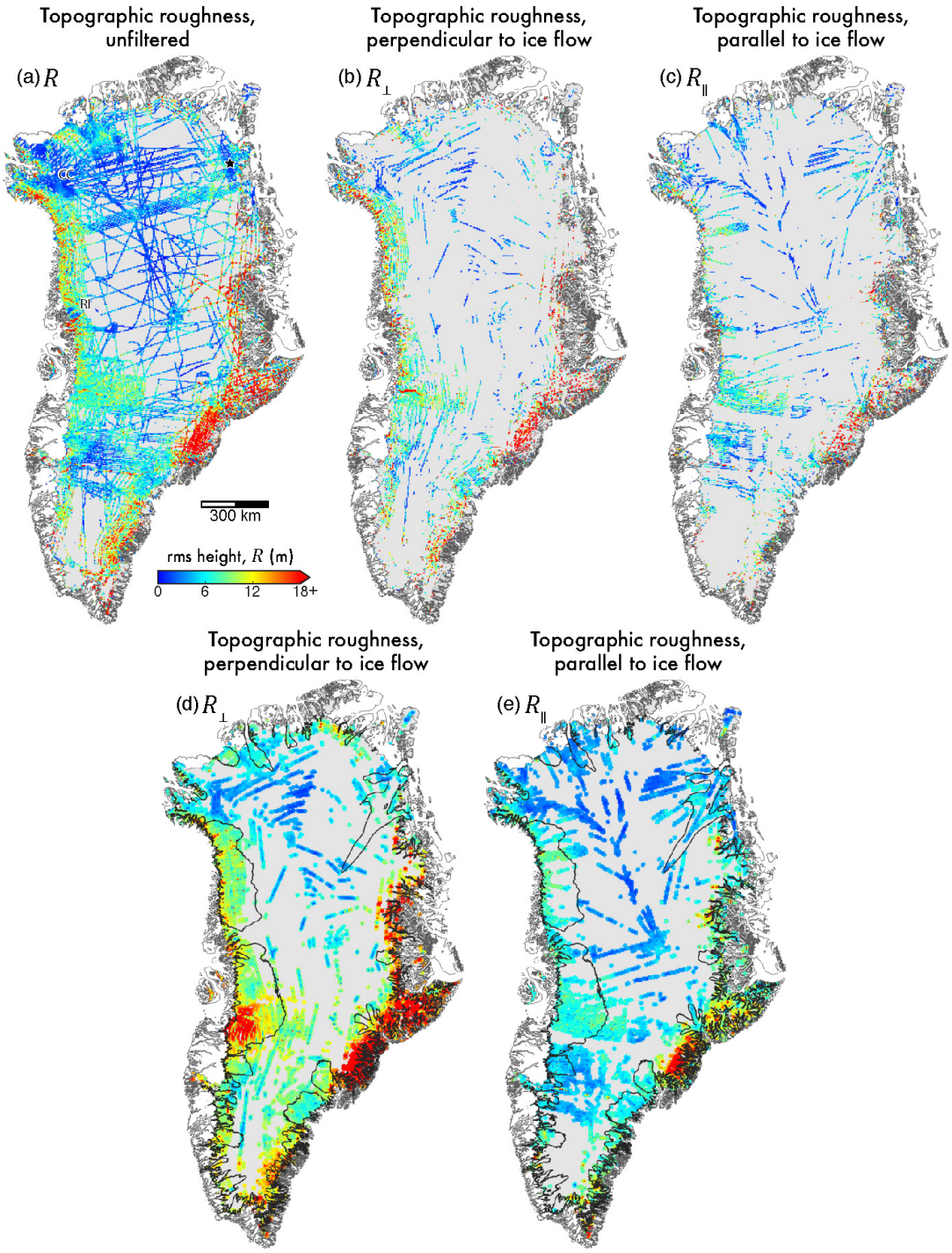

Figure 5.5: Topographic roughness (R) across the GrIS. (a) R unfiltered by flow direction. (b) $R_\perp$. (c) $R_\parallel$. (d) and (e) shows spatial interpolation of (b) and (c) to a width of 20 km, respectively, for improved visualisation.

the south of the ice sheet we observe more distinct behaviour between $R_\perp$ and $R_\parallel$ values (see Sect. 5.5.2). Overall, $R_\parallel$ exhibits more uniform roughness values across fast- and slow-flowing regions, particularly within the north and west, where $R_\perp$ presents a notable difference between fast- (rough) and slow-flowing regions (smooth).

We observe a remarkably similar spatial distribution of unfiltered R (Fig. 5.5(a)) to those previously quantified for Greenland using an rms residual technique (see Fig. 4 in Layberry and Bamber, 2001), and through a frequency-domain approach (FFTs) undertaken at a much larger length-scale (10 km; see Fig. 1 in Rippin, 2013); in these studies, general conclusions for a smooth interior and rough margin were made. Rippin (2013) additionally notes a localised smooth bed underlying the trunk of Petermann Glacier, where Layberry and Bamber (2001) notes a smooth basin for both Humboldt and Petermann glaciers. However, as these studies do not filter with respect to surface flow direction, the main differences between the quantification of the subglacial environment in this study presents notable roughness anisotropy in R across the ice sheet.

Scattering-derived roughness, ξ

Figure 5.6(a) presents the spatial distribution of scattering-derived subglacial roughness, ξ, for the GrIS. As noted (Sect. 5.4.3), these values are inversely correlated to the peakiness index (Λ; Fig. 5.6(b)), due to the scattering model relationship. The spatial distributions observed within scattering-derived roughness are broadly similar to those observed for unfiltered R, including a notable link between fast flow and high values of ξ (more rough beds). Regions that present the smoothest subglacial environment also reflect those mentioned above notably the vicinity of the CC drilling site; a coherent patch south-east of Petermann Glacier; towards the outlet of the NEGIS; and, in the vicinity of Rink Isbræ (marked on Fig. 5.6(a)). Low (smooth) values of ξ are also observed along the central ice divide. Contrasting to measures of R, however, and concordant with the broad-scale relationship of ξ to $|v|$, the fastest-flowing trunks of Humboldt and Petermann Glacier present a rougher bed. Other differences between topographic and scattering-derived roughness include a corridor of high ξ extending south of Petermann Glacier and across the ice divide (see Fig. 5.6), as well as a generally more 'mixed' roughness behaviour in the ice sheet interior.

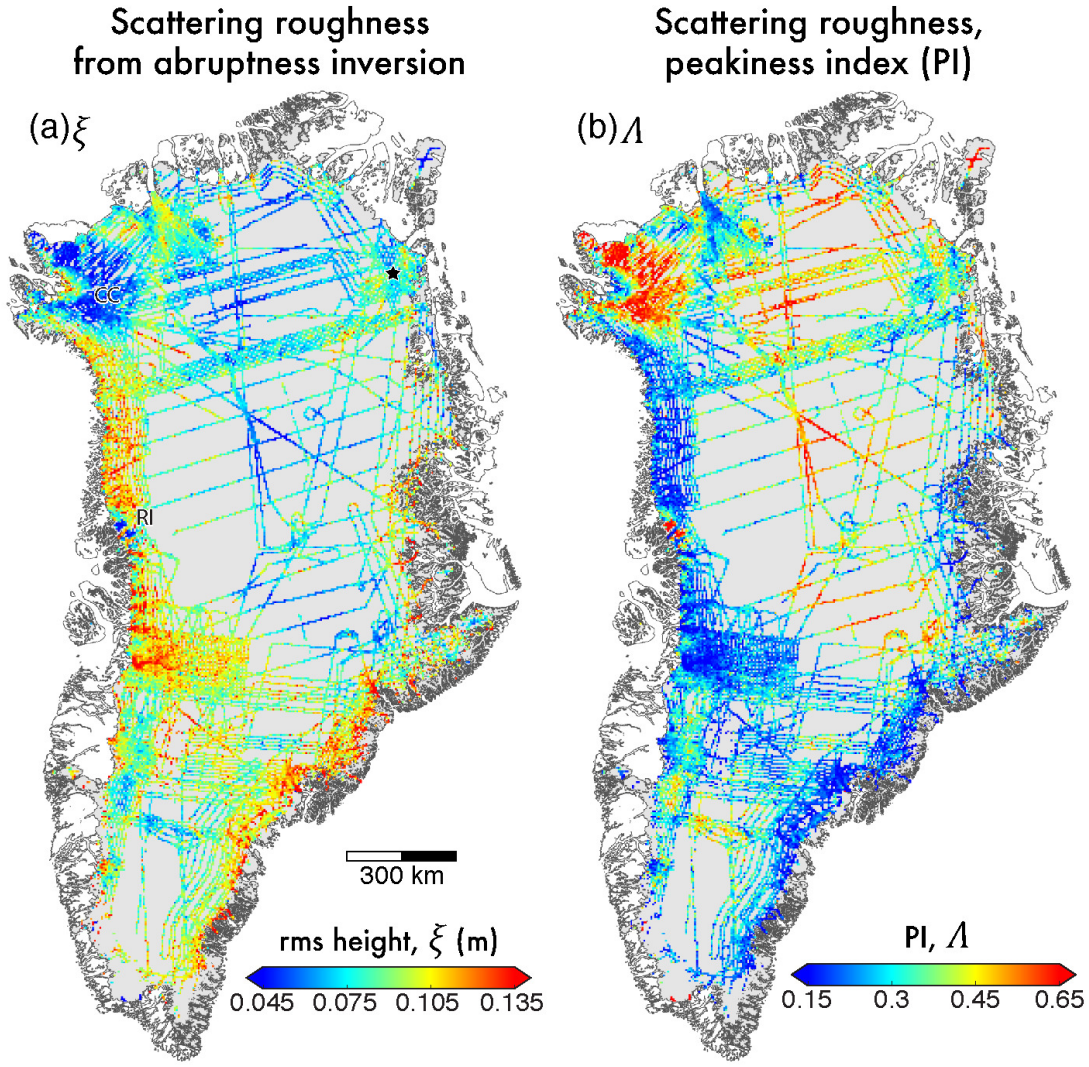

Figure 5.6: Scattering-derived roughness (ξ) across the GrIS. (a) ξ. (b) Non-dimensional peakiness index (Λ) determined from the bed-echo waveform.

Previous studies quantifying the properties of bed-echo waveforms at the bed (*e.g.*, Oswald and Gogineni, 2008, 2012) are better compared to the calculated Λ (Fig. 5.6(b)). The spatial distribution of Λ, and in particular regions of the highest Λ (smoothest beds), are remarkably similar to the spatially contiguous, large ($>$ 1,000 km^2) regions previously concluded to be thawed at the bed, or hosting ponded water (see respective Figs. 8 & 13 in Oswald and Gogineni, 2012; Oswald et al., 2018).

5.5.2 Relationship with contemporary ice velocity

Ice sheet scale

As stated, owing to the isotropic nature of ξ, we limit more comprehensive assessment of the relationship between contemporary ice velocity and subglacial roughness to topographic roughness, R, only. Figure 5.7 presents an assessment of the relationship between quantified topographic subglacial roughness R, with respect to surface ice flow direction, in fast-flowing regions ($|v| > 50$ ma^{-1}). The difference in distributions between $R_\perp$ and $R_\parallel$ (Figs. 5.7(a) & (b)) highlights that roughness perpendicular to flow direction is greater (*i.e.* more 'rough;' mean=9.39 m, compared to 6.27 m), and exhibits higher variance (92.21 m^2, compared to 43.02 m^2).

Calculated mean surface ice velocity magnitude ($|\bar{v}|$) for logarithmic bins (at 0.25 intervals) of $R_\perp$ and $R_\parallel$ are shown in Figs. 5.7(c) and (d), respectively. A marked difference between the calculated ice speed averages is observed: for all bins of $R_\perp$, $|\bar{v}|$ is seen not to exceed 250 ma^{-1}, whereby the lower bound for $|\bar{v}|$, calculated for $R_\parallel$, is > 350 ma^{-1}. This scaling relationship is broadly in agreement with those previously observed in the literature for Antarctica (Bingham and Siegert, 2007) and Greenland (Lindbäck and Pettersson, 2015); however, it is notable that this relationship is evident for the ice sheet as a whole, compared to these regional studies. Additionally, if we are to assume that $|v|$ increases with proximity to the grounding line, the exhibited scaling relationship for $R_\parallel$ is in agreement with previous studies where roughness is observed to decrease (Bingham and Siegert, 2007, 2009). Increasingly smooth beds parallel to flow direction, therefore, are indicative of fast ice velocity. The limit to which this relationship holds is $R = 10^{1.25}$ (also delineated in distribution histograms by the dashed black line in Figs. 5.7 (a) and (b)). This value is the approximate

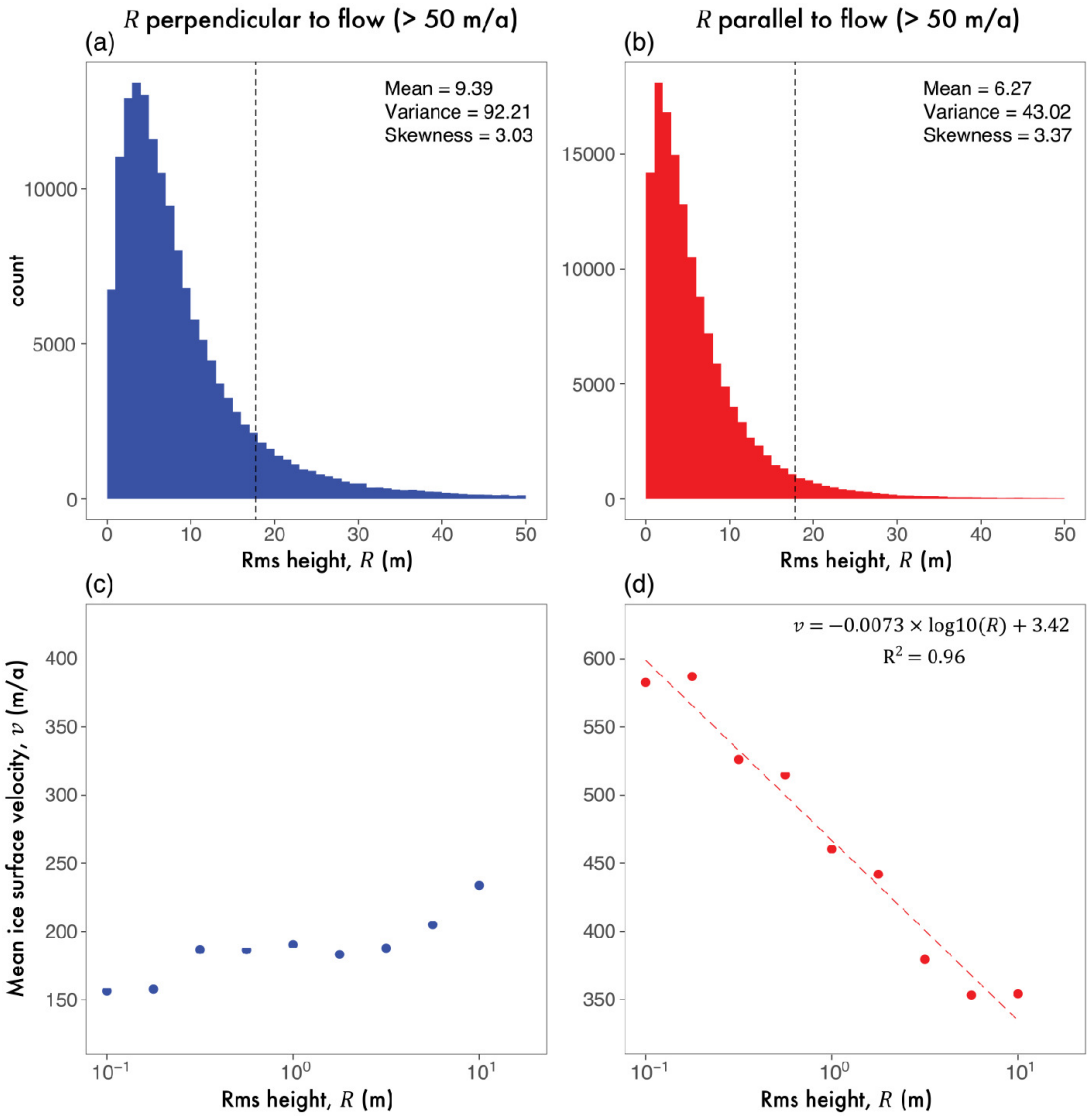

Figure 5.7: Relationship between $R_\perp$ and $R_\parallel$ and surface ice for fast-flowing ($|v| > 50$ ma^{-1}) regions of the GrIS. (a) and (b) present distributions $R_\perp$ and $R_\parallel$, respectively. (c) and (d) show mean ice surface velocity magnitude, $|v|$, calculations for logarithmic R bins (at 0.25 m intervals). This is a linear–log plot, where the limit of the horizontal axis (R) is $10^{1.25}$ m, noted by the dashed black lines in (a) and (b). It should be noted the vertical exaggeration of these two plots are constant. Colours here are consistent with Fig 5.3 (c) for alignment with surface flow direction.

upper limit of R that can reasonably quantified using eq. 5.1 (Section 5.6.4). Conversely, a weak positive relationship is observed between $R_{\perp}$ and mean ice surface velocity magnitude (Fig. 5.7(c)). $R_{\parallel}$, however, exhibits a strong negative exponential scaling relationship with mean ice surface velocity magnitude (Fig. 5.7(d)), which is statistically significant above the p =0.001 confidence level.

Figure 5.8(a) presents the spatial relationship of calculated anisotropy ratio (Ω) across the ice sheet, where coincident values of $R_{\perp}$ and $R_{\parallel}$ are quantified. It is clear that fast-flowing outlet regions (the ice sheet margins) are generally more smooth parallel to surface flow direction (where $\Omega \rightarrow -1$). In the ice sheet interior a more varied/ random distribution in Ω is apparent. Calculated mean surface ice velocity magnitude for bins of Ω, at 0.1 intervals, in fast- and slow-flowing regions (Figs. 5.8(b) & (c)), reinforces this observed spatial relationship in subglacial roughness. A strong linear relationship with regards to $|v|$ is exhibited within fast-flowing regions; in regions of slow-flow no such relationship is observed.

Fast flow regions and outlet glaciers

To assess any spatial-heterogeneity in the exhibited exponential scaling relationship, local regions of fast flow were selected. These regions are centred around important outlet glaciers (Fig. 5.9), and, where possible, encompass only individual outlet glaciers (*e.g.* Humboldt [Region 1], Petermann [2], and Kangerdlugssuuaq [4]); however, where outlets are spatially-dense, wider regions of fast flow were used (*i.e.* 'Jakobshavn+' [Region 6]). Regionally, we observe the same exponential scaling relationship as exhibited ice sheet-wide. The calculated regression line for each region is statistically significant at, or above, the p =0.01 confidence level, with the exception of Region 3 (encompassing NEGIS) at p =0.05. A marked difference in the regression gradients is also observed, spanning four orders of magnitude; where Region 3 exhibits the shallowest gradient (-1.01×10^{-1} a^{-1}), and Regions 4 & 5 have the the steepest (-9.39×10^{-4} a^{-1} and -7.66×10^{-4} a^{-1}, respectively). Echoed by the shallow regression gradient and the lower confidence level of statistical significance, the NEGIS region [3] also exhibits the lowest r-squared value (0.35). As previously described, both unfiltered R and ξ values reveal a contiguous smooth bed signal, aligned near-perpendicular to flow direction (marked on Figs. 5.5(a) & 5.6(a); further described in Section 5.6.3). 'Downstream' from this, towards the ice sheet margin, a coincident increase in

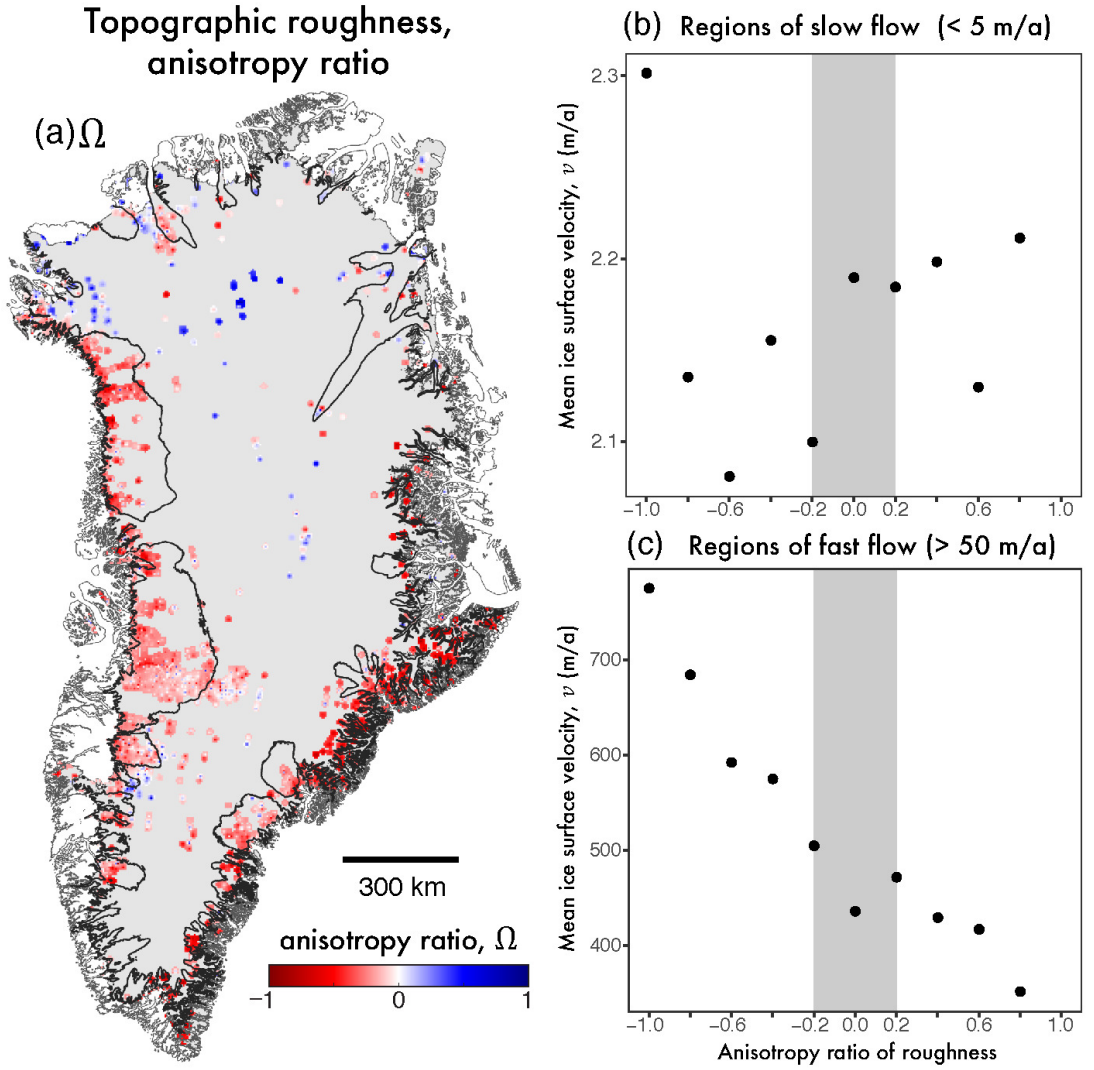

Figure 5.8: Calculated anisotropy ratio for R. (a) Anisotropy ratio, Ω, where values of -1 dictate a dominance of smoothness parallel to flow direction, $+1$ a dominance of smoothness perpendicular to flow (*i.e.* parallel roughness), and values of 0 suggest isotropy. (b) and (c) present mean ice surface velocity, $|v|$, calculated for anisotropy ratio bins (at 0.1 intervals) for slow- and fast-flowing regions, respectively.

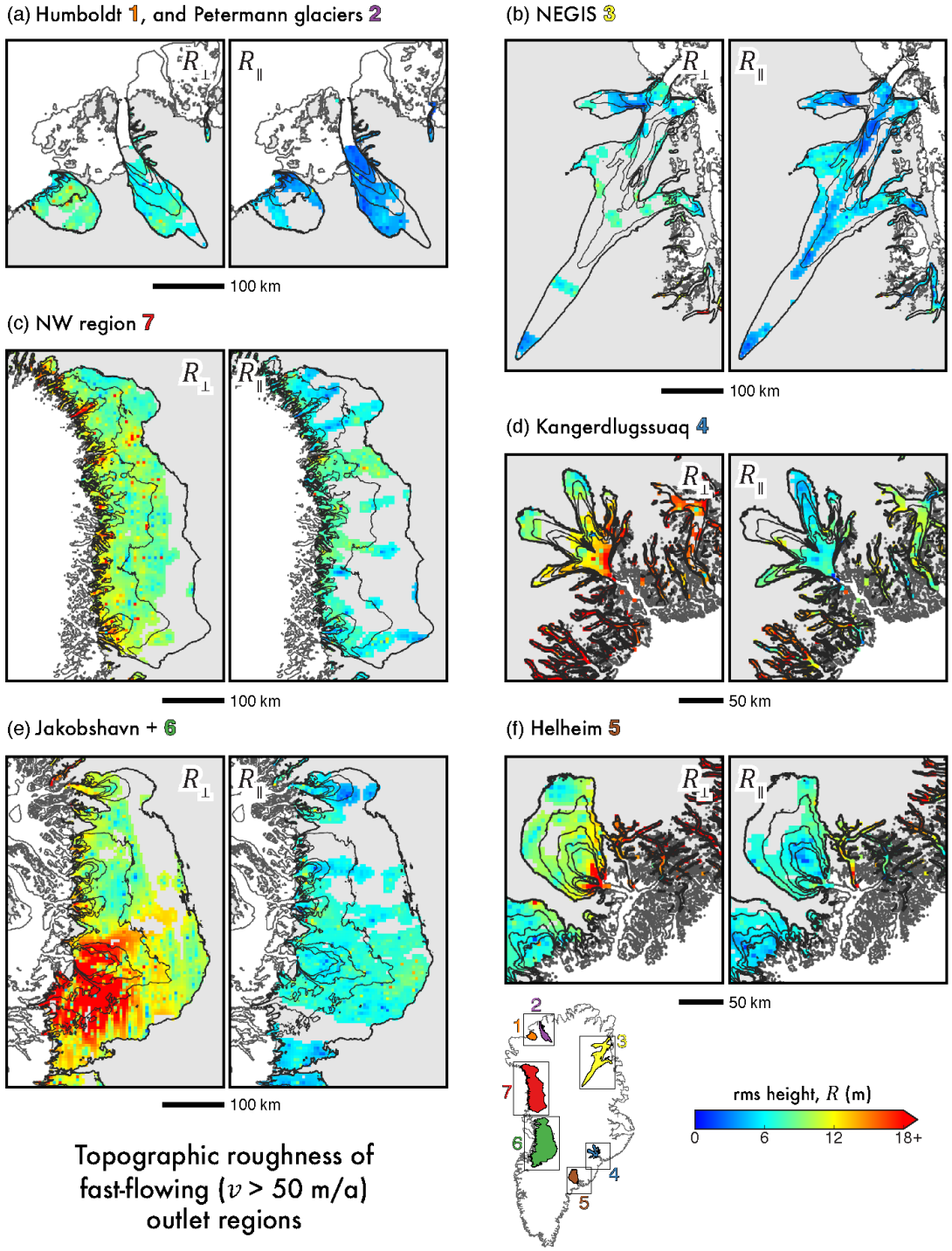

Figure 5.9: Local subsets of $R_\perp$ and $R_\parallel$ in fast-flowing outlet glacier regions. Interpolated $R_\perp$ and $R_\parallel$ (as Fig. 5.5) is shown for the fast-flowing regions of: (a) Humboldt [1] and Petermann [2] glaciers; (b) the North East Greenland Ice Stream (NEGIS) [3]; (c) the North West (NW) [7] fast flow region; (d) Kangerdlugssuaq [4]; (e) Jakobshavn Isbrae and surrounding glaciers [6]; and (f) Helheim [5]. The location of these regions is inset, where regions are colour-coded for further analysis (see Figure 5.10).

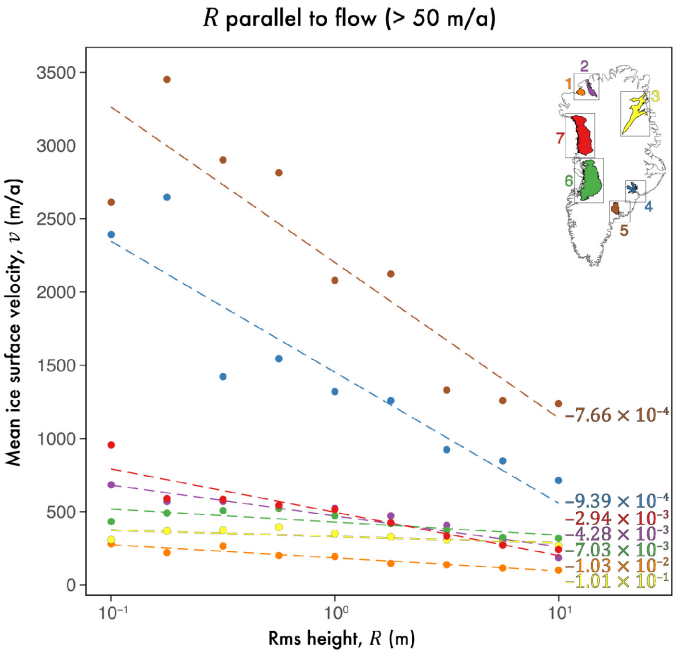

Figure 5.10: Relationship between $R_{\|}$ and surface velocity $|v|$ for fast-flowing outlet glacier regions. This is a linear–log plot as per Figure 5.7 (d), depicting the calculated mean ice surface velocity magnitude, $|v|$, for logarithmic R bins (at 0.25 m intervals) at each of the 7 regions shown in 5.9; the gradient of the linear model (with units of a^{-1}) for each region is shown in ascending order (less negative).

subglacial roughness and $|v|$ is observed. Additionally, there is a notable sampling bias in the radar sounding across Region 3, where fewer tracks are aligned parallel to the flow direction (Figs. 5.3(c) & 5.9(b)). Together, these factors may be responsible for the weaker scaling relationship observed between $|\bar{v}|$ and R.

More interestingly, however, two distinct 'groups' are observed, showing a clear separation in regression slope gradients (Fig. 5.10). The first group (see bottom; Fig. 5.10) are mostly-homogenous in terms of their regression slopes, *i.e.* the relationship between roughness and velocity magnitude here is broadly similar. However, Regions 4 & 5 in south-east Greenland (Kangerdlugsuuaq and Helheim, respectively) exhibit marked increase in gradient, indicative of a stronger scaling relationship at these sites.

5.5.3 Contiguous smooth beds in slow-flow regions

As previously described, we observe coherent, contiguous 'smooth' regions present across the GrIS across both roughness metrics (Figs. 5.5 & 5.6). These regions include north-west Greenland (around CC; Fig. 5.11); south-east of Petermann Glacier (Fig. 5.12); and bisecting central Greenland bounded west–east by Rink Isbræ and Geikie Palteau, respectively (Fig. 5.13). Owing to its isotropic nature, and inherent sensitivity to more fine-scale roughness information, we have focused on measures of ξ for these regions. High abruptness values (comparable to Λ; Fig. 5.4(b)) in several of these regions have previously been observed (*e.g.*, Fig.6(c) in Jordan et al., 2017; Oswald and Gogineni, 2012). For the most part, these are coincident with regionally high, and flat, bed elevation (Morlighem et al., 2017), slow surface ice speed (Joughin et al., 2016), and a frozen basal thermal state (MacGregor et al., 2016).

5.6 Discussion

5.6.1 Interpretation of spatial patterns

Weertman-style hard-bed sliding laws are theoretically influenced/limited by basal traction exerted on the ice column by small-scale basal 'features' (order 1 m) (Weertman, 1957; Nye, 1970; Durand et al., 2011). However, the most prevalent methods of quantifying subglacial roughness (*i.e.* through statistical analysis of along-track bed elevation, as in this study) are limited to evaluating basal information at the order of 100–1000-metres. Nevertheless, in regional studies of West Antarctica, a smooth bed has widely been considered a control on the location of fast-flowing, streaming ice (Siegert et al., 2004; Bingham and Siegert, 2009), and in constrast, slow-flowing regions have been observed to widely exhibit more-rough beds (Siegert et al., 2004; Bingham and Siegert, 2007; Rippin et al., 2006, 2014).

However, when assessed across Greenland, it is evident that the spatial relationship between subglacial roughness and $|v|$ appears to be non-universal. In direct contrast, rough beds have been observed to be coincident with contemporary fast-flowing ice both in Antarctica (Schroeder et al., 2014), and previously in Greenland (Rippin, 2013; Jordan et al., 2017). In this study, as exhibited across

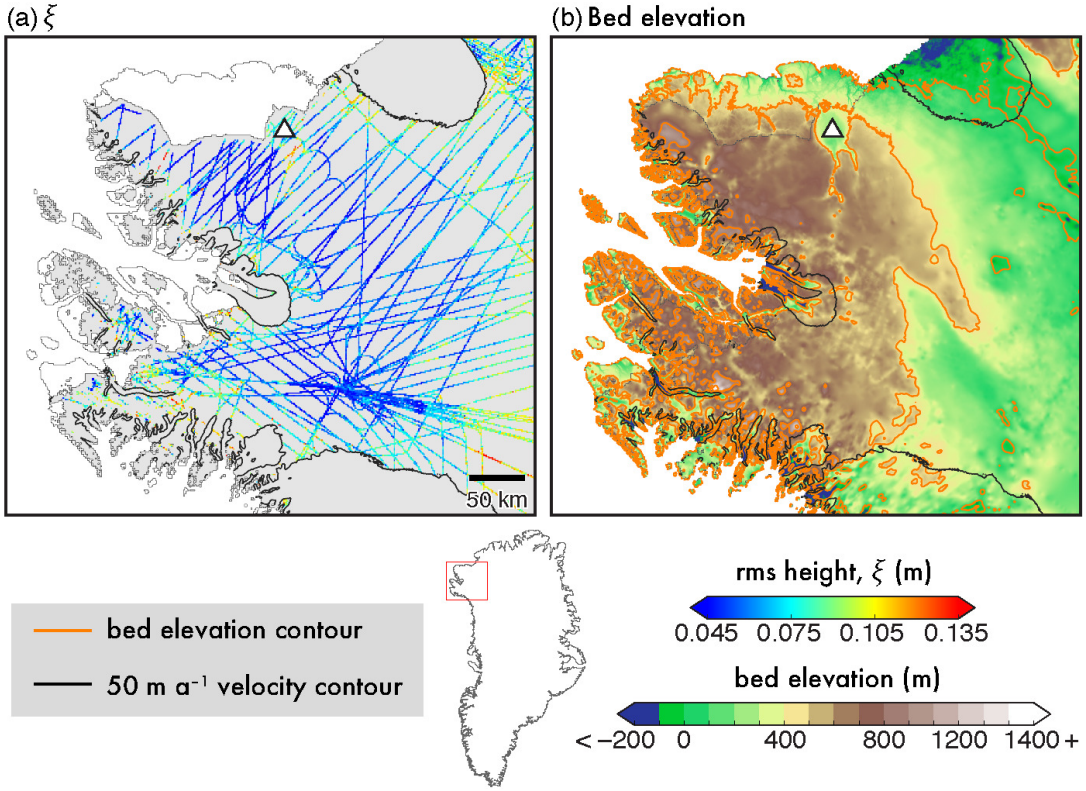

Figure 5.11: Geological interpretation using scatting-derived roughness, ξ, near Camp Century. (a) ξ, with values in fast-flowing regions (delineated by black contour; $|v| > 50$ ma^{-1}) masked. (b) Bed elevation (BedMachine, v3; Morlighem et al., 2017) with contours at 400 m intervals. Location inset.

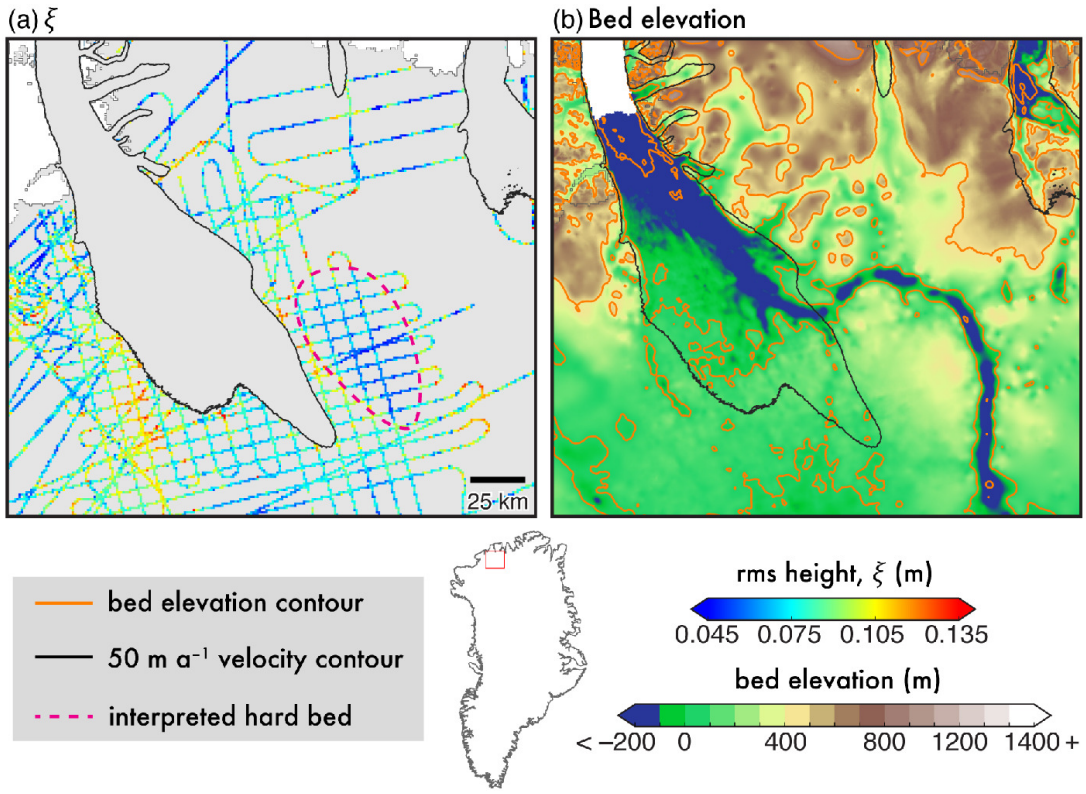

Figure 5.12: Geological interpretation using scatting-derived roughness, ξ, at Petermann Glacier. (a) ξ, with values in fast-flowing regions (delineated by black contour; $|v| > 50$ ma^{-1}) masked. Interpreted smooth, hard bedrock geology delineated by pink dashed line. (b) Bed elevation (BedMachine, v3; Morlighem et al., 2017) with contours at 400 m intervals. Location inset.

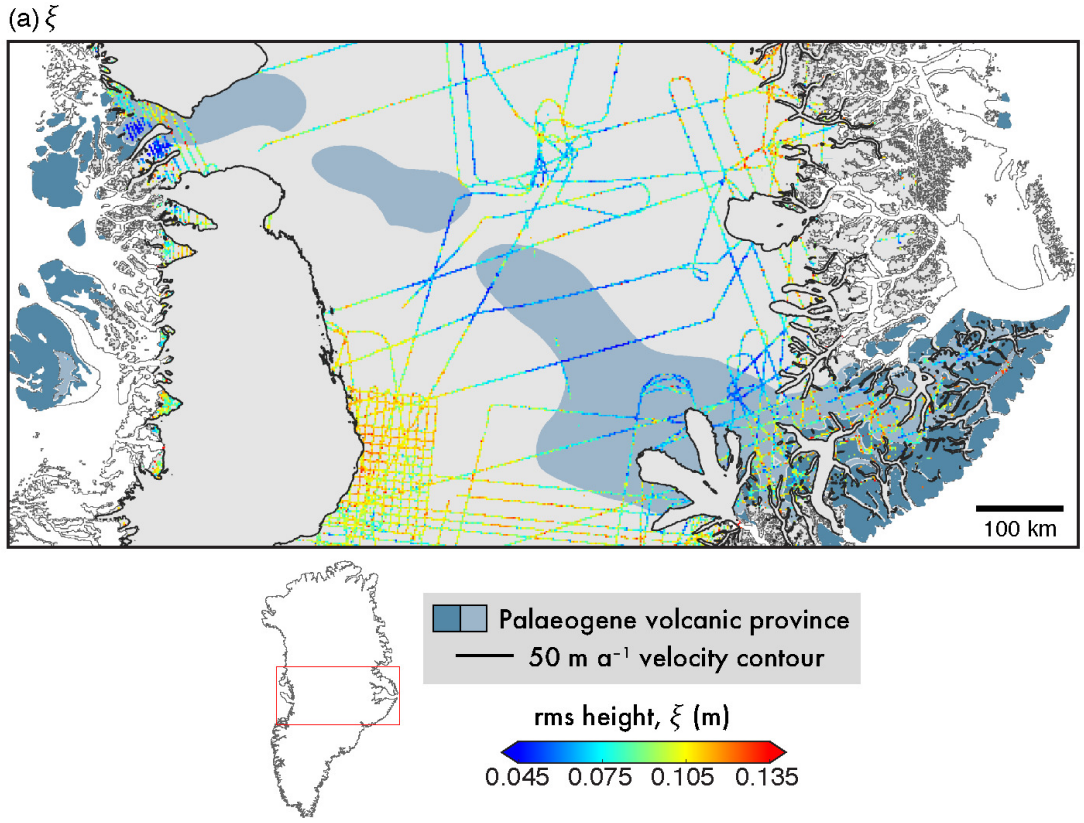

Figure 5.13: Geological interpretation using scatting-derived roughness, ξ, central Greenland. Values of ξ in fast-flowing regions are masked (delineated by black contour; $|v| > 50$ ma^{-1}). Predicted extent of Palaeogene volcanic province (Dawes, 2009) is underlain, bounded west–east by Rink Isbræ and Geikie Plateau, respectively. Location inset.

both unfiltered topographic roughness (R) and the more-fine scale, scattering-derived roughness (ξ) measure, a similar spatial relationship to $|v|$ is observed (Figs. 5.5(a) & 5.6(a)). Rough beds are seen to dominate fast-flowing regions, where slow-flowing regions are predominantly smooth. This relationship, therefore, does not fit within a classical interpretation of roughness influencing basal traction, nor does it suggest that smooth beds a a necessary condition for fast flow across Greenland. This is in broad agreement with a recent evaluation of basal motion across Greenland's outlet glaciers, whereby basal traction is concluded not to be a fundamental control under a Weertman-style hard-bed sliding law, but rather the influence of soft beds and/ or the presence of basal water (Stearns and van der Veen, 2018). Further interpretation of the relationship between subglacial roughness, namely flow-filtered topographic roughness ($R_\perp$ & $R_\parallel$), and $|v|$ is given below (Sect. 5.6.2).

Where a direct influence upon basal traction is elusive, the interpretation of subglacial roughness has been centred on geomorphic means. One such framework is outlined by Bingham and Siegert (2009), whereby smooth-bedded regions have been associated with the presence of deformable sediment, perhaps attributable to marine sedimentation (*e.g.* Rippin et al., 2006, 2011, 2014; Bingham and Siegert, 2007), or as a result of enhanced erosion resulting in topographic streamlining within bedrock (*e.g.* Siegert et al., 2005; Rippin et al., 2014). Low-lying topographic basins, particularly with a marine setting, may promote a smooth-bed owing to marine deposition/sedimentation during interglacial periods (Bingham and Siegert, 2009). In this vein, the localised, relatively smooth bed observed underlying NEGIS may be a likely candidate for deformable sediment (marked, Fig. 5.5(a) & 5.6(a)). Christianson et al. (2014) characterises the presence of subglacial till in this region through seismic analysis; this is coincident with a marine-overdeepening underlying NEGIS as well as low R and ξ values (smooth beds) as quantified in this study (Figs. 5.5(a) & 5.6(a)). More in-depth assessment of the presence of sediment, alongside the evaluation of hard (non-deformable) beds, is further discussed below (Sect. 5.6.3).

Much of the ice sheet interior is characterised as having a likely frozen basal thermal state (MacGregor et al., 2016), which, alongside low $|v|$, suggests that rates of erosion or sediment transport (deposition) is negligible. Smooth beds in regions slow-flow, have previously been characterised as markers of palaeo-ice streams, or fast flow, in regional Antarctic studies (*e.g.*, Siegert et al., 2005;

Bingham and Siegert, 2009; Lindbäck and Pettersson, 2015). Whilst such an interpretation to describe the smooth-bedded interior across Greenland (Figs. 5.5(a) & 5.6(a)) is not feasible, it may be plausible to attribute this to the waxing and waning of the GrIS over multiple interglacial cycles. However, owing to the spatial extent examined here when compared to regional Antarctic studies, an inherent complexity arises when considering the relative smooth and rough patches.

5.6.2 Interpretation of roughness-velocity scaling relationships

As noted above, the consideration of orientation within subglacial roughness interpretation is important (Gudlaugsson et al., 2013; Falcini et al., 2018), despite having been limited previously to a regional focus (*e.g.*, Bingham and Siegert, 2007; Lindbäck and Pettersson, 2015). Analysis of flow-filtered R values demonstrates a pronounced anisotropy of the subglacial roughness. Not only is this observed ice sheet-wide at crossover measures via the anisotropy ratio (Ω; Fig. 5.8), but also in the marked difference in roughness behaviour in fast-flowing regions ($|v| > 50$ ma^{-1}; Fig. 5.7). Distributions of $R_{\perp}$ and $R_{\parallel}$ values suggest that the subglacial environment of Greenland is not only more smooth aligned parallel to flow direction on average, but that $R_{\parallel}$ tends towards smaller values (Figs. 5.7(a) & (b)), giving rise to different relationships between $|\bar{v}|$ and $R_{\perp}$ and $R_{\parallel}$ (Figs. 5.7(c) & (d), respectively).

Where the length-scale of R is too great to directly relate to basal traction within a Weertman-style hard-bed sliding law (Weertman, 1957; Nye, 1970), and the low-likelihood of such a control on ice motion (Stearns and van der Veen, 2018), it is clear a different interpretation must be made with reference to the exhibited roughness-velocity scaling relationships. As such, increasing $|v|$ is unlikely to be explained by a decrease in $R_{\parallel}$ values; this change is more likely attributable to enhanced erosion or sediment transport (increasing with $|v|$), resulting in a streamlining/elongation of bed features, possibly within deformable sediment (*e.g.,* mega-scale glacial lineations (MSGLs) observed in King et al., 2009; Bingham et al., 2017). Additionally, the, albeit weak, positive relationship between $|\bar{v}|$ and flow-parallel roughness could be plausibly explained by enhanced erosion increasing cross-feature amplitude (greater $R_{\perp}$ values) of streamlined beds.

Generally, the spatial distribution of $R_{\perp}$ values present a more marked difference between fast- and slow-flow regions, when compared to values of $R_{\parallel}$. This is most likely influenced by the influence of velocity-controlled bed morphology, including both large-scale troughs/valleys linear bedforms, such as MSGLs.

The roughness-velocity scaling relationship observed parallel to flow direction is seen to be locally-variable (Fig. 5.10). The likely cause for the clear separation, or 'grouping,' within the regression gradients is due to the nature of the underlying topography. Kangerdlugsuuaq (Region 5) and Helheim (4) glaciers are classically defined as being 'topographically-constrained,' by which flow is topographically-steered to the margin through steep-sided valleys/troughs. This influences the onset of flank flow, providing more lateral control to fast-flowing ice and basal motion, impacting upon local rates of erosion and/or deposition. Although Jakobshavn Isbræ is also considered to be topographically constrained,, we do not see such a pronounced relationship for the 'Jakobshavn+' region (Region 6; Fig. 5.10). This is likely because we have conglomerated neighbouring glaciers together due to their spatial density; however, this does suggest that topography provides less lateral control in this region as remarked by Rippin (2013).

5.6.3 Interpreting a hard bed

In fast-flowing regions ($|v| > 50$ ma^{-1}), we observe mixed behaviour in subglacial roughness. Parallel to ice flow direction ($R_{\parallel}$), smooth beds are a likely a result of enhanced erosion controlled by $|v|$, whilst isotropic measures exhibit rough beds (high values of ξ and R) coincident with fast-flowing regions (Sects. 5.5.2 & 5.6.2). However, it is clear that fast flow is not a necessary condition for low roughness values (Figs 5.11–5.13). Where ice motion is thought not to be driven by basal sliding (in regions of slow-flow), a condition largely controlled by basal thermal state, rates of erosion are limited (van der Veen, 2013; MacGregor et al., 2016). It is, therefore, in these regions where we consider an alternative 'control' with regards to low ξ and R values (smooth beds), further elucidating characteristics of the subglacial environment.

High waveform abruptness (A) values, here normalised across radar sounders as Λ, have when combined with radar bed-echo reflectivity, been used to discriminate basal thermal state, where larger, contiguous regions have been associated

with bodies of electrically-deep water (Oswald and Gogineni, 2008, 2012; Oswald et al., 2018). However, recent comparison alongside ice core temperature data and a synthesis for likely basal thermal state (MacGregor et al., 2016) in north-west Greenland, shows this relationship to be largely inconsistent, particularly at the spatial scales (extent) seen here (*e.g.*, Fig. 5.11; Jordan et al., 2017). To build upon Jordan et al. (2017) we integrate existing knowledge of bed geology (Dawes, 2009) and information from complementary geophysical survey (*i.e.,* gravity and magnetic anomalies Tinto et al., 2015), to highlight that low values of ξ may indeed indicate a hard bed geology, particularly where large, contiguous regions are observed (> 1000 km^2). Due to the impermeability of igneous rocks, however, low values of ξ may also be as a result of increased water at the ice-bed interface, giving rise to increased specularity in reflected bed-echoes (high Λ).

Camp Century

Fig. 5.11 presents one such contiguous region of smooth bed in the vicinity of the CC drilling site; where an increase in ξ is observed towards the east and south-east, nearing Humboldt outlet glacier. Fast-flowing regions have been masked, owing to the isotropic nature of scattering-derived roughness, and the anisotropic behaviour of topographic roughness outlined above (Sect. 5.5.2). As the bed is likely frozen in this region (MacGregor et al., 2016), where we also observe a high elevation plateau and slow-flowing ice (and local ice divide), it is not feasible to interpret this signal as the presence of electrically-deep basal water. From the albeit limited knowledge of subglacial geology in this region (see Fig. 1 in Dawes, 2009), we predict that this signal (of low ξ) is in fact caused by a non-deformable bed, related to underlying geology overlain by little–no sediment. This surface, reminiscent of pre-glacial erosion surfaces observed in Antarctica (Rose et al., 2015), also is likely to have been largely untouched by long-term glacial erosion.

Also observed in this region are elevated ξ values coincident with a depression in bedrock topography near Hiawatha outlet glacier, associated with channelised features (triangle; Fig. 5.11). Whilst higher values of ξ may well be due to the interference from off-nadir echoes (as explained above; see Sect. 5.6.4), it is plausible that, by contrast, this may be a marker for a soft-bed (*i.e.* presence of deformable sediment), as a result of enhanced sediment transport.

Igneous intrusion, Petermann Glacier

Figure 5.12 depicts scattering-derived roughness and bed elevation near Petermann Glacier, north-west Greenland. East of the streaming ice and bounded to the north and east by the palaeofluvial 'mega-canyon' (Bamber et al., 2013b), we observe a contiguous low-ξ region where surface flow speed is < 50 ma^{-1}. This signal is observed coincident with a local topographic high (with a prominence of 300 m), which, unlike the surrounding topography, is largely left unmarked or dissected by bedrock channels. Previous geophysical interpretation, using both gravity and magnetic anomalies derived from OIB data (see Fig. 2 in Tinto et al., 2015), has established this unit as an intruded igneous body. The unaltered nature, and geological interpretation, of this feature further lend credibility to our interpretation of low ξ values as denoting a hard bed. Additionally, recent assessment of basal thermal state, and basal water prediction derived from RES, suggest that this region is not predominantly 'wet' (MacGregor et al., 2016; Jordan et al., 2018; Chu et al., 2018) further suggesting the interpretation of water ponding by high Λ is unlikely to hold here.

Volcanic province, central Greenland

Well-constrained by exposed the geology at the ice-free margins of Greenland (bounded west–east by Rink Isbræ and Geikie Plataeu, respectively), is the presence of a volcanic province from the Palaeogene (Fig. 5.13; see also Fig. 1 in Dawes, 2009); under the inland ice in central Greenland, however, the exact extent of the presence of the underlying basaltic rocks cannot be accurately determined (Dawes, 2009). At each margin of the GrIS, where $|v|$ is < 50 ma^{-1}, we see good spatial agreement between ξ and better-constrained ice-free geology. If we are to conclude that low values of ξ delineate hard-bed geology, it may then be possible to re-draw the boundary of the volcanic province further inland from the western margin (Fig. 5.13). The eastern end of this 'smooth' region is spatially-coherent with predicted elevated geothermal heat flux, as a result of the long-term tracking of the Iceland hot-spot, lithosphere thickness, and an underplated body discussed by Rogozhina et al. (2016) and Martos et al. (2018).

Delineating deformable/non-deformable beds

In many assessments of subglacial roughness in Antarctica, smooth beds have been associated with the presence of deformable sediment beneath fast-flowing outlet glaciers (*e.g.,* Bingham and Siegert, 2009; Rippin et al., 2014; Bingham et al., 2017) (Sect. 5.6.2). It is clear from the above examples, however, that fast flow is not a necessary condition for large, coherent regions of 'smooth' bed. Where basal conditions are not indicative of enhanced basal motion (*i.e.,* slow-flowing, cold-based regions), we suggest that low values of ξ are indicative of a non-deformable, hard bed. Whilst we reject that such contiguous signals as evident here are evidence of ponded basal water, or indeed basal thaw, it is plausible that small-scale patches of high abruptness values (high Λ/ low ξ values) could still be interpreted this way.

If we are to extend our conclusion that ξ may be used to demarcate underlying hard beds, focus should then also be drawn to regions where sediment transport is likely to take place. As discussed, the majority of fast-flowing outlet regions exhibit high values of ξ (Fig. 5.6(a); and unfiltered R, Fig. 5.5(a)); which, by $R_{\|}$, we interpret as exhibiting basal 'streamlining' influenced by $|v|$ (akin to that observed by Bingham et al. (2017), albeit at a different scale). This, alongside the recent evaluation that many of Greenland's outlet glaciers are driven by the availability of sediment (Stearns and van der Veen, 2018), may suggest that high values of ξ may well be useful additionally as a proxy to demarcate deformable beds.

Contrastingly, however, a markedly smooth region (low ξ and R values) beneath NEGIS is quantified across both roughness metrics (star; Figs. 5.5(a) & 5.6(a)). This catchment also appears to show the weakest relationship with regard to surface ice speed and flow direction. The contiguous smooth signal near the margin extending north–south, and near-perpendicular to flow direction, is coincident with low bed elevation. As previously noted, where the subglacial topography here exhibits a large marine over-deepening, this is a candidate for marine sedimentation (*e.g.*, Bingham and Siegert, 2009; Christianson et al., 2014).

5.6.4 Roughness scale-separation and breakdown in complex terrain

As the quantification of topographic roughness (R) uses defined length-scale (L =200 m), the interpretable scale of subglacial roughness information, and roughness 'features,' is fixed at this order of magnitude; however, understanding the scale of information provided by scattering-derived roughness (ξ), and the scale-separation between both roughness measures, is not only more complex, but likely to be variable across the ice sheet. Theoretically, scattering-derived roughness is sensitive to roughness information at, or between, the scale of wavelength (order 1-metre) and that of the Fresnel zone (order 100-metres) (Shepard and Campbell, 1999). However, as the observed spatial distribution of ξ is seen to be broadly similar to that of unfiltered R (Figs. 5.5(a) & 5.6(a), respectively), it may be reasonable to suggest that this measure (scattering-derived roughness) may be more appropriately interpreted as defining roughness characteristics at the larger scale.

Local topography ultimately leads to the breakdown of both subglacial roughness metrics presented here, but also likely affects the degree of scale-separation across the ice sheet. Notably, this occurs where a large step-change is observed in bed elevation is observed ('cliff-like' regions; *i.e.* deep subglacial valleys/trough). In these regions bed-echoes are likely to exhibit more diffuse waveform characteristics due to off-nadir echoes from the valley sides; these will present erroneously high values of ξ (a 'false' rough ice-bed interface), thus adversely affecting interpretation. For this reason, it may be sensible to use quantified values of topographic roughness to infer whether values of ξ are providing useful information. For example, if coincident measures of R and ξ are low (topographically smooth), and high, respectively, it may be clear that the subglacial environment is exhibiting more fine-scale roughness information.

Additionally, it is important to note that measures of R also breakdown in similarly complex terrain, where cliff-like changes in along-track bed topography fall within the sampling window. An example of this is illustrated by the transparent grey bar on Fig. 5.2. Both metrics, however, assume a Gaussian distribution about a mean surface; where local topography exhibits such step-changes it appears that this statistical model for roughness no longer holds. As such, the main conclusion we draw in this study with regard to R and ice-sheet motion remains

unaffected, as the exhibited exponential scaling relationship (Figs. 5.7(d)) holds for the lower-end of $R_{\parallel}$ values ($R_{\parallel} \leq 10^{1.25}$), accounting for the vast majority of calculated values in fast-flowing regions.

5.7 Summary and Conclusions

Here, we have presented the first systematic approach to quantifying subglacial roughness across the GrIS using two independent methods: statistical analysis of topography, and the properties of the bed-echo waveform/scattering. Not only have we provided updates to the 'maps' of the spatial distribution of subglacial roughness characteristics in Greenland (*c.f.*, Layberry and Bamber, 2001; Rippin, 2013), but we have been able to investigate further its relationship with ice-sheet motion and other spatially-heterogenous aspects of the subglacial environment. For our measure of topographic roughness (R), we have provided near-complete spatial coverage, making use of data from all publicly-available CReSIS radar sounding campaigns (1993–2016). Filtering R with respect to surface ice velocity characteristics (*i.e.,* speed and direction) has enabled the assessment of roughness anisotropy both at the ice sheet scale and more-locally in certain regions and at specific outlet glaciers.

Values for subglacial roughness, quantified using both topographic- and scattering-derived metrics, suggest that the majority of fast-flowing outlet glaciers are underlain by rough beds, when roughness direction is not included in the analysis. This suggests that enhanced glacier flow (*i.e.,* basal sliding) in Greenland is unlikely to be controlled by basal traction, following a Weertman-style hard-bed sliding parametrisation (Weertman, 1957). It is clear, however, that there is pronounced anisotropy in topographic roughness with respect to ice flow direction, in fast-flowing regions ($|v| > 50$ ma^{-1}), whereby topographic roughness exhibits an exponential scaling relationship with ice velocity parallel, but not perpendicular, to flow direction. At the length-scale used to calculate topographic roughness (*i.e.,* 200 m), the observed anisotropy and scaling relationships observed are likely due to enhanced rates of subglacial erosion resulting in a streamlining of bed features, possibly within deformable sediment (*e.g.,* MSGLs observed in King et al., 2009; Bingham et al., 2017). We, therefore, suggest that consideration of roughness anisotropy is required with a view to infer relationships with ice motion

and subglacial processes. Additionally, in many slow-flowing regions we conclude that contiguous smooth regions of the bed are likely due to the presence of hard-bed geology, rather than the presence of deformable sediment. In this vein, this study provides scope for a spatially variable soft bed/hard bed (deformable/non-deformable) boundary constraint for ice sheet models.

Chapter 6

Surface expressions of the Greenland Ice Sheet

6.1 Preface

For the most part, this chapter has been published in *Geophysical Research Letters*, under the full citation:
Cooper, M. A., Jordan, T. M., Siegert, M. J., and J. L. Bamber (in review), Surface expression of basal and englacial processes on the Greenland Ice Sheet, *Geophys. Res. Lett., 46.* https://doi.org/10.1029/2018GL080620

The analysis, interpretation, and writing were conducted by M. A. Cooper, with the remaining authors providing guidance, insight, and review. Further helpful to this chapter were provided at the review stage by Matteo Spagnolo and an anonymous reviewer. The bulk of this chapter remains unchanged to that published. However, 'supplementary information' for this manuscript has been added in-line where appropriate. Some additional work was conducted outside of the scope of the submitted manuscript; this work is also is presented here following the manuscript conclusions (see Section 6.7).

6.2 Abstract

Radar-sounding surveys measuring ice thickness in Greenland have enabled an increasingly "complete" knowledge of basal topography and glaciological processes.

Where such observations are spatially limited, bed elevation has been interpolated through mass conservation or kriging. Ordinary kriging fails to resolve anisotropy in bed geometry, however, leaving complex topography misrepresented in elevation models of the ice sheet bed. Here, we demonstrate the potential of new high-resolution ($\leq$5 m) surface topography data (ArcticDEM) to provide enhanced insight into basal and englacial geometry and processes. Notable surface features, quantified via residual surface elevation, are observed coincident with documented subglacial channels, and new, smaller-scale tributaries (<2,000 m in width) and valley-like structures are clearly identified. Residual surface elevation also allows the extent of basal ice units to be mapped, which in conjunction with radar data indicate that they act as "false bottoms," likely due to a rheological contrast in the ice column.

6.3 Introduction

Advances in understanding basal processes of the Greenland Ice Sheet (GrIS) have primarily been driven by the need to refine projections of the ice sheet's response to climate change using numerical models. An increase in observations of ice thickness, obtained using airborne ice-penetrating radar (hereafter termed, radio-echo sounding, RES), has enabled improved representation of Greenland's bed topography and, consequently, the production of progressively accurate and spatially "complete" (without holes) bed digital elevation models *DEMs; e.g.* Bamber et al., 2001, 2013a; Morlighem et al., 2014, 2017). RES data, therefore, provide a necessary input to ice sheet modeling and also allow for the assessment of more specific basal and englacial properties, including subglacial roughness and its anisotropy (*e.g.* Rippin, 2013; Lindbäck and Pettersson, 2015; Jordan et al., 2017; Chapter 5 of this thesis); ice rheology, through the measurement of englacial stratigraphy (*e.g.* Karlsson et al., 2013; MacGregor et al., 2015a); englacial temperature from radar attenuation (*e.g.* MacGregor et al., 2015b); and determining the distribution of basal water from bed-echo reflectivity (*e.g.* Jordan et al., 2018; Oswald et al., 2018). Despite the influence of basal processes upon ice dynamics being theoretically well constrained (Cuffey and Paterson, 2010; van der Veen, 2013), our understanding of spatial variation in subsurface conditions and processes remains restricted by the paucity of RES data; conse-

quently, observation-led interrogation is required to understand the magnitude of their effects *in situ*.

While the number of RES ice-thickness observations has roughly tripled in the past decade there remain large swathes of the GrIS left unobserved (see Figure 3.4 in this thesis, after Morlighem et al., 2017). Limitations in RES coverage, and spatial bias due to variation in observation density often result in the mapping and assessment of basal geometry and processes being reliant on spatial interpolation between flight tracks. Interpolation has primarily been applied to bed topographies (Bamber et al., 2013a; Morlighem et al., 2017), but also the tracing of englacial stratigraphy (MacGregor et al., 2015a; Bons et al., 2016), and the mapping of subglacial roughness (Rippin, 2013). Interpolated bed DEMs have enabled the "discovery" of large-scale landscape systems beneath the GrIS (*e.g.* Bamber and Aspinall, 2013; Cooper et al., 2016; Livingstone et al., 2017) confirming that the identification of more nuanced interrelationships between basal topography and the overlying ice is now possible. In this vein, process-based assessments have attempted to understand the relationship between ice flow and bed topography, with focus on aspects of landscape genesis, evolution, preservation and inheritance in Antarctica (Rose et al., 2013; Ross et al., 2014; Rose et al., 2015; Bingham et al., 2017) and Greenland (Cooper et al., 2016, Chapter 4 of this thesis; Livingstone et al., 2017).

The most recent data sets for Greenland bed topography have employed a "mass conservation" interpolation between flightlines in fast-flowing regions (Morlighem et al., 2014, 2017). However, the majority of the bed in the latest product (BedMachine v3, referred to here as BM3), primarily the slow-flowing ice sheet interior, was interpolated using ordinary (isotropic) kriging (Figure 3.4 after Morlighem et al., 2017). In observation-sparse areas, this approach generates surfaces that fail to represent the "true" geometry of anisotropic basal features (i.e., quasi-linear geometries): Rendered surfaces can appear artificially smooth (Williams et al., 2017), or result in "bulls-eye" anomalies manifesting as a series of isolated peaks and/or hollows (Dentith and Mudge, 2014). Although BM3 is provided at a posting of 150 m, the true resolution of the estimated surface is dependent upon the local observation density (*i.e.* the level of clustering) and sampling regime (*i.e.* the flight-line spacing) (Morlighem et al., 2017). Since parallel track spacing over the ice sheet interior is up to 75 km, it is important, therefore, to consider the need for a spatially consistent method through which

to assess basal morphology and associated basal and englacial processes without the artefacts associated with interpolation.

The transfer of basal information from "bed-to-surface" has long been appreciated, with knowledge of local ice velocity and flow parameters being used to calculate bed topography along a profile of the surface (Budd, 1970). More recently, surface and subsurface data have been used to better constrain this transfer of basal information, with particular reference to spatial variability in basal traction (Gudmundsson, 2003; Gudmundsson and Raymond, 2008; De Rydt et al., 2013). However, it is widely understood that local variations in flow regime and surface topography are more suitably explained by undulations in subglacial topography (De Rydt et al., 2013). It is yet to be determined whether this modelled basal transfer (as in Gudmundsson, 2003) can be applied generally, especially where ice thickness and speed vary considerably. This is perhaps exemplified through the application of mass conservation interpolation being limited to regions of fast flow (Morlighem et al., 2014, 2017). While recent efforts have been made to characterize basal information transfer across the interior of the GrIS, where velocity is low and basal slip is spatially heterogenous, the success of this is limited to more large-scale patterns, arguably by computational means(Ignéczi et al., 2018; Ng et al., 2018). Outside theoretical frameworks, and particularly in the interior of Antarctica, numerous observational studies have demonstrated the relationship between surface and basal geometry (Rémy and Minster, 1997; Rose et al., 2014; Ross et al., 2014; Rose et al., 2015; Le Brocq et al., 2008). For example, subglacial lakes manifest as flat surfaces in the overlying ice sheet, due to the negligible basal friction above them (Ridley et al., 1993; Siegert and Ridley, 1998). Such research has benefited from high accuracy ice sheet surface topography, including analyses of surface curvature, to determine bed features and subglacial landscape (Le Brocq et al., 2008; Rose et al., 2014; Ross et al., 2014; Rose et al., 2015)

While both ice surface observation- and model-led approaches reveal important information about subsurface processes in areas of sparse observational data, much of the small-scale topography of the Greenland interior remains uncharted; this is primarily due to the relative coarseness (spatial resolution) of previously available surface imagery (*e.g.*, Moderate Resolution Imaging Spectroradiometer surface brightness, as used in Ross et al., 2014), and the complexities in modeling transfer of information from bed to surface (De Rydt et al., 2013). However, with

the recent release of a new high-resolution ($\leq$5 m) pan-Arctic DEM (ArcticDEM; Morin et al., 2016; https://www.pgc.umn.edu/data/arcticdem/), there is an opportunity to improve our knowledge of spatially heterogeneous basal conditions using the ice surface topography rather than, or in conjunction with, RES data.

Here, we explore the potential for ArcticDEM ice surface information—specifically the residual surface elevation (RSE)—to provide a "lens" for subsurface processes in Greenland. From this, we present evidence for previously undocumented complex basal topographies, and characterize the influence of ice dynamics on the ice surface. We also provide evidence that some surface expressions are likely a result of englacially discrete, rheological boundaries, and improve the mapping of "units of disrupted radiostratigraphy" (UDRs) (Bell et al., 2014; Wolovick et al., 2014; Dow et al., 2018; Vieli et al., 2018). We compare results inferred from surface data with BM3 and highlight the importance of topographic anisotropy and scale both in the planning of geophysical surveys and spatial interpolation. Finally, to understand the relationship between the surface expression and basal processes we compare with complementary data sets: basal water (Jordan et al., 2018), geothermal heat flux (Martos et al., 2018), basal slip (MacGregor et al., 2016), and ice velocity (Joughin et al., 2016, 2017).

6.4 Calculating RSE

The ArcticDEM is a newly released collection of Earth surface DEMs produced using high-resolution ($\sim$0.5 m) stereopair imagery, collected by DigitalGlobe Inc. optical satellites. The DEM is supplied by the Polar Geospatial Center in two formats: the "ArcticDEM Strip" format (2-m resolution) and tiled "Mosaic" format (5-m resolution). The Mosaic format was used here owing to both its spatial regularity (50 km 50 km; 2,500-km^2 tiles), increased data coverage, improved absolute accuracy, and fewer artefacts. A total of 36 tiles, covering an area of $\sim$90,000 km^2 over northwest Greenland, south of Petermann Glacier, defines the study region (6.1). This region was chosen due to its relatively high, and spatially dense, coverage of RES data (6.1; additionally, studies mapping and understanding of both englacial (*e.g.,* Bell et al., 2014; Chu et al., 2018) and basal features/properties (*e.g.,* Bamber et al., 2013b; Livingstone et al., 2017) have also focused on this region. This facilitates both the comparison and val-

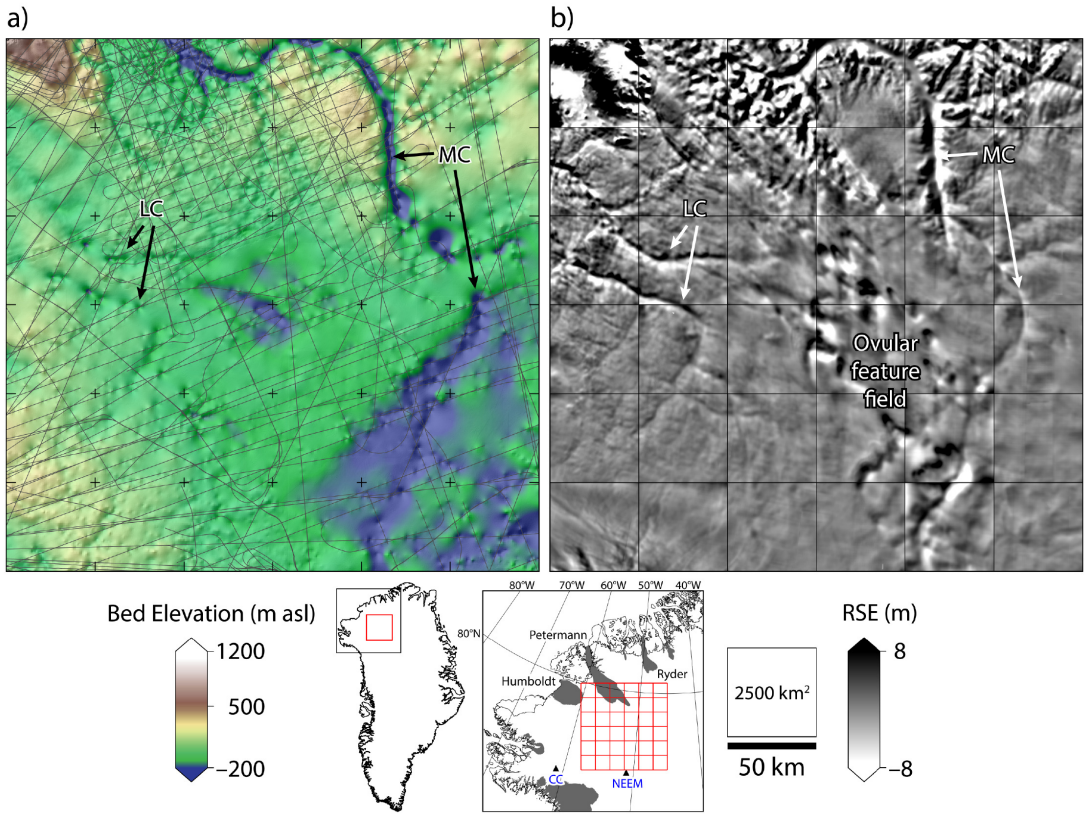

Figure 6.1: Bed topography and RSE for Northwest Greenland. Study location inset, including: fast-flowing ice (> 50 ma^{-1} [grey]); and ice core drilling sites. (a) BM3 (Morlighem et al., 2017). RES survey coverage (dark grey). (b) RSE. Red and black grids show the spatial extent of individual ArcticDEM tiles; labels LC and MC refer to subglacial channel systems, documented by Livingstone et al. (2017) and Bamber and Aspinall (2013), respectively.

idation of this paper's conclusions, in order to better assess the capability of high-resolution surface information in extracting subsurface information.

Ice sheet surface topography (Figure 6.2) is influenced by underlying basal conditions (i.e., geometry) and processes (*e.g.* Rémy and Minster, 1997; Gudmundsson, 2003). Compared to the dominant signal of an ice sheet's surface slope (which is approximately parabolic, or dome-like), however, this influence yields a much smaller change at the ice surface, both in terms of amplitude and wavelength. To help resolve the influence of basal geometry, large-scale surface slopes must be removed. We calculated a third-order polynomial trend surface for each ArcticDEM tile, using least squares regression, to detrend surface topography, leaving the RSE (Figure 6.4(b)). The RSE preserves local surface features

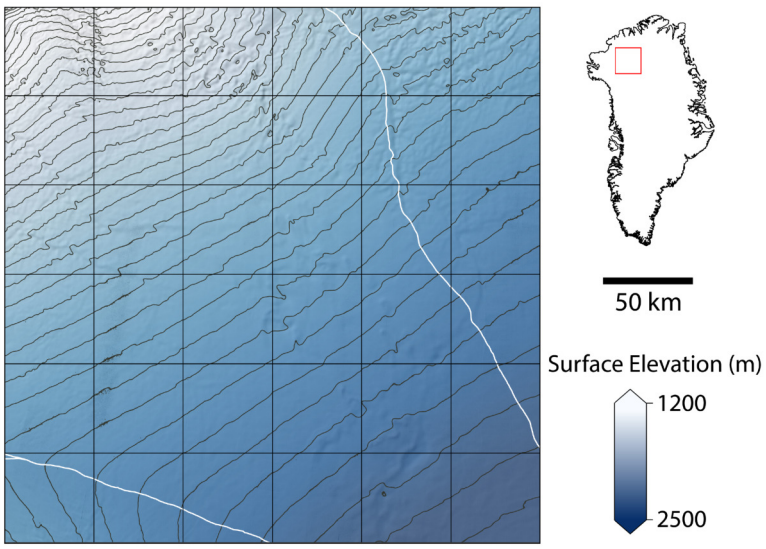

Figure 6.2: Ice sheet surface digital elevation model (ArcticDEM; Morin et al., 2016). Data are provided at a 5 m spatial resolution in individual 2500 km^2 (50-km-by-50-km) tiles, as per black grid. Elevation contours (dark grey) are at 50 m intervals. Major GrIS drainage basins are delineated (white; Zwally et al., 2012). Location inset.

down to a minimum wavelength of about 1 km, which are then interpreted as manifestations of basal topography or englacial surfaces (Section 6.5). While the ArcticDEM boasts a much finer scale than this, it is probable that smaller-wavelength features are not resolvable due to the dampened transfer of basal information as a result of ice thickness (De Rydt et al., 2013); for such features "direct" observation using RES data are likely necessary. Additional second- and fourth-order polynomial surfaces were used; however, no marked improvement, in terms of interpretable "features," was observed. By contrast, the third-order surface performed better over ice divides and at ice margins when compared to fitting a second-order polynomial.

Various feature extraction methods have been employed to obtain bed geometry from ice surface topographies, and surface brightness. This includes edge detectors (*e.g.* Ekholm et al., 1998) and isolating local topographic change through the calculation of profile curvature (of Moderate Resolution Imaging Spectroradiometer imagery, *e.g.*, Ross et al., 2014). While these methods are usually dimensionless (without vertical information) and only reveal relative changes at the bed, spatial patterns in basal geometry can still be interpreted. We repeated

these approaches for the new ArcticDEM (Figures 6.3a–c), alongside a calculation of RSE for a more coarse surface topography (90-m resolution) DEM (6.3(d); Greenland Ice Mapping Project, GIMP; Howat et al., 2014). Although a 30-m GIMP DEM is available, the latter comparison was undertaken to explicitly assess whether topography at a greater spatial resolution (i.e., ArcticDEM) can provide enhanced subsurface information. RSE calculated for the 30-m GIMP DEM provides a near-similar level of information provided by the ArcticDEM; however, for the purpose of this paper we rely on the new, and higher-resolution ArcticDEM for further analysis.

6.5 Interpreting surface expressions

RSE (Figure 6.1(b)) can be interpreted similar to a relative DEM, where surface undulations are attributed to bed undulations or, as we later demonstrate, basal-englacial UDRs. Various geometric features, including lineations, troughs, and peaks, are visible in the RSE. Interpretation of these features is facilitated by the comparison with BM3, (Morlighem et al., 2017) and along-track radargrams from National Aeronautics and Space Administration's Operation IceBridge ((Rodriguez-Morales et al., 2014); Figure 6.1(a), as well as with complementary data sets (Figure 6.4), including interferometric synthetic aperture radar-derived surface ice velocity (Joughin et al., 2016), radar-derived basal water (Jordan et al., 2018), and magnetic-derived geothermal heat flux (Martos et al., 2018). On initial comparison to BM3, the RSE (Figure 6.1(b) replicates fundamental landscape features. Most notably these are large, and previously documented, dendritic channel networks, such as the "mega-canyon" flowing toward Petermann Glacier (Bamber et al., 2013b), and the two channels linked with Humbolt Glacier (Livingstone et al., 2017; MC and LC, respectively; Figure 6.1(a)). Further, RSE broadly simulates the overall trends in basal topography (acting similarly to a topographic "hillshade," Figure 6.4(a), and in observation-sparse regions it delineates previously undocumented morphological features (see sections 6.5.1 and 6.5.2 and Figure 6.1(b)). This confirms that the ice surface can be used to explore basal geometries, which are poorly constrained by the shortcomings of isotropic interpolation between sparse/transect-based observations.

There are, however, notable signals and features present in the RSE that

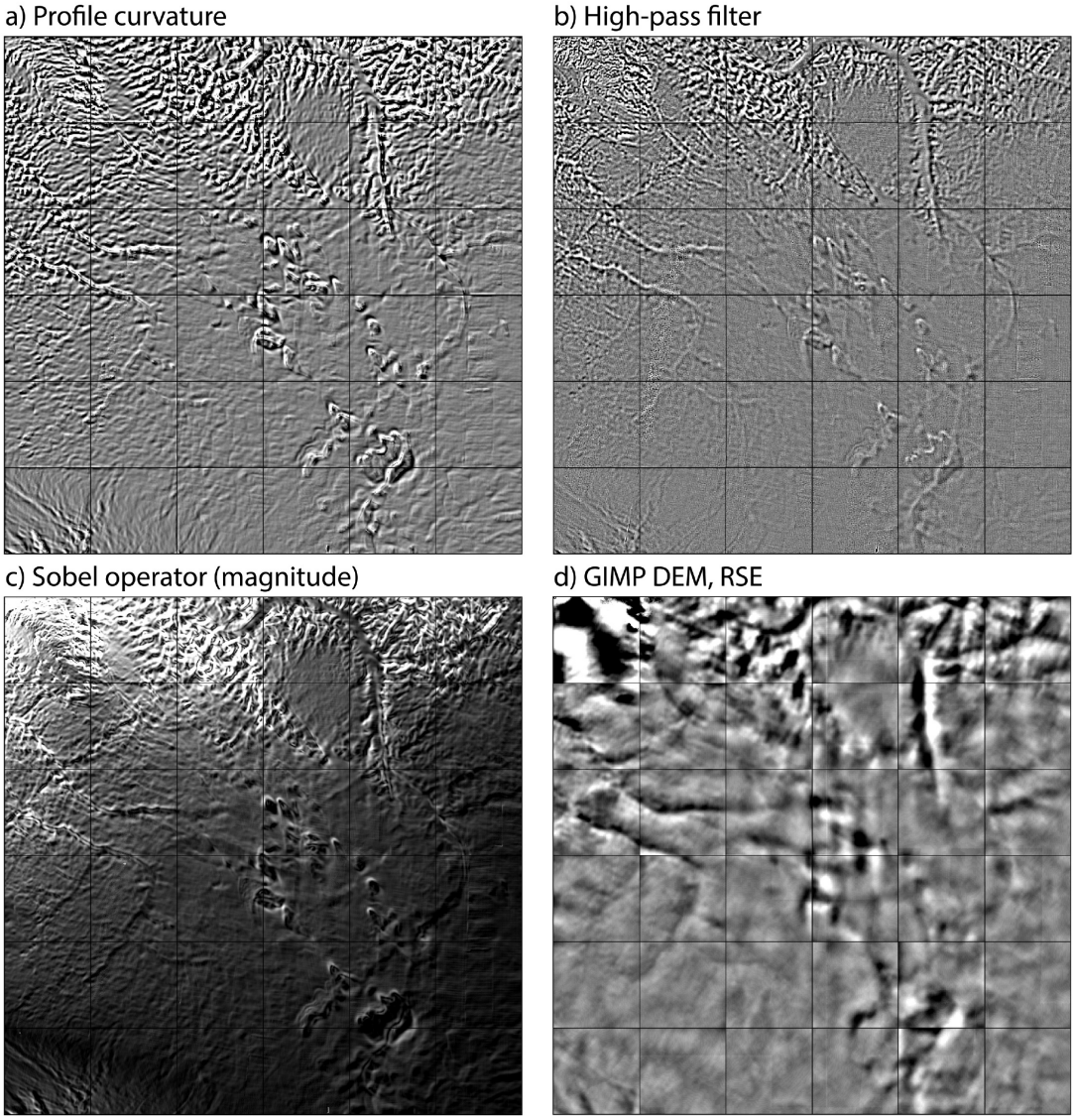

Figure 6.3: Alternative surface feature extraction methods used in glaciological research. Location as per Figures 6.1 & 6.2. (a) Profile Curvature calculated using ArcticDEM tiles (after Ross et al., 2014); (b) High-pass filter (3x3) calculated over ArcticDEM tiles (after Ekholm et al., 1998); (c) Magnitude of the image gradient calculated using the Sobel operator (Sobel and Feldman, 1968) using ArcticDEM tiles; (d) Residual surface elevation (RSE) calculated using previous, lower resolution, GIMP DEM for Greenland (Howat et al., 2014).

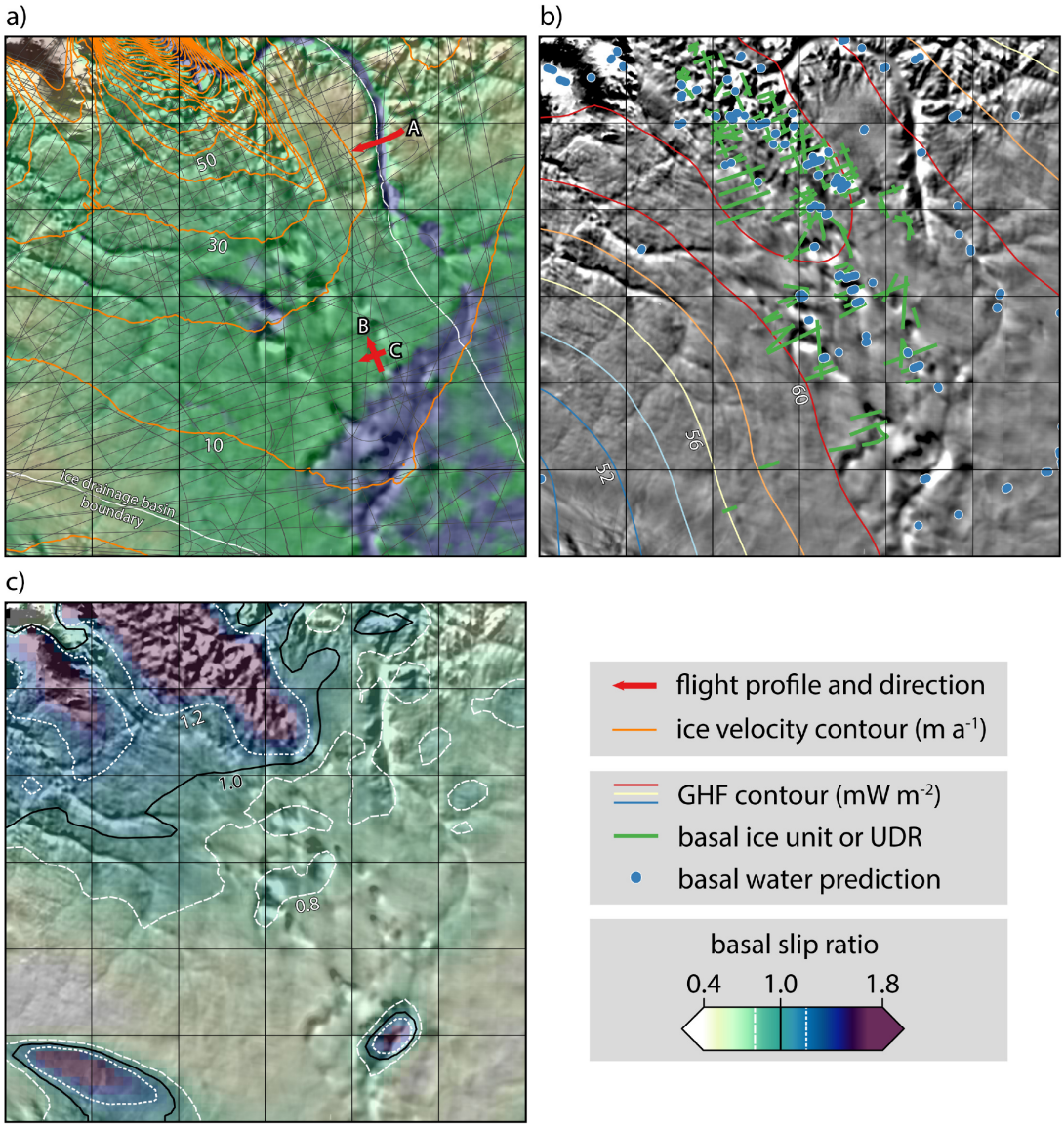

Figure 6.4: Comparison of observed surface features to auxiliary geophysical data. (a) RSE with BedDEM transparency (as Figure 6.1(a)). RES coverage as per Figure 6.1(a), and GrIS drainage basins are delineated (Zwally et al., 2012); ice surface velocity contours at 10 m a^{-1} intervals (Joughin et al., 2010); and profiles A–C are presented in Figure 6.6. (b) RSE with GHF contours at 2 mW m^{-2} intervals (Martos et al., 2018); radar predictions for basal water (Jordan et al., 2018); and, locations of 'basal ice units' (Bell et al., 2014). (c) RSE with basal slip ratio transparency (MacGregor et al., 2016), values of 0.8 (dashed), 1.0 (black), and 1.2 (dotted) are delineated.

do not appear to reflect likely basal topography; instead, these features result from ice dynamics and/or UDRs. In the first instance, a marked "rippling" is observed in the RSE coincident with Petermann Glacier, extending southeast (Figure 6.1(b)). While this signal appears linked to a spatial transition in the ice speed, there is no direct relationship to magnitude (Figures 6.4(a) and 6.5). Evidence of streaming ice is identified by the tight spacing of velocity contours, delineating pronounced shear margins (Figure 6.4(a)) and an elevated basal slip ratio (Figure 6.4(c); MacGregor et al., 2016). It is at shear margins, where strain rates and shear stress are high, and within fast-flowing ice, that ice is likely to become decoupled from the bed (Cuffey and Paterson, 2010). Spatial similarity between the observed RSE rippling features, shear margins as evidenced by velocity contours, and modelled driving and basal shear stress is observed (see Figure 3 in Sergienko et al., 2014). It is, therefore, plausible that the coincident response in ice surface topography may result from changes in ice flow parameters (i.e., decoupling) and a more efficient transfer of large-scale basal undulations, resulting from increased slip (Gudmundsson, 2003; De Rydt et al., 2013).

On the other hand, south of Petermann Glacier, in a relatively flat and low-lying area of the bed (Figure 6.1(a)), multiple ovular features are observed in the RSE (Figure 6.1(b)). UDRs have been documented across this sector of the GrIS in radiostratigraphy (Bell et al., 2014; Wolovick et al., 2014; Dow et al., 2018; Vieli et al., 2018). The established locations of most of these units correspond to the ovular/lobed features observed in the RSE (Figure 6.4(b)). The genesis and interrelationship with local ice flow parameters of these UDRs are discussed below.

6.5.1 'Ground truthing' RSE

To disentangle the primary causes of the surface features (Figure 6.1(b))), comparison can be made against radar-derived bed elevation and stratigraphy. Three illustrative profiles are shown in Figure 6.6. Profile A provides a near-perpendicular cross-section of the MC (Bamber and Aspinall, 2013), where profiles B and C present near-orthogonal bisectors of a UDR. Although a marked response in RSE is apparent along all three transects, the nature of these differ (Figures 6.6(a)–(c)). RSE along profile A follows basal topography with a corresponding negative, smoothed, facsimile of bed elevation; however, this response is notably

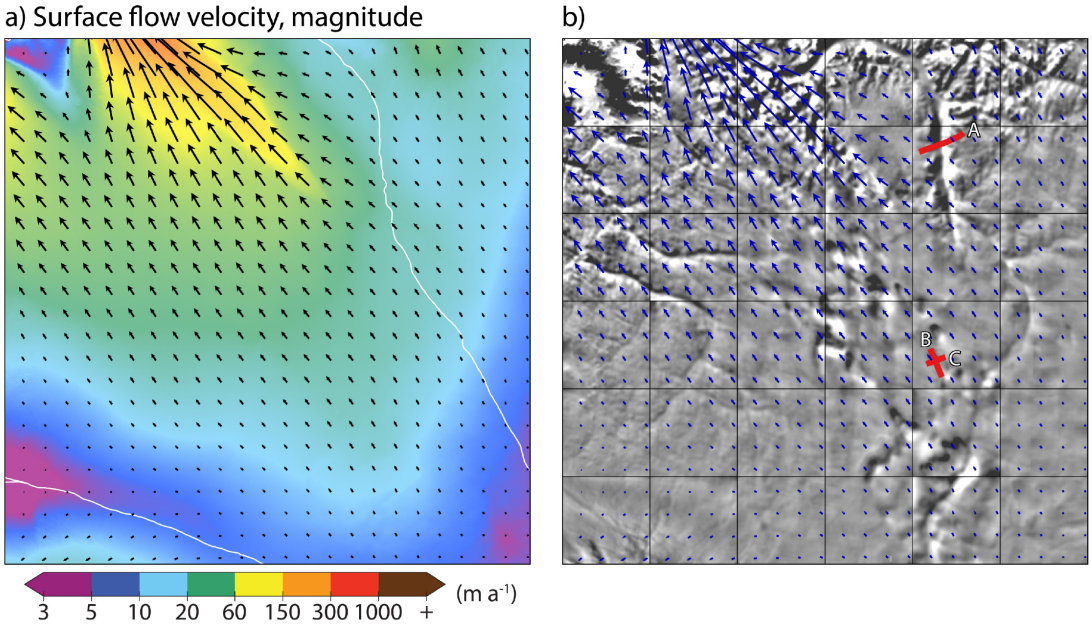

Figure 6.5: Ice sheet surface flow velocity magnitude with overlain flow velocity direction (black) (Joughin et al., 2016) (a). (b) RSE with overlain flow velocity direction (blue). Labelled profiles (A–C) are depicted in Figure 6.4d–f.

out of phase. This is likely a function of ice-flow direction (∼65° from profile; Figure 6.5), as well as ice rheology, thickness, and thermal regime, all of which affect the efficiency of bed-to-surface transmission (Gudmundsson, 2003; De Rydt et al., 2013). This informs us that although additional influences impinge the bed-to-surface transfer, we can still extract information regarding the scale and geometry of the basal feature using RSE. While a large positive response in RSE is observed along profiles B and C, little variation is observed in sampled bed elevation (standard deviation ≤19 m); it is unlikely, therefore, that basal topography is the primary cause.

When considering returned-power across the MC (profile A; Figure 6.6(d)), englacial stratigraphy generally conforms with basal topography. Specifically, some layer disturbance is partially visible towards the base of the ice column, however at this depth the ice has few radio-reflecting horizons. The dashed white line on all profiles indicates the transition in englacial stratigraphy between the Holocene ice above, and the "softer" ice of the Last Glacial Period, below (Dahl-Jensen and Gundestrup, 1987; Huybrechts, 1994; Chu et al., 2018). Above the canyon (Figure 6.6(d)) this better documents the "dampening" effect in the trans-

fer of basal information in englacial stratigraphy towards the surface (De Rydt et al., 2013), presenting a smoother transfer of the bed geometry in the RSE (Figure 6.6(a)).

Radargrams from profiles B and C (Figures 6.6(e), 6.6(f), and 6.7) depict a significant UDR (Figure 3a, Bell et al., 2014 and Figure 1, Wolovick et al., 2014), with a thickness up to one half of the ice column (∼1,000 m). When comparing the observed structure and reflectance characteristics of the UDR (Figures 6.6(e), 6.6(f), and 6.7) against similar features described in Greenland (Wolovick et al., 2014) and Antarctica (Wrona et al., 2017), we see several similarities. Large-scale cylindrical folding of this unit is also present, with the axis aligned perpendicular to flow (Figure 6.6e); more notably, a lobular extension from the top of the basal ice, elongated in the direction of surface ice flow, is similar to the "finger structures" observed in Antarctica formed through the entrainment of the softer basal unit into the overlying ice (Wrona et al., 2017). Across flow a central "eyelet" is observed within the UDR (asterisk, Figure 6.6f), indicative of extension/deformation of the unit parallel to the flow direction, characteristic of sheath folding (Wolovick et al., 2014; Wrona et al., 2017). The radiostratigraphy broadly shows the overlying ice flow "up-and-over" the UDR (Figures 6.6e and 6.6f) mostly undisturbed; this reflects the likely cause of the positive rise in RSE (Figure 6.6(b)), whereby the basal unit is hypothesized to act as a "false topographic bed," over which the upper ice layers conform. It is, therefore, possible that by using RSE we are able to better map or extrapolate the 2-D areal/horizontal extent of UDRs where directly observed in radargrams; however, in observation-sparse regions (away from RES flight lines), the cause of such ovular surface expressions is likely to be more ambiguous, as internal surfaces and certain bed geometry (e.g., basins and topographic rises) could present similarly, as such "additional" UDRs (those not previously documented) cannot be confidently mapped using RSE. To better answer this would require the implementation of a bed-to-surface transfer framework (as in Gudmundsson, 2003; De Rydt et al., 2013), which is beyond the scope of this paper.

Specifically, at the point of bisection between profiles B and C, we can use radar power anisotropy to make a preliminary assessment of vertical changes in the horizontal dielectric anisotropy of the ice column and related asymmetry of the ice crystal orientation fabric (COF; Hargreaves, 1978; Fujita et al., 2006). Radar power anisotropy is influenced by both birefringent propagation (associ-

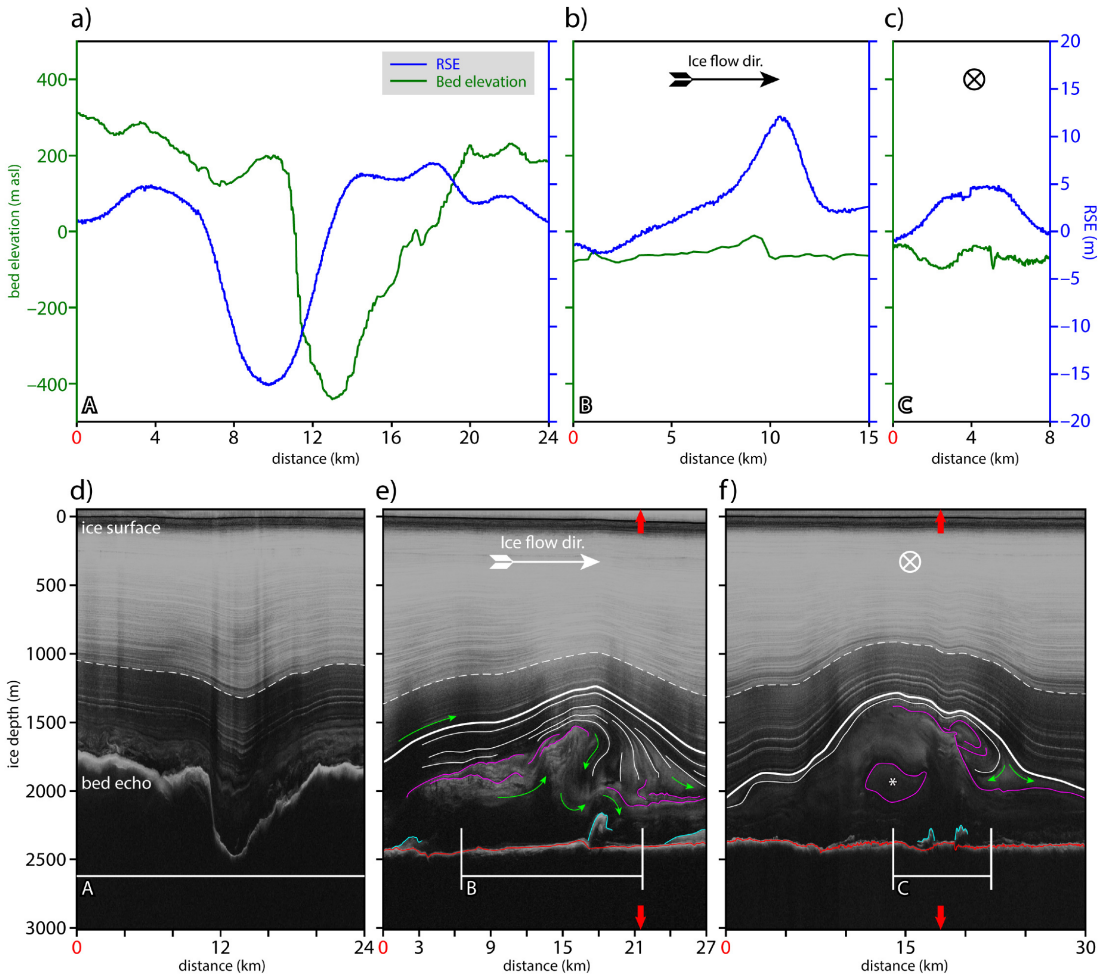

Figure 6.6: Bed elevation, RSE, and radargrams at locations A–C. Ice surface flow direction along profiles B and C is marked, where for profile A this oblique to the page (∼65°). Profile length has been extended in (e) & (f); labelled cutlines depict the original length. (d–f) are annotated for englacial stratigraphy interpreted in text. Englacial layers that correlate with 'surface ice' are shown (white lines), where the thickest line represents the first complete layer above the UDR; dashed white line denotes the separation between Holocene ice (above) and LGP ice (below). Radio-stratigraphy within reflective basal ice are purple, and near-bed reflectors beneath non-reflective ice are blue. The asterisk in (f) is interpreted as an inner ellipse within a sheath fold. Bed-echo (red) and ice surface returns are labeled. Red arrows x-axes (e & f) mark the location at which (f) orthogonally (∼90.1°) bisects the plane of (e). There is a vertical exaggeration by a factor of 19.35 and 11.45, for (a–c) and (d–f), respectively.

ated with horizontal COF anisotropy that varies smoothly with ice depth) and anisotropic scattering (associated with sharp vertical transitions in the COF; e.g., Fujita et al., 2006). Specifically, at mid-depths (∼900—1,700 m), we observe oscillations in the across/along-flow power difference as a function of depth (Figure 6.7(b)). The ∼10-dB amplitude and smoothly varying depth periodicity are seen to be consistent with power modulation dominated by birefringent radio wave propagation through the ice column (Fujita et al., 2006; Matsuoka et al., 2012). This implies smoothly varying horizontal asymmetry of the COF (i.e., the presence of either a vertical girdle fabric distribution or elongated single maximum). In both more shallow and deeper ice, the power difference shows greater isotropy, implying a weaker horizontal asymmetry of the COF. This is likely representative of a near-random fabric in shallow ice and a strengthened single maximum in deeper ice. As previously noted, the Holocene-Last Glacial Period transition is marked by a change in returned power (Chu et al., 2018) and is observed at ∼900 m (Figures 6.6d–f and 6.7a), approximately coincident with the point at which we infer the development of horizontal asymmetry in the COF.

Multiple hypotheses surrounding the inception of UDRs exist, including bottom-up accretion through supercooling and basal freeze-on (Bell et al., 2014; Vieli et al., 2018), thermomechanical changes resulting from anisotropic ice rheology, or changes in rheology affected by "stick-slip" mechanisms (Bons et al., 2016; Weertman, 1976; Wolovick et al., 2014). The latter of these mechanisms, initiated either by velocity changes within the ice column or in basal thermal state, would give rise to large-scale folding and deformation like that seen here (Weertman, 1976; Wolovick et al., 2014). While it has been noted that some UDRs in Greenland do not have a clear relationship to known basal water networks (Wolovick et al., 2014), the distribution of observed features is consistent with radar basal water predictions (Chu et al., 2018; Jordan et al., 2018). Additionally, these are within a region of elevated geothermal heat flux (> 58 mW m^{-2}; Martos et al., 2018; Figure 6.4b), and transitional basal thermal state (MacGregor et al., 2016; Chu et al., 2018). While hydrological modelling suggests minimal basal freeze-on rates (MacGregor et al., 2016; Dow et al., 2018), the correlation with these complementary geophysical properties, as well as evidence of multi-lobed sheath folding, may be symptomatic of heterogeneous basal sliding or altered ice rheology, ultimately leading to the formation of UDRs. This is compounded not only by an enhanced predicted basal motion over a particularly large UDR-feature

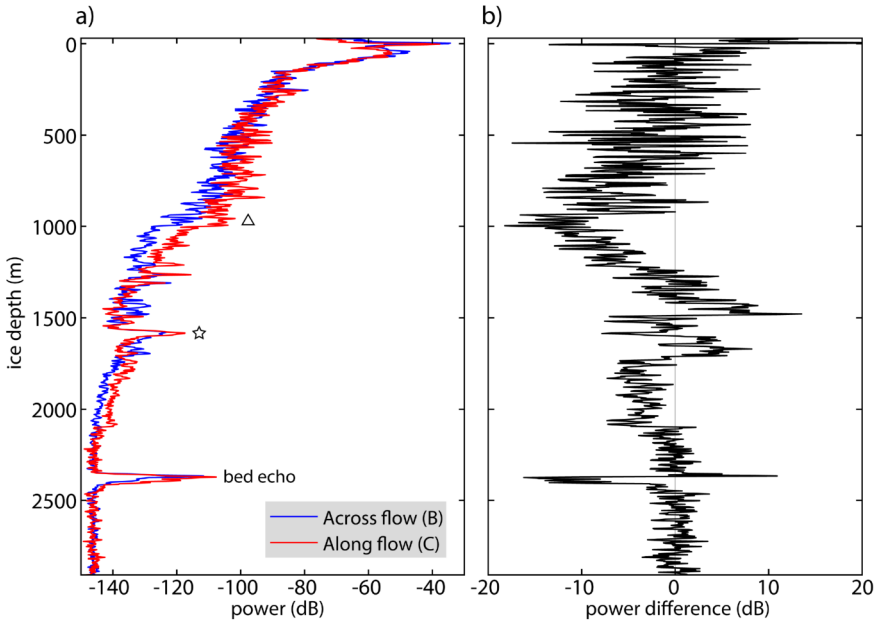

Figure 6.7: Returned power from internal layering at the orthogonal crossover between profiles B and C (Figure 6.4(a); 6.6(e)–(f)). The angle of crossover between these profiles is 90.1°. (a) Returned power (dB) from profile B across (blue) and profile C along (red) ice flow. Depth-transition from Holocene to LGP ice at ∼900 m is marked (triangle) and links to transition in Figure 6.6 (white dashed line). A strong reflector at the top of the basal unit is also highlighted (star marker). (b) Difference in returned power for across–along flow (dB). The radar antenna/polarization plane is aligned with the along-track direction.

observed in the RSE (Figures 6.4(c); asterisk, 6.8; MacGregor et al., 2016) but also through the inferred depth transitions from a near horizontally isotropic to horizontally anisotropic COF (Figure 6.7). Altogether, this suggests that these UDR features may act, dynamically, as "false beds" with localized englacial "decoupling" across the upper boundary.

6.5.2 Mapping basal characteristics

Although the presence, and causes, of surface expressions observed in the RSE can be directly attributed to basal topographies and associated subglacial processes using RES data, much of the true extent of these features cannot be realized due to sparse/absent observations. Figure 6.8 presents an annotated RSE, including our interpretation for the primary origin of surface expressions. We can map with greatest confidence quasi-linear topographic features, such as channel systems and dendritic fluvial landscape morphologies, though it is apparent that sites of significant basal UDRs, and velocity induced changes, plausibly indicative of glacier-bed decoupling, are also interpretable.

We are able to discern prominent bed geometries in the RSE, notably the additional detail in the landscape surrounding the MC and the northeast of the study region. Multiple, sinuous tributaries exist, as well as complex channel network and dendritic valley-like structures, suggestive of headwater catchments with several "minor" channels visible ($<$ 2,000 m in width; e.g., HS, Figure 6.8). Further, we see in tile E4 (Figure 6.8) that the MC appears to split into two upstream tributaries. It should be noted that where the RSE calculated for the more coarse resolution (90 m) GIMP DEM (Figure 6.3d) provides prominent basal channels (i.e., the MC), "fine" scale detail (i.e., HS, Figure 6.8) is not interpretable from the more "smoothed" information. While many channels are aligned quasi-parallel to contemporary ice flow direction, there are some channels that are aligned perpendicular to flow and, in one example, span the present-day ice divide (DC, Figure 6.8). Complex landscapes such as these are indicative of past fluvial activity and are often interpreted as inherited or partially preserved ancient fluvial systems, predating the inception of contemporary ice sheet. More "major" channels (in terms of great width and relative depth), and associated channel networks, are seen to influence contemporary ice flow and the routing of contemporary subglacial water (Bamber, et al., 2013; Cooper et al., 2016;

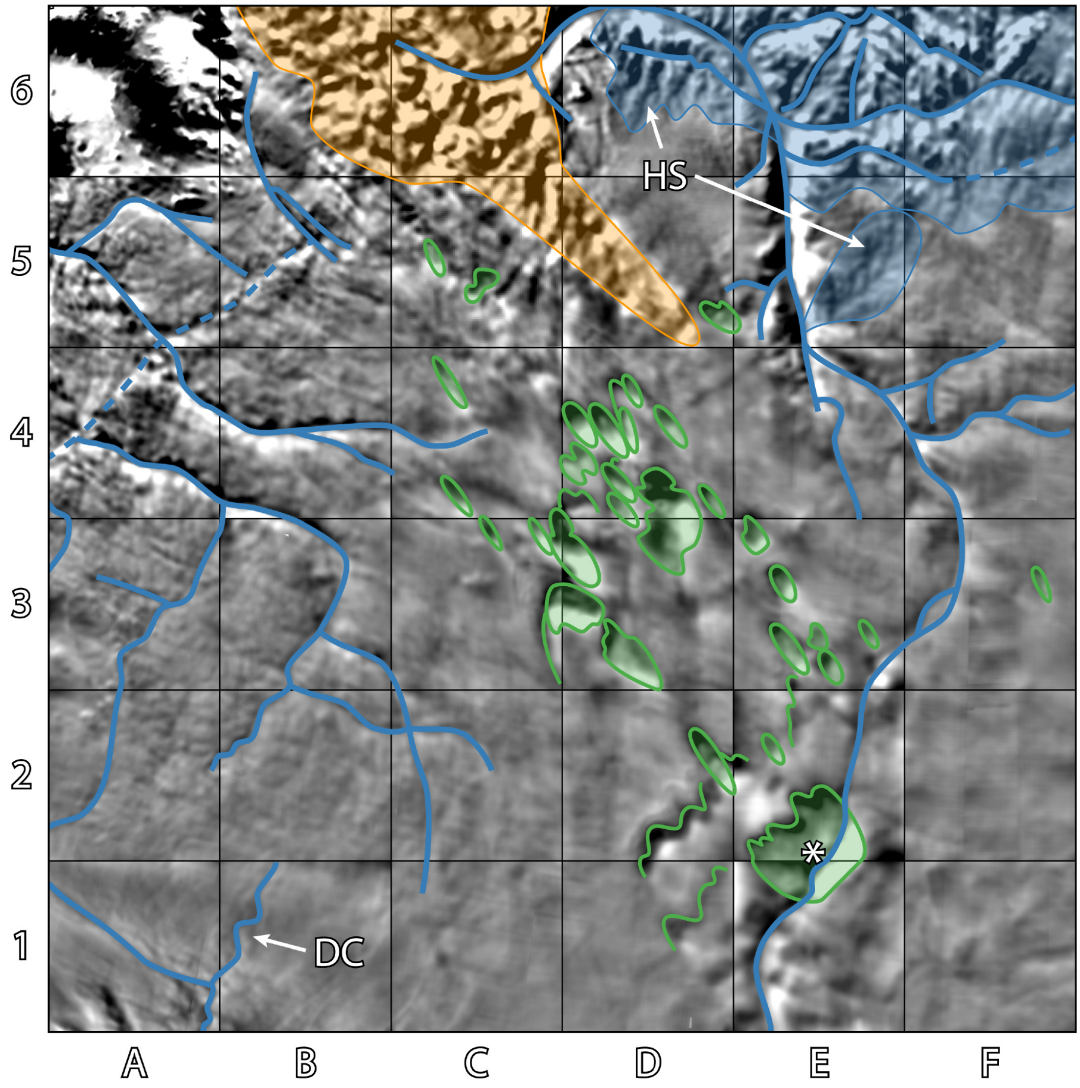

Figure 6.8: Summary of RSE with reference to basal and englacial processes and landforms. Subglacial channel features are delineated (blue lines), valley-like areas (blue-shade), with possible headstream catchments labelled (HS); DC depicts channel structure 'flowing' across the ice divide. UDRs are marked (green); whereby an asterisk marks a large-scale, multi-lobed UDR seen to be coincident increased basal slip (Figure 6.4(c)). Ice velocity-driven manifestations upon surface topography are also shown (orange). Alphanumeric grid labels are used in text to further describe and highlight features.

Bingham et al., 2017; Livingstone et al., 2017; Jordan et al., 2018;).

6.6 Conclusions

Here, we established the potential of the high-resolution (5 m) ArcticDEM to elucidate basal geometry with previously unobtainable detail. Where current geostatistically-derived bed topographies rely on isotropic methods of interpolation (*i.e.,* ordinary kriging), RSE provides a spatially-complete proxy to constrain local (horizontal length scales ∼1–10 km) morphology. This approach is particularly advantageous for anisotropic features within the ice sheet interior. Additionally, via combination with complementary RES data, we can constrain dynamical basal features (*e.g.,* subglacial drainage pathways) and englacial processes (*e.g.,* the 2-D areal extent of UDRs). Via analysis of bisecting radargrams, we assessed how UDRs form, and their dynamic relationship with the ice column. This permits correlation with, and influences of, and upon, surface flow characteristics (*e.g.,* sheath folding, fold elongation, and localized englacial decoupling).

In summary, we illustrate a complex subglacial and englacial system in northwest Greenland, notably improving the delineation of anisotropic geometric features that had previously been possible, or poorly captured, using isotropic interpolation. While qualitative, knowledge regarding the presence of complex basal topography, or indeed basal and englacial processes, may prove valuable not only in facilitating the further understanding of bed-to-surface transfer, but also in working to constrain future interpolation methods, and aiding the design of more directed geophysical campaigns. In the first instance, RSE is able to provide vertical information (in meter units), absent in previous edge detection and curvature methods (Figures 6.3). Where additionally, the positive identification of quasi-linear channels and dendritic valley networks can provide channel centerlines for physically based, anisotropic interpolation of bed topographies (exemplified in Herzfeld et al., 2011; Goff et al., 2014; Williams et al., 2017).

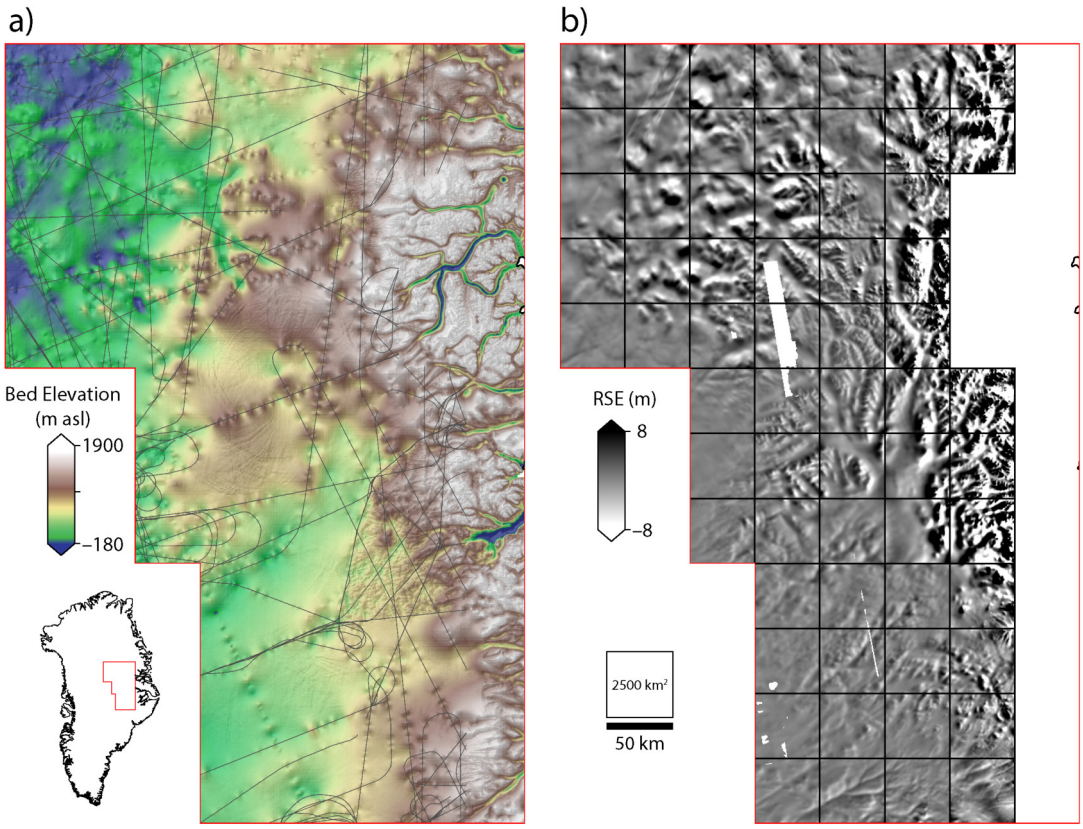

Figure 6.9: Bed topography and RSE for eastern Greenland. Study location inset. (a) BM3 (Morlighem et al., 2017). RES survey coverage (dark grey). (b) Calculated RSE. Black grid shows the spatial extent of individual ArcticDEM tiles.

6.7 Addendum: further insight

6.7.1 'Unveiling' complex terrain in east Greenland

Whilst outside of the immediate scope of the manuscript presented above, similar analysis was undertaken elsewhere over the GrIS. A notable example of this analysis is shown here, whereby RSE is seen to 'unveil' previously undocumented (within BM3) complex terrain at the eastern margin of the ice sheet. Figure 6.9 depicts BM3 (a), alongside calculated RSE for the same region (b); this is a region of the ice sheet where paucity of observation manifests as large smooth, flat regions within the interpolated bed topography, with large errors (see Figure 6.10(a)).

As is noted for the 'Petermann subset' presented above (Figure 6.1), the RSE

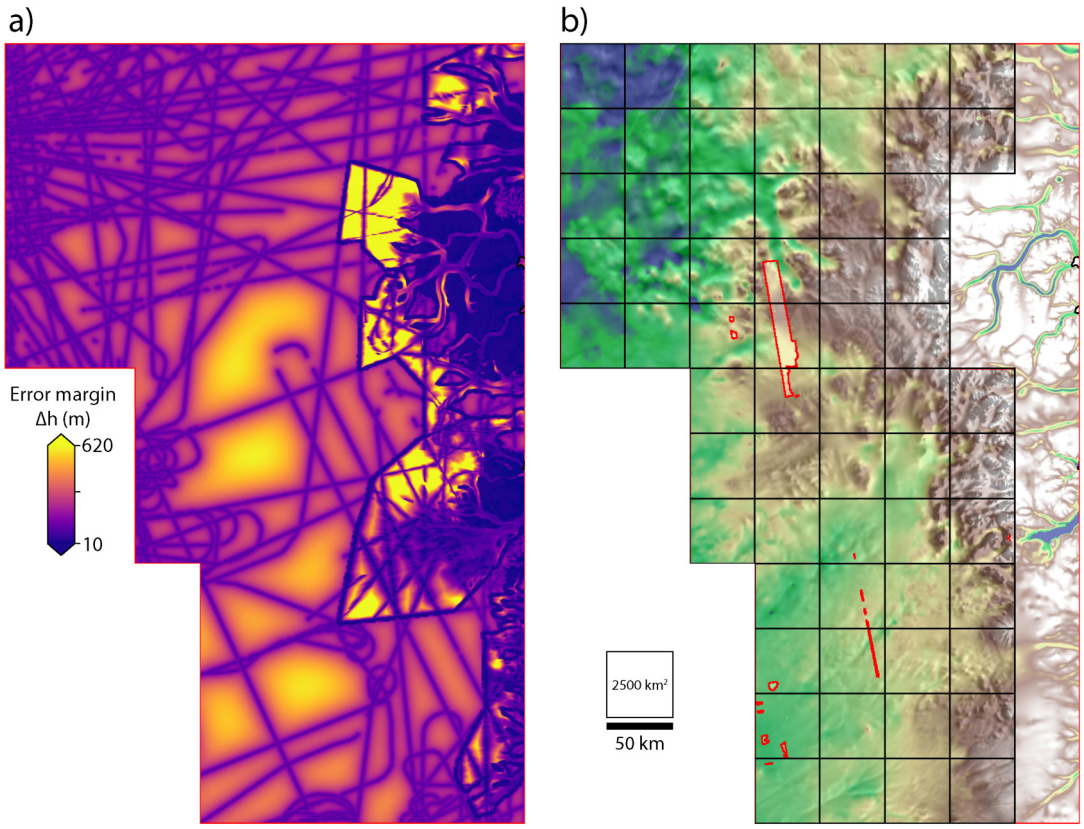

Figure 6.10: Bed topography, with regard to associated error, compared to RSE. Study location as per Figure 6.9. (a) BM3 error margin (Morlighem et al., 2017). (b) BM3 overlain on RSE. Red delineates where no data are present within surface topography.

exhibits clear potential to resolve complex and anisotropic topography. This is particularly emphasised here, as the observed surface expressions (Figure 6.9(b)) suggest that the complex fjord system at the ice sheet margin appear to continue a long distance into the interior. Additionally. in the north of the subset, velocity-driven manifestations in the RSE mark the onset of fast flow, and shear margins of the NEGIS; where more linear channels and tributaries are observed in the south, flowing south-west (Figure 6.9(b)).

Although the application of the RSE here is not as in-depth as the assessment in north-west Greenland it is clear that "unveiling" subglacial topography of this nature will present implications for contemporary, and projected ice dynamics. Furthermore, these subglacial channels, acting as part of a valley system may influence the routing of basal waters.

This subset is perhaps more clear in documenting the "failings" of isotropic interpolation, where numerous symptomatic "bull-eye" errors are observed (Figure 6.9(a)); though it should be noted this is primarily due to sparse observation. Data such as these may prove instrumental in planning more directed geophysical surveys, whereby the orientation and anisotropy of the underlying landscape may be mapped more appropriately.

Chapter 7

Conclusions

The purpose of this thesis was to provide new, in-depth assessment of Greenland's subglacial environment, making use of the recent increase in, and the relatively 'untapped' wealth of, available RES data across the GrIS, and facilitated by the use of complementary datasets (as described in Chapter 3). This research has been framed by the specific, overarching aim: to identify and better constrain the inter-relationships between aspects of the subglacial environment and the Greenland Ice Sheet, with specific reference to subglacial processes, ice-sheet motion and the solid earth.

As outlined in the introductory chapters of this thesis (Chapter 2), the influence, and exertion of 'control' between ice dynamics (namely ice motion) and the subglacial environment are not always clear cut. However, driven by the necessity to better constrain projections of mass loss under contemporary climatic perturbation, the influence of subglacial properties relating to ice motion (*e.g.,* sliding velocities) is often inferred from surface observations. Lacking any direct, *in situ* observations or process-based understanding, these parametrisations are seen as a source of great uncertainty.

This chapter acts to summarise the key findings of this thesis, providing a discussion of the conducted research with specific reference to the research aims and objects outlined in Chapter 1. As part of this, the implications for wider scientific understanding, and advances to current scientific literature are presented. Further, this chapter highlights potential future research avenues with regard to the findings presented here, which would act either to extend the application of, or to improve upon, the methods employed.

7.1 Summary of results and findings

7.1.1 Landscape inheritance and ice-sheet motion

The scope of chapter 4 was to identify the influence of broad, landscape-scale topography upon the GrIS, and vice-versa; this was undertaken in an attempt to clarify the apparent 'chicken-or-egg' relationship between the bed and ice, with reference to previous assessments of glacial 'erasure' (by erosive means), contrasting to more recent examples of landscape preservation in Antarctica. A proxy for pre-glacial bed topography was used to both identify the geomorphic origin and long-term evolution of the underlying landscape; this highlighted the 'minimal' influence of glacial erosion since the inception of the GrIS, in turn presenting a consideration for 'landscape inheritance.'

Chapter 4 documented evidence for a large-scale drainage basin underlying much of southern Greenland, aligned with the present-day Jakobshavn Isbræ, Greenland's largest outlet glacier. This basin, through topographic and morphometric analysis, was concluded to be of palæofluvial origin, whereby deep, V-shaped channels have been preserved within the slow-flowing ice sheet interior. The observed channel network is likely to have influenced subsequent selective glacial erosion, exemplified in the modification of the channel/trough at the basin's outlet, presenting a characteristic glacial over-deepening. The ancient bed topography here presents, through landscape inheritance, a defining influence on the modern ice-sheet configuration and contemporary dynamics, acting to constrain the flow of ice, thus explaining the location, size, and velocity of the Jakobshavn Isbræ ice stream both now and over several glacial cycles.

This research provided the first interpretation Greenland's underlying topography, with respect to the established literature on the selective nature of glacial erosion, and landscape preservation beneath ice sheets. This built upon the observation of the large-scale 'mega-canyon' in north Greenland (Bamber et al., 2013b), thought to be instrumental in the transport of basal waters and sediment to the ice sheet margin. Furthermore, this has opened further discussion for the understanding of the two-way relationship between ice motion and pre-existing topography, through long-term landscape evolution and landscape inheritance. Following the publication of this chapter, Livingstone et al. (2017) has presented further evidence for both the preservation of pre-glacial channel systems, associ-

ated with Humboldt outlet glacier.

7.1.2 Subglacial roughness and ice-sheet motion

Prediction of the Greenland Ice Sheet's future contribution to global sea level relies on numerical modelling to project its dynamic response, and thus rates of mass loss, to a changing climate. Mass loss is principally driven by the movement of ice over the grounding line, which is largely influenced by basal sliding (and sliding velocity). As previously noted, various properties of the subglacial environment influence basal sliding. These include, basal thermal regime; presence of basal water; geotechnical bed properties (*i.e.* presence of deformable sediment); and basal traction/drag (*i.e.* resistance from roughness) (Clarke, 2004; Durand et al., 2011; Iverson and Zoet, 2015; Brondex et al., 2017; Stearns and van der Veen, 2018). Whilst theoretically well understood, these properties are often not directly implemented into ice sheet models, whereby sliding laws (and basal traction) are parametrised via the inversion of surface velocities. Previous assessments, whilst limited in their ability to resolve basal undulations at a scale critical for influencing sliding velocity (order 1-metre), have concluded that subglacial roughness, and in particular smooth beds, are an important control on fast-flowing, streaming ice.

This purpose of this chapter was not only to improve upon previous ice sheet-wide quantifications of subglacial roughness in Greenland, but also to draw conclusions based upon the spatial distribution observed within the calculated measures, and their relationship to aspects of ice-sheet motion. Two independent methods of quantification were presented: firstly, via statistical analysis of along track bed elevation (facilitating the assessment of ice-sheet anisotropy); and secondly by the quantification of electromagnetic scattering (to extract more fine-scale information). This research provides key advances in elucidating the spatially-heterogenous aspects of Greenland's subglacial environment, making assessment with regard to the 'non-universal' behaviour exhibited within roughness information across Greenland and Antarctica.

It is concluded that smooth beds are not a necessary condition for fast flow, nor necessary markers for the presence of deformable sediment. Contrastingly, the majority of fast-flowing regions are seen to exhibit rough beds across both metrics, and smooth beds, within slow-flowing regions are likely indicative to the

presence of hard-bed geology. As such, this chapter hopes to provide scope for a spatially variable hard bed/soft bed boundary constraint for ice sheet models. Additionally, subglacial roughness shows strong anisotropy across the ice sheet, with a more marked signal within regions of fast flow; here, 'topographic roughness' exhibits a strong exponential scaling relationship with ice velocity parallel, but not perpendicular, to flow direction. This relationship is thought to be driven by the influence of erosion acting to streamline, or elongate bed features, possibly within deformable sediment (*e.g.,* mega-scale glacial lineations, Bingham et al., 2017). This chapter hopes to provide scope for a spatially variable hard bed/soft bed boundary constraint for ice sheet models.

7.1.3 Surface expression of basal and englacial processes

Knowledge of bed topography/geometry provides an instrumental boundary condition for ice-sheet modelling; this has driven successive releases of basal topography products for Greenland, improving in both spatial resolution and accuracy (*e.g.,* Bamber et al., 2013b; Morlighem et al., 2017). However, limited by spatial-bias in sampling regimes, paucity in observations and isotropic interpolation techniques, these products often fail to represent the 'true' geometry of both small-scale, and anisotropic basal features. The transfer of information from the bed-to-surface had been previously discussed, both theoretically and through data-driven means. However, with the release of a new high-resolution dataset (the ArcticDEM; 5 m), it was the primary aim of Chapter 6 to establish the potential of the ArcticDEM to elucidate basal geometry and other subsurface processes.

Calculated residual surface elevation provides a spatially-complete proxy to constrain local (horizontal length scales ∼1–10 km) basal morphology, as well as providing the 2-D areal extent of basal units within the region. Further analysis of bisecting radargrams provided insight into how these units form, as well as their dynamic relationship with the ice column. This permits correlation with, and influences of, and upon, surface flow characteristics, notably localised englacial 'decoupling').

This chapter illustrates a complex subglacial and englacial system in northwest Greenland, notably improving delineation of anisotropic geometric features that had previously been poorly captured using isotropic interpolation. Whilst qual-

itative, this knowledge regarding the presence of complex basal topography, or indeed basal and englacial processes, is valuable in constraining future anisotropic interpolation methods (as in Goff et al., 2014; Williams et al., 2017), and designing more directed geophysical campaigns.

7.2 Considerations for future research

Whilst each research chapter in this thesis has pointed towards specific methodological limitations and aspects for further consideration, there are numerous, more in-depth research avenues for future research with implications for wider research.

7.2.1 Further characterisation of subglacial environment

A key finding from the analysis presented in Chapter 5 suggests that smooth beds are not necessarily indicative of deformable sediment. In slow-flowing regions, three such contiguous regions were concluded as likely underlain by a hard-bed geology, or rather, lacking deformable sediment. To facilitate future analysis, it is recommended that roughness information be used alongside coincident magnetic and gravity anomaly data (as exemplified south of Petermann Glacier in Chapter 5; *i.e.* Tinto et al., 2015). Doing so would aid confirmation of underlying geology in these regions, and widely across the ice sheet. Additionally, the use of seismic data could prove useful when establishing a link between the presence of deformable sediment (as in Christianson et al. (2014)) and subglacial roughness. The ability to fully demarcate deformable–non-deformable beds presents implications not only with regard to erosive processes, preservation landscape evolution (as in Chapter 4), but will also provide pertinent information with regard to basal sliding, with a view to better constrain forward modelling and sliding law parametrisation.

Where the current scope of the present research drew comparison between subglacial roughness information and contemporary surface velocity, these could be re-framed to consider calculated sliding and deformation velocities (such as those given in MacGregor et al., 2016). Basal sliding is, for the most part, responsible for fast flow, and rates of enhanced erosion; it would, therefore, be useful to examine whether any relationship is exhibited between fine-scale roughness

information and sliding at the bed.

Subglacial roughness and landscape development

Finally, in a more geomorphological extension to the delineation of soft-beds, the roughness datasets published through this research could aid interpretation to factors/conditions promoting rough and smooth beds. For example, this may follow a schematic framework similar to that outlined by Bingham and Siegert (2009), with reference to erosion and deposition, geographical setting, and to both palaeo- and contemporary ice dynamics. In doing so, important information regarding the history of long-term landscape evolution of Greenland may be made evident, with a potential to describe what influences both contemporary and pre-glacial landscapes have and will have on the GrIS at a higher-order (*i.e.,* the influence of landscape inheritance, already documented in Greenland (Chapter 4; Cooper et al., 2016; Livingstone et al., 2017).

This framework will need to take into account local characteristics of subglacial roughness (across both metrics in Chapter 5); contemporary ice speed and flow orientation; basal relief; as well as any information regarding the erodibility of the bed. Creating such a framework has the potential to be difficult, as the above characteristics are already documented to be well intertwined. Whilst a simplistic approach regarding parallel bed smoothness and fast ice flow is likely a marker for glacial erosion, as previously discussed (Chapter 5), more complex developmental relationships may well exist.

Additionally, work towards such a framework may benefit from the use of, or conjunction with with the 'landscape classifier' pilot study in this thesis (Section 3.2). Rather than using this to identify primarily 'glacial' landscapes, utilising it as more of a general 'morphometric classifier,' alongside both ice and roughness characteristics may well help to further understand the landscape development of Greenland.

7.2.2 Further examining surface expression (RSE)

The research presented in Chapter 6 defines a clear and significant potential for the use of newly [publicly] available high-resolution surface imagery for elucidating subsurface processes and geometry.

The scope of the initial chapter (Chapter 6) was spatially-limited—drawing focus primarily to north-west Greenland—the first avenue for further research would be to employ the methods described herein across the entirety of the ice sheet. This would prove instrumental in examining the subsurface properties and processes across the GrIS, working to: identify complex subglacial topography, and the extent of basal units (or UDRs). These features are seen to be pertinent to ice motion and thus a constraint upon forward-modelling, characterising a new potential for localised englacial decoupling (resulting in slip/sliding). A first step for future research and analysis could be to extend this methodology and approach ice-sheet wide, pursuing an analysis of subsurface information across Greenland, as well as identifying areas where the methodology employed may break-down (such as at the margins).

Finding an empirical relationship

It should be noted, however, that the analysis of residual surface elevation (RSE) is fundamentally qualitative; whilst width and areal extent of basal geometry is preserved, absolute elevation, and the amplitude are not extracted. Furthermore, shifts in the bed-to-surface transfer, owing to ice motion (amongst other factors) may lead to spatial 'misdiagnosis,' whereby the location of an observed feature is shifted laterally. It is, therefore, necessary to consider and investigate to what level the extraction of bed-to-surface information can be quantified, and how local factors may influence surface manifestations. A key method to test the efficacy of using RSE as a proxy for bed elevation would be the use of comparative, cross-correlation metrics (as in De Rydt et al. (2013)); this would also enable greater precision with regard to the peak wavelengths/frequencies of the bed-to-surface transfer.

Automatic feature extraction

In chapter 6, various 'features' were identified from surface information, and analysed. Within this chapter I described the image analysis tools previously used to 'extract' such features within the literature. These methods, present as simple edge detector tools (*e.g.,* surface curvature, and, high-pass and, sobel filters), and provide similar visual information to that provided by the RSE calculated in this thesis. Whilst these tools provide a useful starting point for subsequent visual in-

spection and analysis, they do little to extract 'self-contained' features or indeed a characterisation or classification of the observed surface expression; more complex methods of feature extraction, and perhaps automated fuzzy classification may well prove instrumental in extracting useful subsurface information.

Various techniques may be applied, either through some level of computer vision to better detect 'real' morphology, extracting and classifying surface information into expressions of englacial features (potential UDRs), and basal geometry (*e.g.,* valley structures). A more 'involved,' but less computationally-complex, process may perhaps utilise a decision-tree-based approach, similar to that in the pilot study for this thesis (section 3.2); this technique would require certain measures of relief and linearity which may, however, prove difficult.

Future survey planning

With the ability of the RSE to reveal underlying complex terrain with high spatial resolution (Chapter 6), further advances could be made in planning future RES surveys. As touched upon previously, a stronger quantitative relationship could perhaps be derived between the surface information and underlying bed topography; direct observation from RES, however, has greater potential to elucidate further basal (and englacial) characteristics (*e.g.,* subglacial roughness in this thesis, Chapter 5). Therefore, the provision of higher-order geometry could be used to better inform the placement of radar flightlines, aligning both across and along subglacial features (*i.e.,* lineated valleys), which would not only help to better constrain interpolation, but also to more complex landscapes which are likely to influence the flow of ice.

Finally, with the recent release of the Reference Elevation Model for Antarctica (REMA) providing surface topography at a similar spatial resolution (8 m), similar analysis could be undertaken with a view to improve the current subsurface 'poles of ignorance' as a result of the paucity in RES observations.

7.3 Closing remarks

The research presented here, through Chapters 4–6, has not only documented broad-scale controls at the bed, but has also elucidated the influence, and behaviour, of more-localised subglacial–englacial processes. This thesis provides

particular significance to the current understanding of the spatially-heterogeneous characteristics of the subglacial environment, enabling further constraint of the non-universal inter-relationships between the bed and overlying ice motion. It is, therefore, hoped that this thesis will work to improve the understanding of glacial response to contemporary climatic perturbation, and to improve projections of future contributions to global sea level.

Bibliography

Alley, R. B., Andrews, J. T., Brigham-Grette, J., Clarke, G. K. C., Cuffey, K. M., Fitzpatrick, J. J., Funder, S., Marshall, S. J., Miller, G. H., Mitrovica, J. X., Muhs, D. R., Otto-Bliesner, B. L., Polyak, L., and White, J. W. C. (2010). History of the Greenland Ice Sheet: paleoclimatic insights. *Quaternary Science Reviews*, 29(15–16):1728–1756.

Anderson, R. S., Molnar, P., and Kessler, M. A. (2006). Features of glacial valley profiles simply explained. *Journal of Geophysical Research: Earth Surface*, 111(F1):F01004.

Andrews, J. T., Milliman, J. D., Jennings, A. E., Rynes, N., and Dwyer, J. (1994). Sediment thicknesses and holocene glacial marine sedimentation rates in three east Greenland fjords (ca. 68 °N). *The Journal of Geology*, 102(6):669–683.

Arthern, R. J., Hindmarsh, R. C. A., and Williams, C. R. (2015). Flow speed within the Antarctic ice sheet and its controls inferred from satellite observations. *Journal of Geophysical Research: Earth Surface*, 120(7):1171–1188.

Bamber, J. L. and Aspinall, W. P. (2013). An expert judgement assessment of future sea level rise from the ice sheets. *Nature Climate Change*, 3(4):424–427.

Bamber, J. L., Griggs, J. A., Hurkmans, R. T. W. L., Dowdeswell, J. A., Gogineni, S. P., Howat, I., Mouginot, J., Paden, J., Palmer, S., Rignot, E., and Steinhage, D. (2013a). A new bed elevation dataset for Greenland. *The Cryosphere*, 7(2):499–510.

Bamber, J. L., Layberry, R. L., and Gogineni, S. P. (2001). A new ice thickness and bed data set for the Greenland ice sheet: 1. Measurement, data reduction, and errors. *Journal of Geophysical Research: Atmospheres*, 106(D24):33773–33780.

Bamber, J. L., Siegert, M. J., Griggs, J. A., Marshall, S. J., and Spada, G. (2013b). Paleofluvial mega-canyon beneath the central Greenland Ice Sheet. *Science*, 341(6149):997–999.

Baroni, C., Noti, V., Ciccacci, S., Righini, G., and Salvatore, M. C. (2005). Fluvial origin of the valley system in northern Victoria Land (Antarctica) from quantitative geomorphic analysis. *Geological Society of America Bulletin*, 117(1-2):212–228.

Bartoli, G., Sarnthein, M., Weinelt, M., Erlenkeuser, H., Garbe-Schönberg, D., and Lea, D. W. (2005). Final closure of Panama and the onset of northern hemisphere glaciation. *Earth and Planetary Science Letters*, 237(1–2):33–44.

Baynes, E. R. C., Attal, M., Niedermann, S., Kirstein, L. A., Dugmore, A. J., and Naylor, M. (2015). Erosion during extreme flood events dominates Holocene canyon evolution in northeast Iceland. *Proceedings of the National Academy of Sciences*, 112(8):2355–2360.

Bell, R. E., Tinto, K., Das, I., Wolovick, M., Chu, W., Creyts, T. T., Frearson, N., Abdi, A., and Paden, J. D. (2014). Deformation, warming and softening of Greenland's ice by refreezing meltwater. *Nature Geoscience*, 7(7):497–502.

Berry, M. V. (1973). The statistical properties of echoes diffracted from rough surfaces. *Philosophical Transactions of the Royal Society of London. Series A*, 273(1237):611–654.

Berry, M. V. (1975). Theory of radio echoes from glacier beds. *Journal of Glaciology*, 15(73):65–74.

Bingham, R. G., Rippin, D. M., Karlsson, N. B., Corr, H. F. J., Ferraccioli, F., Jordan, T. A., Le Brocq, A. M., Rose, K. C., Ross, N., and Siegert, M. J. (2015). Ice-flow structure and ice dynamic changes in the Weddell Sea sector of West Antarctica from radar-imaged internal layering. *Journal of Geophysical Research: Earth Surface*, 120(4):2014JF003291.

Bingham, R. G. and Siegert, M. J. (2007). Radar-derived bed roughness characterization of Institute and Möller ice streams, West Antarctica, and comparison with Siple Coast ice streams. *Geophysical Research Letters*, 34(21):L21504.

Bingham, R. G. and Siegert, M. J. (2009). Quantifying subglacial bed roughness in Antarctica: implications for ice-sheet dynamics and history. *Quaternary Science Reviews*, 28(3–4):223–236.

Bingham, R. G., Siegert, M. J., Young, D. A., and Blankenship, D. D. (2007). Organized flow from the South Pole to the Filchner-Ronne ice shelf: An assessment of balance velocities in interior East Antarctica using radio echo sounding data. *Journal of Geophysical Research: Earth Surface*, 112(F3).

Bingham, R. G., Vaughan, D. G., King, E. C., Davies, D., Cornford, S. L., Smith, A. M., Arthern, R. J., Brisbourne, A. M., De Rydt, J., Graham, A. G. C., Spagnolo, M., Marsh, O. J., and Shean, D. E. (2017). Diverse landscapes beneath Pine Island Glacier influence ice flow. *Nature Communications*, 8(1):1618.

Böhner, J. and Conrad, O. (2007). SAGA-GIS.

Bons, P. D., Jansen, D., Mundel, F., Bauer, C. C., Binder, T., Eisen, O., Jessell, M. W., Llorens, M.-G., Steinbach, F., Steinhage, D., and Weikusat, I. (2016). Converging flow and anisotropy cause large-scale folding in Greenland's ice sheet. *Nature Communications*, 7:11427.

Braun, A., Kim, H. R., Csatho, B., and von Frese, R. R. B. (2007). Gravity-inferred crustal thickness of Greenland. *Earth and Planetary Science Letters*, 262(1–2):138–158.

Brondex, J., Gagliardini, O., Gillet-Chaulet, F., and Durand, G. (2017). Sensitivity of grounding line dynamics to the choice of the friction law. *Journal of Glaciology*, 63(241):854–866.

Budd, W. F. (1970). Ice flow over bedrock perturbations. *Journal of Glaciology*, 9(55):29–48.

Bull, W. B. and McFadden, L. D. (1977). Tectonic geomorphology north and south of the Garlock fault, California. In Doehring, D. O., editor, *Geomorphology in Arid Regions: A Proceedings Volume of the Eighth Annual Geomorphology Symposium Held at the State University of New York at Binghamton, September 23-24, 1977 Proceedings of the eighth annual geomorphology symposium. State University of New York, Binghamton*, pages 115–138. George Allen & Unwin, New York, NY.

Carr, J. R., Vieli, A., Stokes, C. R., Jamieson, S. S. R., Palmer, S. J., Christoffersen, P., Dowdeswell, J. A., Nick, F. M., Blankenship, D. D., and Young, D. A. (2015). Basal topographic controls on rapid retreat of Humboldt Glacier, northern Greenland. *Journal of Glaciology*, 61(225):137–150.

Christianson, K., Peters, L. E., Alley, R. B., Anandakrishnan, S., Jacobel, R. W., Riverman, K. L., Muto, A., and Keisling, B. A. (2014). Dilatant till facilitates ice-stream flow in northeast Greenland. *Earth and Planetary Science Letters*, 401:57–69.

Chu, W., Schroeder, D. M., Seroussi, H., Creyts, T. T., and Bell, R. E. (2018). Complex basal thermal transition near the onset of Petermann Glacier, Greenland. *Journal of Geophysical Research: Earth Surface*, 123(5):985–995.

Clarke, G. K. (2004). Subglacial processes. *Annual Review of Earth and Planetary Sciences*, 33(1):247–276.

Conrad, O. and Olaya, V. (2004). SAGA-GIS: Terrain Analysis – Hydrology.

Cooper, M. A., Michaelides, K., Siegert, M. J., and Bamber, J. L. (2016). Paleofluvial landscape inheritance for Jakobshavn Isbræ catchment, Greenland. *Geophysical Research Letters*, 43(12):6350–6357.

Cowton, T., Nienow, P., Bartholomew, I., Sole, A., and Mair, D. (2012). Rapid erosion beneath the Greenland ice sheet. *Geology*, 40(4):343–346.

Cuffey, K. M. and Paterson, W. S. B. (2010). *The Physics of Glaciers*. Academic Press, Cambridge, Mass.

Dahl-Jensen, D. and Gundestrup, N. (1987). Constitutive properties of ice at Dye3, Greenland. In *International Association of Hydrological Sciences Publications*, number 170, pages 31–43. Vancouver Symposium, IAHS Publ.

Dahl-Jensen, D., Gundestrup, N., Gogineni, S. P., and Miller, H. (2003). Basal melt at NorthGRIP modeled from borehole, ice-core and radio-echo sounder observations. *Annals of Glaciology*, 37:207–212.

Dawes, P. R. (2009). The bedrock geology under the inland ice: the next major challenge for greenland mapping. *Geological Survey of Denmark and Greenland Bulletin*, (17):57–60.

De Rydt, J., Gudmundsson, G. H., Corr, H. F. J., and Christoffersen, P. (2013). Surface undulations of Antarctic ice streams tightly controlled by bedrock topography. *The Cryosphere*, 7(2):407–417.

Dentith, M. and Mudge, S. T. (2014). *Geophysics for the Mineral Exploration Geoscientist*. Cambridge University Press, Cambridge, United Kingdom.

Dow, C. F., Karlsson, N. B., and Werder, M. A. (2018). Limited impact of subglacial supercooling freeze-on for Greenland Ice Sheet stratigraphy. *Geophysical Research Letters*, 45(3):1481–1489.

Drewry, D. J. (1986). *Glacial Geologic Processes*. E. Arnold, London.

Durand, G., Gagliardini, O., Favier, L., Zwinger, T., and Meur, E. l. (2011). Impact of bedrock description on modeling ice sheet dynamics. *Geophysical Research Letters*, 38(20).

Ebert, K., Hall, A. M., Kleman, J., and Andersson, J. (2015). Unequal ice-sheet erosional impacts across low-relief shield terrain in northern Fennoscandia. *Geomorphology*, 233:64–74.

Echelmeyer, K. and Clarke, T. S. (1991). Surficial glaciology of Jakobshavns Isbræ, West Greenland: Part I. Surface morphology. *Journal of Glaciology - J GLACIOLOGY*, 37:368–382.

Egholm, D. L., Nielsen, S. B., Pedersen, V. K., and Lesemann, J.-E. (2009). Glacial effects limiting mountain height. *Nature*, 460(7257):884–887.

Ekholm, S., Keller, K., Bamber, J. L., and Gogineni, S. P. (1998). Unusual surface morphology from digital elevation models of the Greenland Ice Sheet. *Geophysical Research Letters*, 25(19):3623–3626.

Eldrett, J. S., Harding, I. C., Wilson, P. A., Butler, E., and Roberts, A. P. (2007). Continental ice in Greenland during the Eocene and Oligocene. *Nature*, 446(7132):176–179.

Evans, S., Drewry, D., and Robin, G. d. Q. (1972). Radio-echo sounding in antarctica, 1971–72. *Polar Record*, 16(101):207–212.

Fahnestock, M. A., Joughin, I., Scambos, T. A., Kwok, R., Krabill, W. B., and Gogineni, S. (2001). Ice-stream-related patterns of ice flow in the interior of northeast Greenland. *Journal of Geophysical Research: Atmospheres*, 106(D24):34035–34045.

Falcini, F. A. M., Rippin, D. M., Krabbendam, M., and Selby, K. A. (2018). Quantifying bed roughness beneath contemporary and palaeo-ice streams. *Journal of Glaciology*, 64(247):822–834.

Fleming, K. and Lambeck, K. (2004). Constraints on the Greenland Ice Sheet since the Last Glacial Maximum from sea-level observations and glacial-rebound models. *Quaternary Science Reviews*, 23(9–10):1053–1077.

Fountain, J., Usselman, T. M., Wooden, J., and Langway, C. C. (1981). Evidence of the bedrock beneath the Greenland Ice Sheet near Camp Century, Greenland. *Journal of Glaciology*, 27(95):193–197.

Fretwell, P., Pritchard, H. D., Vaughan, D. G., Bamber, J. L., Barrand, N. E., Bell, R., Bianchi, C., Bingham, R. G., Blankenship, D. D., Casassa, G., Catania, G., Callens, D., Conway, H., Cook, A. J., Corr, H. F. J., Damaske, D., Damm, V., Ferraccioli, F., Forsberg, R., Fujita, S., Gim, Y., Gogineni, P., Griggs, J. A., Hindmarsh, R. C. A., Holmlund, P., Holt, J. W., Jacobel, R. W., Jenkins, A., Jokat, W., Jordan, T., King, E. C., Kohler, J., Krabill, W., Riger-Kusk, M., Langley, K. A., Leitchenkov, G., Leuschen, C., Luyendyk, B. P., Matsuoka, K., Mouginot, J., Nitsche, F. O., Nogi, Y., Nost, O. A., Popov, S. V., Rignot, E., Rippin, D. M., Rivera, A., Roberts, J., Ross, N., Siegert, M. J., Smith, A. M., Steinhage, D., Studinger, M., Sun, B., Tinto, B. K., Welch, B. C., Wilson, D., Young, D. A., Xiangbin, C., and Zirizzotti, A. (2013). Bedmap2: improved ice bed, surface and thickness datasets for Antarctica. *The Cryosphere*, 7(1):375–393.

Fujita, S., Maeno, H., and Matsuoka, K. (2006). Radio-wave depolarization and scattering within ice sheets: a matrix-based model to link radar and ice-core measurements and its application. *Journal of Glaciology*, 52(178):407–424.

Goff, J. A., Powell, E. M., Young, D. A., and Blankenship, D. D. (2014). Conditional simulation of Thwaites Glacier (Antarctica) bed topography for flow

models: Incorporating inhomogeneous statistics and channelized morphology. *Journal of Glaciology*, 60(222):635–646.

Gogineni, S., Tammana, D., Braaten, D., Leuschen, C., Akins, T., Legarsky, J., Kanagaratnam, P., Stiles, J., Allen, C., and Jezek, K. (2001). Coherent radar ice thickness measurements over the Greenland ice sheet. *Journal of Geophysical Research: Atmospheres*, 106(D24):33761–33772.

Gogineni, S., Yan, J.-B., Paden, J., Leuschen, C., Li, J., Rodriguez-Morales, F., Braaten, D., Purdon, K., Wang, Z., Liu, W., and Gauch, J. (2014). Bed topography of Jakobshavn Isbrae, Greenland, and Byrd Glacier, Antarctica. *Journal of Glaciology*, 60(223):813–833.

Graf, W. L. (1970). The geomorphology of the glacial valley cross section. *Arctic and Alpine Research*, 2(4):303–312.

Grima, C., Schroeder, D. M., Blankenship, D. D., and Young, D. A. (2014). Planetary landing-zone reconnaissance using ice-penetrating radar data: Concept validation in Antarctica. *Planetary and Space Science*, 103:191–204.

Gudlaugsson, E., Humbert, A., Winsborrow, M., and Andreassen, K. (2013). Subglacial roughness of the former Barents Sea ice sheet. *Journal of Geophysical Research: Earth Surface*, 118(4):2546–2556.

Gudmundsson, G. H. (2003). Transmission of basal variability to a glacier surface. *Journal of Geophysical Research: Solid Earth*, 108(B5).

Gudmundsson, G. H. and Raymond, M. (2008). On the limit to resolution and information on basal properties obtainable from surface data on ice streams. *The Cryosphere*, 2(2):167–178.

Gunnell, Y. (2015). Ancient landforms in dynamic landscapes: Inheritance, transience and congruence in Earth-surface systems. *Geomorphology*, 233:1–4.

Hall, A. M., Ebert, K., and Hättestrand, C. (2013). Pre-glacial landform inheritance in a glaciated shield landscape. *Geografiska Annaler: Series A, Physical Geography*, 95(1):33–49.

Hall, A. M. and Kleman, J. (2014). Glacial and periglacial buzzsaws: fitting mechanisms to metaphors. *Quaternary Research*, 81(2):189–192.

Hallet, B., Hunter, L., and Bogen, J. (1996). Rates of erosion and sediment evacuation by glaciers: A review of field data and their implications. *Global and Planetary Change*, 12(1–4):213–235.

Hargreaves, N. D. (1978). The radio-frequency birefringence of polar ice. *Journal of Glaciology*, 21(85):301–313.

Henriksen, N. (2008). *Geological History of Greenland. Four billion years of Earth evolution*. Geological Survey of Denmark and Greenland (GEUS), Copenhagen, 1 edition.

Henriksen, N., Higgins, A., Kalsbeek, F., and Pulvertaft, T. C. R. (2009). Greenland from Archaean to Quarternary - Descriptive text to the 1995 Geological map of Greenland, 1:2,500,000. 2nd edition. *Geological Survey of Denmark and Greenland Bulletin*, 18:1–126.

Herman, F., Beyssac, O., Brughelli, M., Lane, S. N., Leprince, S., Adatte, T., Lin, J. Y. Y., Avouac, J.-P., and Cox, S. C. (2015). Erosion by an Alpine glacier. *Science*, 350(6257):193–195.

Howat, I. M., Negrete, A., and Smith, B. E. (2014). The Greenland Ice Mapping Project (GIMP) land classification and surface elevation data sets. *The Cryosphere*, 8(4):1509–1518.

Huybrechts, P. (1994). The present evolution of the Greenland ice sheet: an assessment by modelling. *Global and Planetary Change*, 9(1):39–51.

Ignéczi, Á., Sole, A. J., Livingstone, S. J., Ng, F. S. L., and Yang, K. (2018). Greenland Ice Sheet surface topography and drainage structure controlled by the transfer of basal variability. *Frontiers in Earth Science*, 6.

Iverson, N. R. and Zoet, L. K. (2015). Experiments on the dynamics and sedimentary products of glacier slip. *Geomorphology*, 244:121–134.

Jamieson, S. S., Stokes, C. R., Ross, N., Rippin, D. M., Bingham, R. G., Wilson, D. S., Margold, M., and Bentley, M. J. (2014). The glacial geomorphology of the Antarctic ice sheet bed. *Antarctic Science*, 26(Special Issue 06):724–741.

Jamieson, S. S. R., Ross, N., Greenbaum, J. S., Young, D. A., Aitken, A. R. A., Roberts, J. L., Blankenship, D. D., Bo, S., and Siegert, M. J. (2016). An extensive subglacial lake and canyon system in Princess Elizabeth Land, East Antarctica. *Geology*, 44(2):87–90.

Jamieson, S. S. R., Sugden, D. E., and Hulton, N. R. J. (2010). The evolution of the subglacial landscape of Antarctica. *Earth and Planetary Science Letters*, 293(1–2):1–27.

Jordan, T. M., Bamber, J. L., Williams, C. N., Paden, J. D., Siegert, M. J., Huybrechts, P., Gagliardini, O., and Gillet-Chaulet, F. (2016). An ice-sheet-wide framework for englacial attenuation from ice-penetrating radar data. *The Cryosphere*, 10(4):1547–1570.

Jordan, T. M., Cooper, M. A., Schroeder, D. M., Williams, C. N., Paden, J. D., Siegert, M. J., and Bamber, J. L. (2017). Self-affine subglacial roughness: consequences for radar scattering and basal water discrimination in northern Greenland. *The Cryosphere*, 11(3):1247–1264.

Jordan, T. M., Williams, C. N., Schroeder, D. M., Martos, Y. M., Cooper, M. A., Siegert, M. J., Paden, J. D., Huybrechts, P., and Bamber, J. L. (2018). A constraint upon the basal water distribution and thermal state of the Greenland Ice Sheet from radar bed echoes. *The Cryosphere*, 12(9):2831–2854.

Joughin, I., Abdalati, W., and Fahnestock, M. (2004). Large fluctuations in speed on Greenland's Jakobshavn Isbræ glacier. *Nature*, 432(7017):608–610.

Joughin, I., Smith, B., Howat, I., and Scambos, T. (2016). MEaSUREs multi-year Greenland Ice Sheet velocity mosaic, version 1.

Joughin, I., Smith, B. E., and Howat, I. M. (2017). A complete map of Greenland ice velocity derived from satellite data collected over 20 years. *Journal of Glaciology*, 64(243):1–11.

Joughin, I., Smith, B. E., Howat, I. M., Scambos, T., and Moon, T. (2010). Greenland flow variability from ice-sheet-wide velocity mapping. *Journal of Glaciology*, 56(197):415–430.

Joughin, I., Tulaczyk, S., Bamber, J. L., Blankenship, D., Holt, J. W., Scambos, T., and Vaughan, D. G. (2009). Basal conditions for Pine Island and Thwaites Glaciers, West Antarctica, determined using satellite and airborne data. *Journal of Glaciology*, 55(190):245–257.

Karlsson, N. B., Dahl-Jensen, D., Gogineni, S. P., and Paden, J. D. (2013). Tracing the depth of the Holocene ice in North Greenland from radio-echo sounding data. *Annals of Glaciology*, 54(64):44–50.

Karlsson, N. B., Rippin, D. M., Bingham, R. G., and Vaughan, D. G. (2012). A 'continuity-index' for assessing ice-sheet dynamics from radar-sounded internal layers. *Earth and Planetary Science Letters*, 335–336:88–94.

King, E. C., Hindmarsh, R. C. A., and Stokes, C. R. (2009). Formation of mega-scale glacial lineations observed beneath a West Antarctic ice stream. *Nature Geoscience*, 2(8):585–588.

Kleiven, H. F., Jansen, E., Fronval, T., and Smith, T. M. (2002). Intensification of Northern Hemisphere glaciations in the circum Atlantic region (3.5–2.4 Ma) – ice-rafted detritus evidence. *Palaeogeography, Palaeoclimatology, Palaeoecology*, 184(3–4):213–223.

Kleman, J. (1994). Preservation of landforms under ice sheets and ice caps. *Geomorphology*, 9(1):19–32.

Kleman, J. and Hättestrand, C. (1999). Frozen-bed Fennoscandian and Laurentide ice sheets during the Last Glacial Maximum. *Nature*, 402(6757):63–66.

Kleman, J., Stroeven, A. P., and Lundqvist, J. (2008). Patterns of Quaternary ice sheet erosion and deposition in Fennoscandia and a theoretical framework for explanation. *Geomorphology*, 97(1–2):73–90.

Koppes, M. N. and Montgomery, D. R. (2009). The relative efficacy of fluvial and glacial erosion over modern to orogenic timescales. *Nature Geoscience*, 2(9):644–647.

Layberry, R. L. and Bamber, J. L. (2001). A new ice thickness and bed data set for the Greenland ice sheet: 2. Relationship between dynamics and basal

topography. *Journal of Geophysical Research: Atmospheres*, 106(D24):33781–33788.

Le Brocq, A. M., Hubbard, A., Bentley, M. J., and Bamber, J. L. (2008). Subglacial topography inferred from ice surface terrain analysis reveals a large un-surveyed basin below sea level in East Antarctica. *Geophysical Research Letters*, 35(16):L16503.

Li, X., Sun, B., Siegert, M. J., Bingham, R. G., Tang, X., Zhang, D., Cui, X., and Zhang, X. (2010). Characterization of subglacial landscapes by a two-parameter roughness index. *Journal of Glaciology*, 56(199):831–836.

Lindbäck, K. and Pettersson, R. (2015). Spectral roughness and glacial erosion of a land-terminating section of the Greenland Ice Sheet. *Geomorphology*, 238:149–159.

Livingstone, S. J., Chu, W., Ely, J. C., and Kingslake, J. (2017). Paleofluvial and subglacial channel networks beneath Humboldt Glacier, Greenland. *Geology*, 45(6):551–554.

MacGregor, J. A., Catania, G. A., Conway, H., Schroeder, D. M., Joughin, I., Young, D. A., Kempf, S. D., and Blankenship, D. D. (2013). Weak bed control of the eastern shear margin of Thwaites Glacier, West Antarctica. *Journal of Glaciology*, 59(217):900–912.

MacGregor, J. A., Fahnestock, M. A., Catania, G. A., Aschwanden, A., Clow, G. D., Colgan, W. T., Gogineni, P. S., Morlighem, M., Nowicki, S. M. J., Paden, J. D., Price, S. F., and Seroussi, H. (2016). A synthesis of the basal thermal state of the Greenland Ice Sheet. *Journal of Geophysical Research: Earth Surface*.

MacGregor, J. A., Fahnestock, M. A., Catania, G. A., Paden, J. D., Prasad Gogineni, S., Young, S. K., Rybarski, S. C., Mabrey, A. N., Wagman, B. M., and Morlighem, M. (2015a). Radiostratigraphy and age structure of the Greenland Ice Sheet. *Journal of Geophysical Research: Earth Surface*, 120(2).

MacGregor, J. A., Li, J., Paden, J. D., Catania, G. A., Clow, G. D., Fahnestock, M. A., Gogineni, S. P., Grimm, R. E., Morlighem, M., Nandi, S., Seroussi,

H., and Stillman, D. E. (2015b). Radar attenuation and temperature within the Greenland Ice Sheet. *Journal of Geophysical Research: Earth Surface*, 120(6):983–1008.

Martos, Y. M., Jordan, T. A., Catalán, M., Jordan, T. M., Bamber, J. L., and Vaughan, D. G. (2018). Geothermal heat flux reveals the Iceland hotspot track underneath Greenland. *Geophysical Research Letters*, 0(0).

Matsuoka, K., Power, D., Fujita, S., and Raymond, C. F. (2012). Rapid development of anisotropic ice-crystal-alignment fabrics inferred from englacial radar polarimetry, central West Antarctica. *Journal of Geophysical Research: Earth Surface*, 117(F3).

Morin, P., Porter, C., Cloutier, M., Howat, I., Noh, M.-J., Willis, M., Bates, B., Willamson, C., and Peterman, K. (2016). ArcticDEM; A Publically Available, High Resolution Elevation Model of the Arctic. volume 18, pages EPSC2016–8396.

Morlighem, M., Rignot, E., Mouginot, J., Seroussi, H., and Larour, E. (2014). Deeply incised submarine glacial valleys beneath the Greenland ice sheet. *Nature Geoscience*, 7(6):418–422.

Morlighem, M., Rignot, E., Seroussi, H., Larour, E., Dhia, H. B., and Aubry, D. (2011). A mass conservation approach for mapping glacier ice thickness. *Geophysical Research Letters*, 38(19).

Morlighem, M., Williams, C. N., Rignot, E., An, L., Arndt, J. E., Bamber, J. L., Catania, G., Chauché, N., Dowdeswell, J. A., Dorschel, B., Fenty, I., Hogan, K., Howat, I., Hubbard, A., Jakobsson, M., Jordan, T. M., Kjeldsen, K. K., Millan, R., Mayer, L., Mouginot, J., Noël, B. P. Y., O'Cofaigh, C., Palmer, S., Rysgaard, S., Seroussi, H., Siegert, M. J., Slabon, P., Straneo, F., van den Broeke, M. R., Weinrebe, W., Wood, M., and Zinglersen, K. B. (2017). BedMachine v3: Complete bed topography and ocean bathymetry Mapping of Greenland from multibeam echo sounding combined with mass conservation. *Geophysical Research Letters*, 44(21):11,051–11,061.

Mudd, S., Hurst, M., Milodowski, D., Grieve, S., Clubb, F., and Valters, D. (2013). Land Surface Dynamics Topography Tool Box.

Ng, F. S. L., Ignéczi, Á., Sole, A. J., and Livingstone, S. J. (2018). Response of surface topography to basal variability along glacial flowlines. *Journal of Geophysical Research: Earth Surface*.

Nick, F. M., Vieli, A., Andersen, M. L., Joughin, I., Payne, A., Edwards, T. L., Pattyn, F., and van de Wal, R. S. W. (2013). Future sea-level rise from Greenland's main outlet glaciers in a warming climate. *Nature*, 497(7448):235–238.

Nolan, M., Motyka, R. J., Echelmeyer, K., and Trabant, D. C. (1995). Ice-thickness measurements of Taku Glacier, Alaska, U.S.A., and their relevance to its recent behavior. *Journal of Glaciology*, 41:541–553.

Nye, J. F. (1970). Glacier sliding without cavitation in a linear viscous approximation. *Proceedings of the Royal Society of London. Series A, Mathematical and Physical Sciences*, 315(1522):381–403.

O'Connor, J. E. and Baker, V. R. (1992). Magnitudes and implications of peak discharges from glacial Lake Missoula. *Geological Society of America Bulletin*, 104(3):267–279.

Oswald, G. K. A. and Gogineni, S. P. (2008). Recovery of subglacial water extent from Greenland radar survey data. *Journal of Glaciology*, 54(184):94–106.

Oswald, G. K. A. and Gogineni, S. P. (2012). Mapping basal melt under the northern Greenland Ice Sheet. *IEEE Transactions on Geoscience and Remote Sensing*, 50(2):585–592.

Oswald, G. K. A., Rezvanbehbahani, S., and Stearns, L. A. (2018). Radar evidence of ponded subglacial water in Greenland. *Journal of Glaciology*, pages 1–19.

Overeem, I., Hudson, B. D., Syvitski, J. P. M., Mikkelsen, A. B., Hasholt, B., van den Broeke, M. R., Noël, B. P. Y., and Morlighem, M. (2017). Substantial export of suspended sediment to the global oceans from glacial erosion in Greenland. *Nature Geoscience*, 10(11):859–863.

Paden, J. (2016). Along-track horizontal resolution of cresis data. personal communication.

Paden, J. (2017). Radar Depth Sounder, Centre for Remote Sensing for Ice Sheets.

Peters, M. E., Blankenship, D. D., and Morse, D. L. (2005). Analysis techniques for coherent airborne radar sounding: Application to West Antarctic ice streams. *Journal of Geophysical Research: Solid Earth*, 110(B6).

Plewes, L. A. and Hubbard, B. (2001). A review of the use of radio-echo sounding in glaciology. *Progress in Physical Geography*, 25(2):203–236.

Rémy, F. and Minster, J.-F. (1997). Antarctica Ice Sheet curvature and its relation with ice flow and boundary conditions. *Geophysical Research Letters*, 24(9):1039–1042.

Ridley, J. K., Cudlip, W., and Laxon, S. W. (1993). Identification of subglacial lakes using ERS-1 radar altimeter. *Journal of Glaciology*, 39(133):625–634.

Rignot, E., Velicogna, I., van den Broeke, M. R., Monaghan, A., and Lenaerts, J. T. M. (2011). Acceleration of the contribution of the Greenland and Antarctic ice sheets to sea level rise. *Geophysical Research Letters*, 38(5):L05503.

Rippin, D., Vaughan, D., and Corr, H. (2011). The basal roughness of Pine Island Glacier, West Antarctica. *Journal of Glaciology*, 57(201):67–76.

Rippin, D. M. (2013). Bed roughness beneath the Greenland ice sheet. *Journal of Glaciology*, 59(216):724–732.

Rippin, D. M., Bamber, J. L., Siegert, M. J., Vaughan, D. G., and Corr, H. F. J. (2006). Basal conditions beneath enhanced-flow tributaries of Slessor Glacier, East Antarctica. *Journal of Glaciology*, 52(179):481–490.

Rippin, D. M., Bingham, R. G., Jordan, T. A., Wright, A. P., Ross, N., Corr, H. F. J., Ferraccioli, F., Le Brocq, A. M., Rose, K. C., and Siegert, M. J. (2014). Basal roughness of the Institute and Möller Ice Streams, West Antarctica: Process determination and landscape interpretation. *Geomorphology*, 214:139–147.

Rodriguez-Morales, F., Gogineni, S., Leuschen, C. J., Paden, J. D., Li, J., Lewis, C. C., Panzer, B., Alvestegui, D. G.-G., Patel, A., Byers, K., Crowe, R., Player,

K., Hale, R. D., Arnold, E. J., Smith, L., Gifford, C. M., Braaten, D., and Panton, C. (2014). Advanced Multifrequency Radar Instrumentation for Polar Research. *IEEE Transactions on Geoscience and Remote Sensing*, 52(5):2824–2842.

Rogozhina, I., Petrunin, A. G., Vaughan, A. P. M., Steinberger, B., Johnson, J. V., Kaban, M. K., Calov, R., Rickers, F., Thomas, M., and Koulakov, I. (2016). Melting at the base of the Greenland ice sheet explained by Iceland hotspot history. *Nature Geoscience*, 9(5):366–369.

Rose, K. C., Ferraccioli, F., Jamieson, S. S. R., Bell, R. E., Corr, H., Creyts, T. T., Braaten, D., Jordan, T. A., Fretwell, P. T., and Damaske, D. (2013). Early East Antarctic Ice Sheet growth recorded in the landscape of the Gamburtsev Subglacial Mountains. *Earth and Planetary Science Letters*, 375:1–12.

Rose, K. C., Ross, N., Bingham, R. G., Corr, H. F. J., Ferraccioli, F., Jordan, T. A., Brocq, A. M. L., Rippin, D. M., and Siegert, M. J. (2014). A temperate former West Antarctic ice sheet suggested by an extensive zone of subglacial meltwater channels. *Geology*, 42(11):971–974.

Rose, K. C., Ross, N., Jordan, T. A., Bingham, R. G., Corr, H. F. J., Ferraccioli, F., Le Brocq, A. M., Rippin, D. M., and Siegert, M. J. (2015). Ancient pre-glacial erosion surfaces preserved beneath the West Antarctic Ice Sheet. *Earth Surface Dynamics*, 3(1):139–152.

Ross, N., Jordan, T. A., Bingham, R. G., Corr, H. F. J., Ferraccioli, F., Brocq, A. L., Rippin, D. M., Wright, A. P., and Siegert, M. J. (2014). The Ellsworth Subglacial Highlands: Inception and retreat of the West Antarctic Ice Sheet. *Geological Society of America Bulletin*, 126(1-2):3–15.

Schroeder, D. M., Blankenship, D. D., Raney, R. K., and Grima, C. (2015). Estimating subglacial water geometry using radar bed echo specularity: Application to Thwaites Glacier, West Antarctica. *IEEE Geoscience and Remote Sensing Letters*, 12(3):443–447.

Schroeder, D. M., Blankenship, D. D., and Young, D. A. (2013). Evidence for a water system transition beneath Thwaites Glacier, West Antarctica. *Pro-*

ceedings of the National Academy of Sciences of the United States of America, 110(30):12225–12228.

Schroeder, D. M., Blankenship, D. D., Young, D. A., Witus, A. E., and Anderson, J. B. (2014). Airborne radar sounding evidence for deformable sediments and outcropping bedrock beneath Thwaites Glacier, West Antarctica. *Geophysical Research Letters*, 41(20):7200–7208.

Sergienko, O. V., Creyts, T. T., and Hindmarsh, R. C. A. (2014). Similarity of organized patterns in driving and basal stresses of Antarctic and Greenland ice sheets beneath extensive areas of basal sliding. *Geophysical Research Letters*, 41(11):3925–3932.

Shepard, M. K., Brackett, R. A., and Arvidson, R. E. (1995). Self-affine (fractal) topography: Surface parameterization and radar scattering. *Journal of Geophysical Research: Planets*, 100(E6):11709–11718.

Shepard, M. K. and Campbell, B. A. (1999). Radar scattering from a self-affine fractal surface: Near-Nadir regime. *Icarus*, 141(1):156–171.

Shepard, M. K., Campbell, B. A., Bulmer, M. H., Farr, T. G., Gaddis, L. R., and Plaut, J. J. (2001). The roughness of natural terrain: A planetary and remote sensing perspective. *Journal of Geophysical Research: Planets*, 106(E12):32777–32795.

Shreve, R. L. (1966). Statistical law of stream numbers. *The Journal of Geology*, 74(1):17–37.

Siegert, M. J. (1999). On the origin, nature and uses of Antarctic ice-sheet radio-echo layering. *Progress in Physical Geography*, 23(2):159–179.

Siegert, M. J. (2001). *Ice Sheets and Late Quaternary Environmental Change*. John Wiley and Sons.

Siegert, M. J. and Ridley, J. K. (1998). An analysis of the ice-sheet surface and subsurface topography above the Vostok Station subglacial lake, central East Antarctica. *Journal of Geophysical Research: Solid Earth*, 103(B5):10195–10207.

Siegert, M. J., Taylor, J., and Payne, A. J. (2005). Spectral roughness of subglacial topography and implications for former ice-sheet dynamics in East Antarctica. *Global and Planetary Change*, 45(1–3):249–263.

Siegert, M. J., Taylor, J., Payne, A. J., and Hubbard, B. (2004). Macro-scale bed roughness of the Siple Coast ice streams in West Antarctica. *Earth Surface Processes and Landforms*, 29(13):1591–1596.

Smith, M. W. (2014). Roughness in the earth sciences. *Earth-Science Reviews*, 136:202–225.

Sobel, I. and Feldman, G. (1968). A 3x3 isotropic gradient operator for image processing.

Stearns, L. A. and van der Veen, C. J. (2018). Friction at the bed does not control fast glacier flow. *Science*, 361(6399):273–277.

Stock, J. D., Montgomery, D. R., Collins, B. D., Dietrich, W. E., and Sklar, L. (2005). Field measurements of incision rates following bedrock exposure: Implications for process controls on the long profiles of valleys cut by rivers and debris flows. *Geological Society of America Bulletin*, 117(1-2):174–194.

Stroeven, A. P., Harbor, J., Fabel, D., Kleman, J., Hättestrand, C., Elmore, D., Fink, D., and Fredin, O. (2006). Slow, patchy landscape evolution in northern Sweden despite repeated ice-sheet glaciation. *Geological Society of America Special Papers*, 398:387–396.

Sugden, D. E. (1974). Landscapes of glacial erosion in Greenland and their relationship to ice, topographic and bedrock conditions. *Institute of British Geographers Special Publication*, 7:177–195.

Sugden, D. E. and John, B. S. (1976). *Glaciers and Landscape: A Geomorphological Approach*. Edward Arnold Ltd., London.

Summerfield, M. (1991). *Global Geomorphology:An Introduction to the Study of Landforms*. Longman Scientific and Technical, Harlow, Essex, England.

Taylor, J., Siegert, M. J., Payne, A. J., and Hubbard, B. (2004). Regional-scale bed roughness beneath ice masses: measurement and analysis. *Computers & Geosciences*, 30(8):899–908.

Ten Brink, N. W. and Weidick, A. (1974). Greenland ice sheet history since the last glaciation. *Quaternary Research*, 4(4):429–440.

Tinto, K. J., Bell, R. E., Cochran, J. R., and Münchow, A. (2015). Bathymetry in Petermann fjord from Operation IceBridge aerogravity. *Earth and Planetary Science Letters*, 422:58–66.

Ulaby, F. T., Moore, R. K., and Fung, A. K. (1982). *Microwave Remote Sensing Active and Passive-Volume II: Radar Remote Sensing and Surface Scattering and Enission Theory*. Addison Wesley Longman, Boston , USA.

van den Broeke, M., Bamber, J., Ettema, J., Rignot, E., Schrama, E., van de Berg, W. J., van Meijgaard, E., Velicogna, I., and Wouters, B. (2009). Partitioning recent Greenland mass loss. *Science*, 326(5955):984–986.

van der Veen, C. J. (2013). *Fundamentals of Glacier Dynamics, Second Edition*. CRC Press. Google-Books-ID: r2HRBQAAQBAJ.

Vaughan, D., Comiso, J., Allison, I., Carrasco, J., Kaser, G., Kwok, R., Mote, P., Murray, T., Paul, F., Ren, J., Rignot, E., Solomina, O., Steffen, K., and Zhang, T. (2013). *Observations: Cryosphere. In: Climate Change 2013: The Physical Science Basis. Contribution of Working Group I to the Fifth Assessment Report of the Intergovernmental Panel on Climate Change*, pages 317–382. Cambridge University Press, Cambridge, United Kingdom and New York, NY, USA.

Velicogna, I. and Wahr, J. (2006). Acceleration of Greenland ice mass loss in spring 2004. *Nature*, 443(7109):329–331.

Vieli, G. J.-M. C. L., Martín, C., Hindmarsh, R. C. A., and Lüthi, M. P. (2018). Basal freeze-on generates complex ice-sheet stratigraphy. *Nature Communications*, 9(1):4669.

Waite, A. H. and Schmidt, S. J. (1962). Gross errors in height indication from pulsed radar altimeters operating over thick ice or snow. *Proceedings of the IRE*, 50(6):1515–1520.

Weertman, J. (1957). On the sliding of glaciers. *Journal of Glaciology*, 3(21):33–38.

Weertman, J. (1972). General theory of water flow at the base of a glacier or ice sheet. *Reviews of Geophysics*, 10(1):287–333.

Weertman, J. (1976). Sliding-no sliding zone effect and age determination of ice cores. *Quaternary Research*, 6(2):203–207.

Williams, C. N., Cornford, S. L., Jordan, T. M., Dowdeswell, J. A., Siegert, M. J., Clark, C. D., Swift, D. A., Sole, A., Fenty, I., and Bamber, J. L. (2017). Generating synthetic fjord bathymetry for coastal Greenland. *The Cryosphere*, 11(1):363–380.

Winkler, P. E. M. (1973). Properties of Stone. In *Stone: Properties Durability in Man's Environment*, number 4 in Applied Mineralogy / Technische Mineralogie, pages 27–50. Springer Vienna.

Wolovick, M. J., Creyts, T. T., Buck, W. R., and Bell, R. E. (2014). Traveling slippery patches produce thickness-scale folds in ice sheets. *Geophysical Research Letters*, 41(24):8895–8901.

Wright, A. P., Siegert, M. J., Le Brocq, A. M., and Gore, D. B. (2008). High sensitivity of subglacial hydrological pathways in Antarctica to small ice-sheet changes. *Geophysical Research Letters*, 35(17):L17504.

Wrona, T., Wolovick, M. J., Ferraccioli, F., Corr, H., Jordan, T., and Siegert, M. J. (2017). Position and variability of complex structures in the central East Antarctic Ice Sheet. *Geological Society, London, Special Publications*, 461:SP461.12.

Young, D. A., Schroeder, D. M., Blankenship, D. D., Kempf, S. D., and Quartini, E. (2016). The distribution of basal water between Antarctic subglacial lakes from radar sounding. *Philosophical Transactions. Series A, Mathematical, Physical, and Engineering Sciences*, 374(2059).

Young, D. A., Wright, A. P., Roberts, J. L., Warner, R. C., Young, N. W., Greenbaum, J. S., Schroeder, D. M., Holt, J. W., Sugden, D. E., Blankenship, D. D., van Ommen, T. D., and Siegert, M. J. (2011). A dynamic early East Antarctic Ice Sheet suggested by ice-covered fjord landscapes. *Nature*, 474(7349):72–75.

Zwally, J. H., Giovinetto, M. B., Beckley, M. A., and Saba, J. L. (2012). Antarctic and Greenland drainage systems.